Preliminary Calibration of the Photometrics PXL1300L CCD Camera[1]

Steve Shiang-Feng Chen*
Jerry Wei-Chieh Li*
Kenneth E. Torrance[2]
S. N. Pattanaik[3]

March 4, 1996

[1]An early version of this report was submitted by the first two authors towards the partial fulfillment of their M.Eng. degree in Mechanical & Aerospace Engineering, under course M&AE 690 (8 credits).

[2]Professor, Sibley School of Mechanical and Aerospace Engineering, Cornell University.
[3]Post Doctoral Research Associate, Program of Computer Graphics, Cornell University.

Abstract

This report describes the preliminary spectroradiometric calibration of a CCD camera system, which consists of a high dynamic range (12 bit), liquid cooled scientific grade CCD camera used in conjunction with a series of narrow band and neutral density filters. The purpose of the calibration is to extend the camera system into a *spectral camera*, capable of measuring scene images that would provide, not only color information, but *quantitative spectrum data* for every pixel of a viewed scene. The measured images from such a *spectral camera* can eventually be compared with the synthetic images generated using physically based algorithms for illumination exchange.

The present report provides spectral transmittance curves for the narrow band and neutral density filters used with the CCD camera, and the results of various linearity checks on the camera. The report provides the *spectral response function* for the camera and *preliminary spectral reconstructions* for wide and narrow band light sources.

Contents

Chapter 1

Introduction

This report contains seven chapters describing a study of a particular charge coupled device (CCD) camera, the Photometrics PXL1300L. In brief, the report includes spectral transmittance measurements for the narrow band (color) filters and neutral density (gray) filters used with the camera (Chapter 4), linearity tests on the camera and the determination of the spectral response function of the camera (Chapter 5), and preliminary spectral recreations for wide and narrow band light sources (Chapter 6).

The camera responds over a wide wavelength range. The mathematical procedure used to obtain spectral recreations or reconstructions of an unknown input source spectrum, using camera measurements of the source taken through a range of color filters, is described. The mathematical inversion procedure employs basis functions. Estimates of errors in reconstructed signals are included.

For background information on the present Photometrics camera and other CCD cameras, the interested reader can consult reports available in the Light Measurement Laboratory of the Program of Computer Graphics [1, 2, 3, 14, 17]. In addition, a useful introductory text on CCD imaging is that of Buil [4]. For a discussion of CCD device physics and limits see [6, 7]; for information on calibration see [5]; and for examples of other laboratories using CCD cameras for computer graphics see [8, 9]. Furthermore, a commercial, self-contained, three filter CCD camera with 288×496 resolution has recently been announced [10]. The present report focuses on an eight filter CCD camera with 1024×1280 resolution and high dynamic range (12 bit; 0-4095 signal range).

Chapter 2 lists the equipment used in the present project. Chapter 3 shows the three major camera setups which describe how the data were gathered for the CCD camera. Chapter 4 shows the transmittance of eight color filters, including seven narrow band and one long-band pass filter, and seven neutral density filters which are used for the camera's spectral calibration and for spectral recreation. Throughout this report, for convenience, we will refer to the set of eight color filters as the narrow band (NB) filter set.

Chapter 5 breaks into 3 sections: Section 5.1 for radiometric calibration, Section 5.2 for spectral calibration and Section 5.3 for pixel response variation.

In Section 5.1, the linearity of the camera is verified by using both wide and narrow band light sources and various F-stops. A comprehensive linearity verification over a range of F-stops and shutter speeds is provided. In Section 5.2, the camera response function is found by using the wide-band light source, eight narrow band filters, and eight orthogonal basis functions which are extracted by applying the QR factorization method to the eight filter functions. The camera response for different regions of interest (ROI) on the CCD chip and two different focal distances are also studied in this section. The extracted response is compared to the manufacturer's published response curve. Section 5.3 describes the variation in CCD pixel response observed when imaging a uniform light source.

Chapter 6 uses the camera response found in Chapter 5 to recreate the spectrum of the wide-band uniform light source in Section 6.1 and of monochromatic light sources in Section 6.2. In Section 6.1.2, the spectra for different ROIs and focal distances establish the uniformity of the CCD chip. Section 6.2 shows the recreation of specific narrow band light sources with various half band widths. All the previous spectrum recreations were carried out at 20 nm discrete intervals over the wavelength range from 360 nm to 1100 nm. In Section 6.3, the spectra of both the wide and narrow band light sources are recreated using 10, 20, and 40 nm constant intervals and eight filter peak intervals. This reveals limitations on accuracy as a function of different discrete intervals for reconstruction and different wide-band and narrow band light sources.

Chapter 6 concludes with a discussion of various error estimates for wide-band spectrum recreations. Section 6.4.1 describes the changes in radiance when an input signal is varied by one percent. It shows the sensitivity to, or dependence on, the filters. In Section 6.4.2, the effects of signal measurement errors on a recreated spectrum are examined. Upper and lower error bounds are calculated using constant wavelength reconstruction intervals of 10, 20 and 40 nm and nonconstant intervals corresponding to the eight filter peaks. In Section 6.4.3, calculation errors are estimated by spectrally integrating a recreated signal.

Chapter 7 summarizes this preliminary work on the calibration of the CCD camera. Various problems/difficulties encountered during this work are listed and suggestions are made for future work.

Chapter 2

Equipment List

Given below is the list of equipment used in this project.

2.1 Filters and Transmittance Measurement Equipment

2.1.1 Narrow Band (NB) Color Filters

- Melles Griot 03FIB002 narrow band filter (NB filter #1 (410 nm))
- Melles Griot 03FIB004 narrow band filter (NB filter #2 (470 nm))
- Melles Griot 03FIB006 narrow band filter (NB filter #3 (510 nm))
- Melles Griot 03FIB008 narrow band filter (NB filter #4 (560 nm))
- Melles Griot 03FIB012 narrow band filter (NB filter #5 (610 nm))
- Melles Griot 03FIB014 narrow band filter (NB filter #6 (640 nm))
- Melles Griot 03FIB016 narrow band filter (NB filter #7 (720 nm))
- Band Pass Filter (NB filter #8)
  - Kodak Wratten Gelatin Filter 1495613, No. 26
  - Kodak Wratten Gelatin Filter 1495795, No. 47B

2.1.2 Neutral Density (ND) Filters

- Melles Griot 03FNQ002 optical density filter (ND filter OD = 0.03)
- Melles Griot 03FNQ003 optical density filter (ND filter OD = 0.1)
- Melles Griot 03FNQ007 optical density filter (ND filter OD = 0.3)

- Melles Griot 03FNQ085 optical density filter (ND filter OD = 0.5)
- Melles Griot 03FNQ015 optical density filter (ND filter OD = 1.0)
- Melles Griot 03FNQ023 optical density filter (ND filter OD = 2.0)
- Melles Griot 03FNQ027 optical density filter (ND filter OD = 3.0)

2.1.3 Transmittance Measurement

The following equipment was used to measure the transmittance. The measurement setup consisted of:

- Optronic Laboratories OL-750-S Monochromator (S/N: 93104016)
- Optronic Laboratories OL-750-C Controller (S/N: 93108025)
- Optronic Laboratories 740-20-D/IR IR/Visible Dual Light Source (S/N: 93200241)
- Optronic Laboratories HD-300 Silicon Detector Head (S/N: 93101021)
- Optronic Laboratories DSM-1A Detector Support Module (S/N: 93100017)
- Optronic Laboratories 65DS Precision Current Source (S/N: 93101964)
- Melles Griot 01LA0138 Achromatic f = 120 mm lens (S/N: G3049)

2.2 CCD Camera

The CCD camera is equipped with a Grade 2 CCD chip [13]. It has a resolution of 1024 × 1280, with pixels of size $16\mu m \times 16\mu m$. The 12 bit dynamic range gives 0 to 4095 integer radiance readings. The liquid cooling unit is capable of cooling the chip down to -50°C. The camera measurements reported in this report were all carried out with a constant CCD chip temperature of -40°C. The various units of the camera are:

- Photometrics PXL Camera Head
- Photometrics PXL Camera Electronics Unit
- Photometrics PXL Liquid Cooling Unit
- Nikon lens (Micro-NIKKOR, Focal Length = 55mm, 1:2.8)

2.3 Wide Band Uniform Light Source

- Lab Sphere SC-5000 Integrating Sphere System Control,
- USS-1200 SF 12-inch Uniform Source Sphere.

This is a 12 inch diameter integrating sphere with four internally mounted IHLS-100-30, 30 watt halogen light sources in the interior. The sphere has an aperture of 4 inch diameter. The radiant uniformity of this integrating sphere is greater than 98% across the entire output aperture. It is used as a wide-band light source. The exit spectral radiance is known by independent calibration and is used for camera calibration.

For additional information on the above equipment the interested reader should consult the equipment acquisition report by S.-C. Foo [3] and the various manufacturers' manuals and catalogs for the equipment [11, 12, 14-18].

Chapter 3

Equipment Setups

This chapter displays the three equipment setups used for measuring the transmittance of the filters, for the linearity test, and for the camera calibration and wide-band source spectrum recreation.

Setup 1: Transmittance measurement for neutral density and narrow band filters used in Chapter 4.

Setup 2: Camera linearity and narrow-band-source spectral resolution tests. Sections 5.1.2 and 6.2.

Setup 3: Camera spectral response calibration and wide-band source spectrum recreation. Sections 5.2, 5.3, 6.1, 6.4.1 and 6.4.2.

Setup 1: Transmittance Measurement

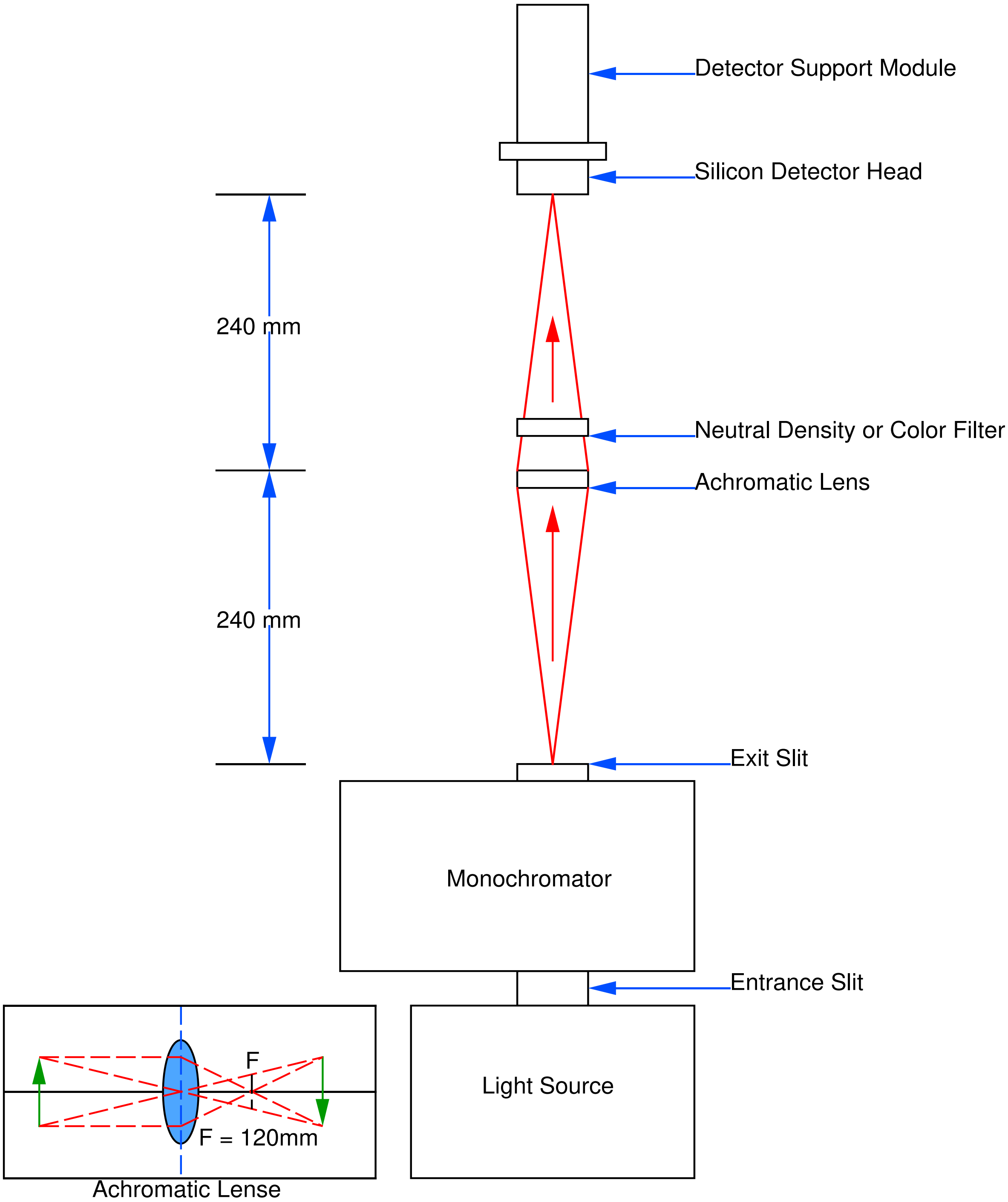

Setup 2: Camera Linearity and Narrow Band Source Resolution Tests

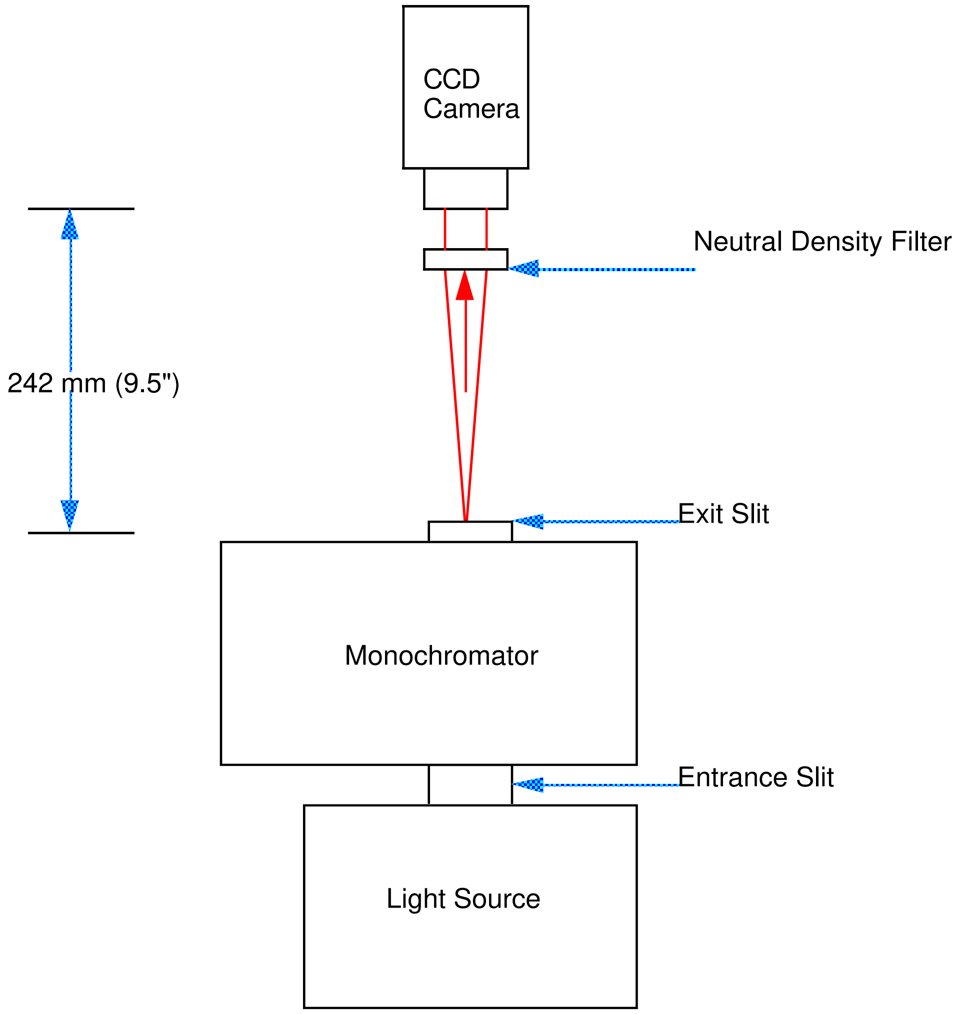

Setup 3: Camera Spectral Response Calibration and Wide Band Source Spectrum Recreation

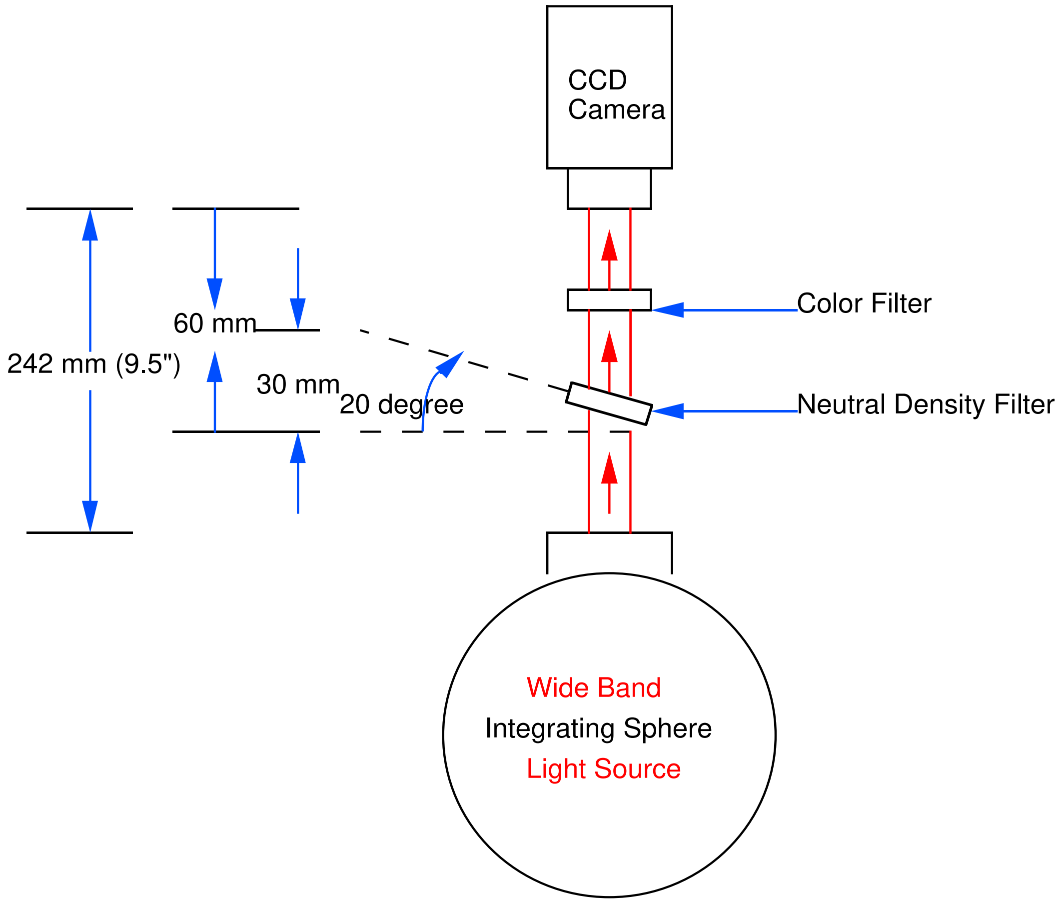

Chapter 4

Filter Transmittance Measurement

Knowledge of the spectral transmittance of the filters is important to this project. The transmission curves of the filters are used to form the basis functions of the mathematical model for the camera calibration and the spectral reconstruction of the radiance of a scene. The spectral transmission of each filter is measured by an accurate sensor using a combination of the Optronic monochromator and silicon detector. The system can measure the transmission in the visible and infrared regions. The filter transmission measurements are presented graphically in this section, and in tabular forms in the Appendices and on a separate $3\frac{1}{2}''$ floppy disk.

4.1 Narrow Band Filters

The light source used for this measurement was a dual source unit which incorporates both a 150-watt Tungsten lamp and an infrared, ceramic glower. The setup appears as Setup #1 in Chapter 3. Since our interest was mainly in the region between wavelengths of 350 nm to 1100 nm, the manual beam switch of the light source was set to the "visible" position. The exit port of the light source was connected to the monochromator which generates a beam with narrow half band width. Of the three available monochromator gratings, we used two. Grating 1 with a dispersion factor of 4 nm/mm was used for transmittance measurements ranging from 350 nm to 900 nm, and grating 2 with a dispersion factor of 8 nm/mm was used for measurements in the range of 900 nm to 1100 nm. The exit and entrance slits of the monochromator determine the half band width (HBW) of the dispersed beam coming out of the exit slit. The HBW was calculated by multiplying the dispersion factor (nm/mm) by the slit width (mm). A slit width of 0.5 mm was chosen for both exit and entrance slits to create a HBW of 2 nm for grating 1 and 4 nm for grating 2.

Since the filters had to be placed between the exit slit of the monochromator and the sensor of the silicon detector, a focusing lens was used to create space for the filters to be tested. An achromatic lens with focal length of 120 mm was chosen. The achromatic lens was a closely spaced combination of positive and negative elements of different refractive indices; therefore the chromatic aberration canceled at two distinct wavelengths, and it had a single focal length value over the entire spectrum. For the detector to get an image of the same size as the exit beam of the monochromator, both monochromator and detector were placed at $2F = 240$mm from either side of the achromatic lens, where F denotes the focal length of the lens.

A High Sensitivity Detector Module (HSDM) which had an effective wavelength range from 200 nm to 1100 nm, was placed at the focal point (Setup #1) on the other side of the achromatic lens. It consisted of a Silicon Detector Head (DH) which contained the detector element, and a Detector Support Module (DSM) which contained the preamplifier. The signal generated by the silicon sensor was sent to the controller after amplification from the DSM.

By using the above setup, a 100 percent calibration measurement was done by scanning the radiant energy from 350 nm to 1100 nm with an interval of 10 nm wavelength using the HSDM. The 100 percent calibration data was then used for transmittance calculation. After the 100 percent calibration was done, seven narrow band (color) filters and one long-band pass filter (filters 1 to 8) were placed between the achromatic lens and the HSDM, one filter at a time. Measurements were then taken of the radiant energy over the wavelength range from 350 nm to 1100 nm with an interval of 10 nm. Dividing the filter data by the 100 percent calibration data, the transmittance of the filters was found. The following eight graphs (Figures 4.1.1-8) show the transmittance curves. Appendix A tabulates the transmittance data of these filters. The average half band width is 7 nm, the wavelength accuracy is 0.05% and the wavelength precision is 0.01%. All the eight filter spectra are shown together in Figure 4.1.9.

The above narrow band, or color, filters are considered quite narrow in bandwidth and very independent even though there were overlaps between them. The independence of the filters can improve the accuracy of the mathematical inversion procedure during spectral camera response calibration and the light source spectrum recreation in Sections 5.2 and 6.1, respectively. During the calibration procedure for the camera, having narrow band color filters along with the smallest F-stop was not enough to reduce the intensity of the incoming light. Therefore neutral density filters were also used. The transmittance measurement for the neutral density filters is described in the next section.

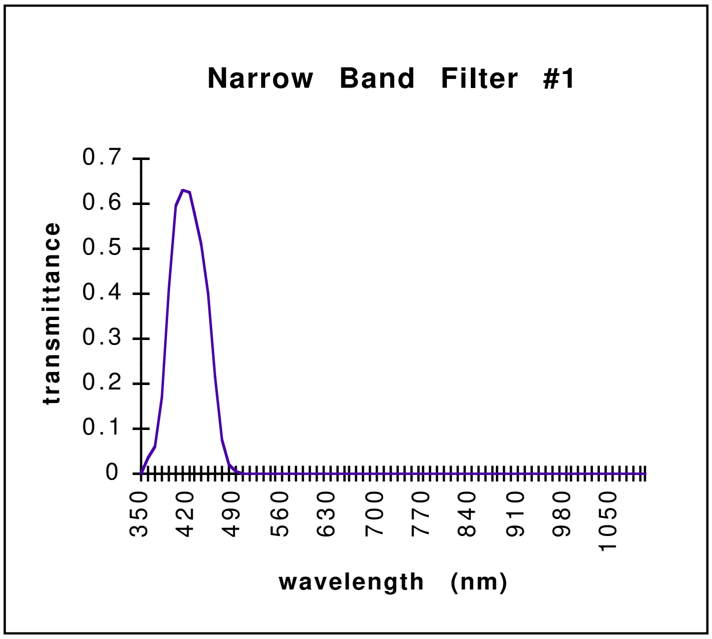

Figure 4.1.1 (Narrow Band Filter # 1 (peak 410 nm))

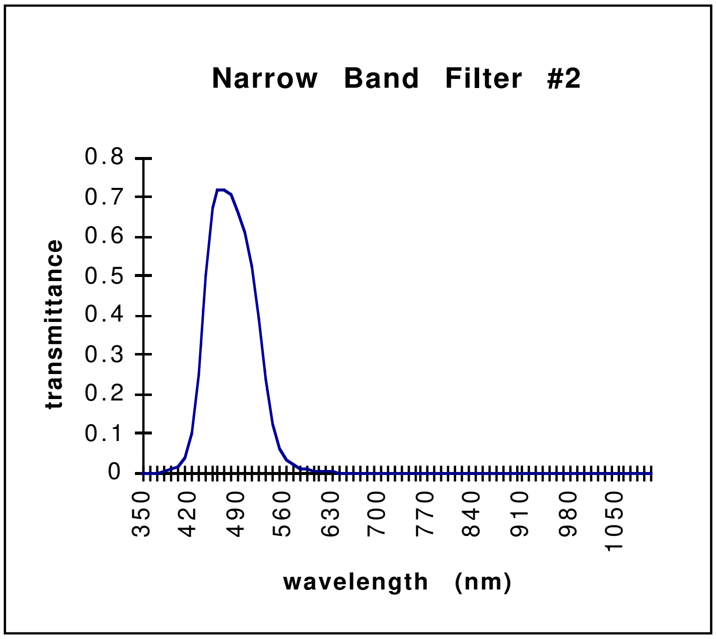

Figure 4.1.2 (Narrow Band Filter # 2 (peak 470 nm))

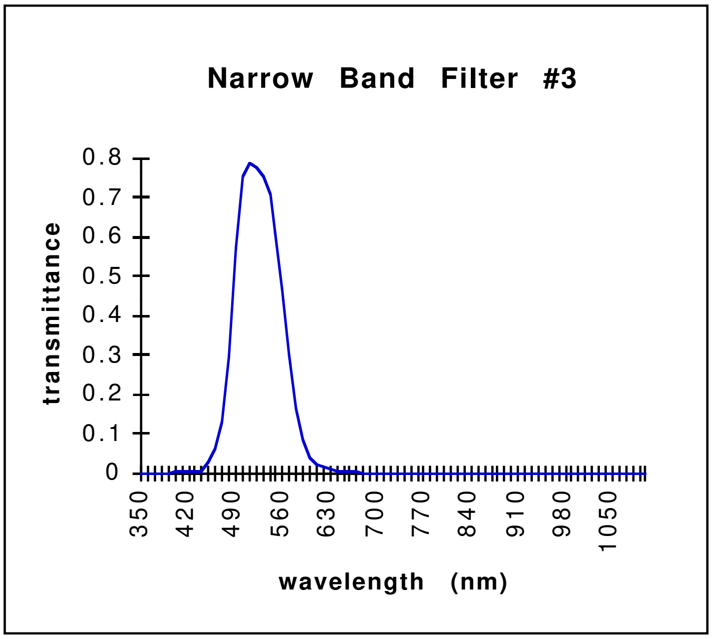

Figure 4.1.3 (Narrow Band Filter # 3 (peak 510 nm))

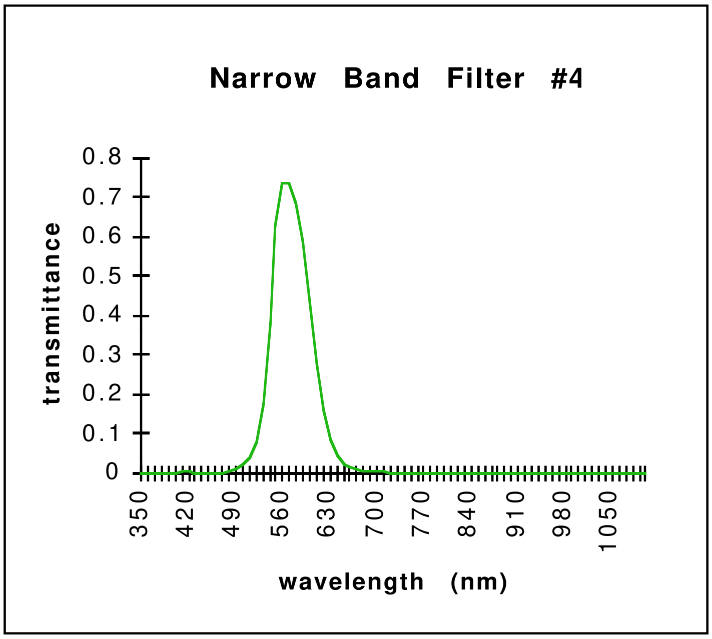

Figure 4.1.4 (Narrow Band Filter # 4 (peak 560 nm))

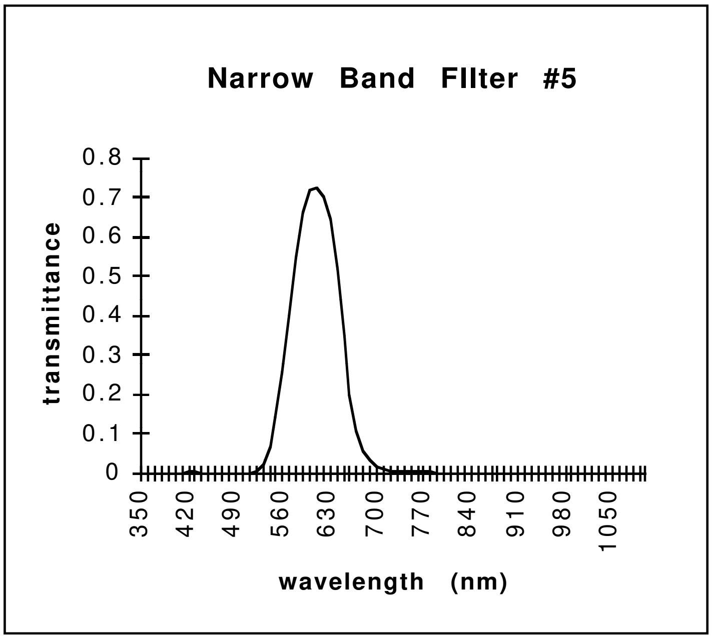

Figure 4.1.5 (Narrow Band Filter # 5 (peak 610 nm))

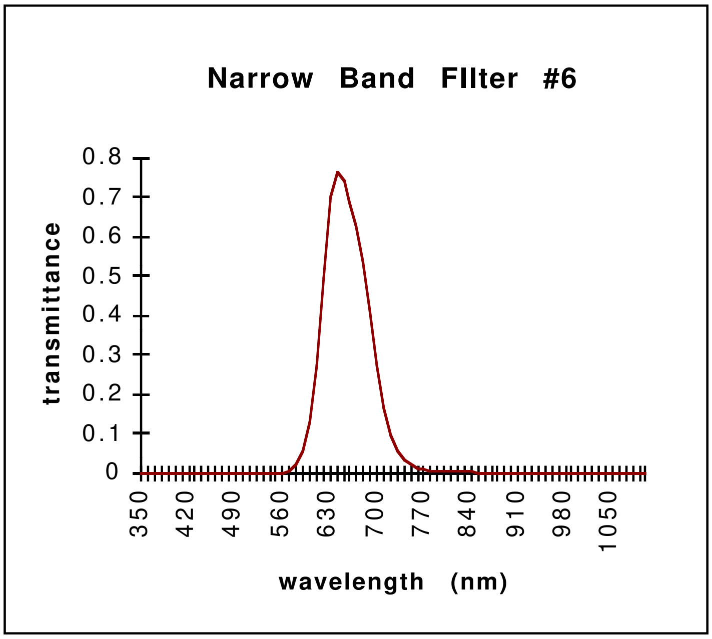

Figure 4.1.6 (Narrow Band Filter # 6 (peak 640 nm))

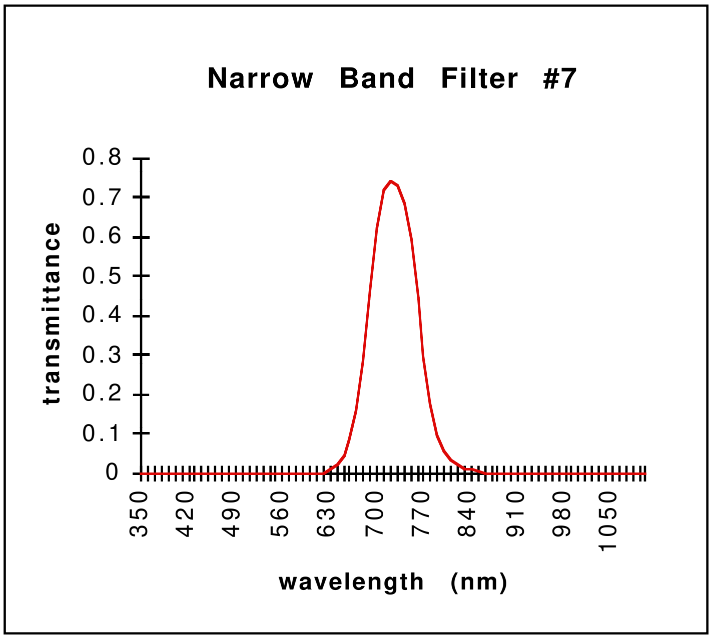

Figure 4.1.7 (Narrow Band Filter # 7 (peak 720 nm))

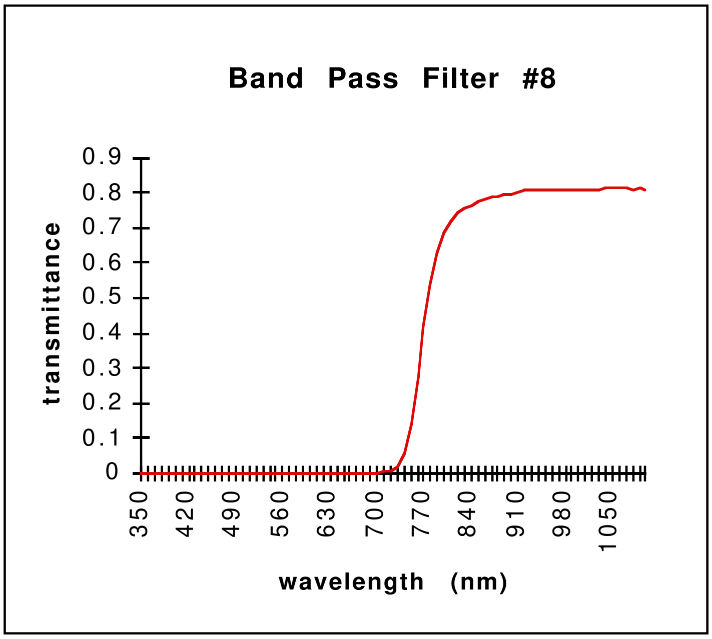

Figure 4.1.8 (Band Pass Filter # 8)

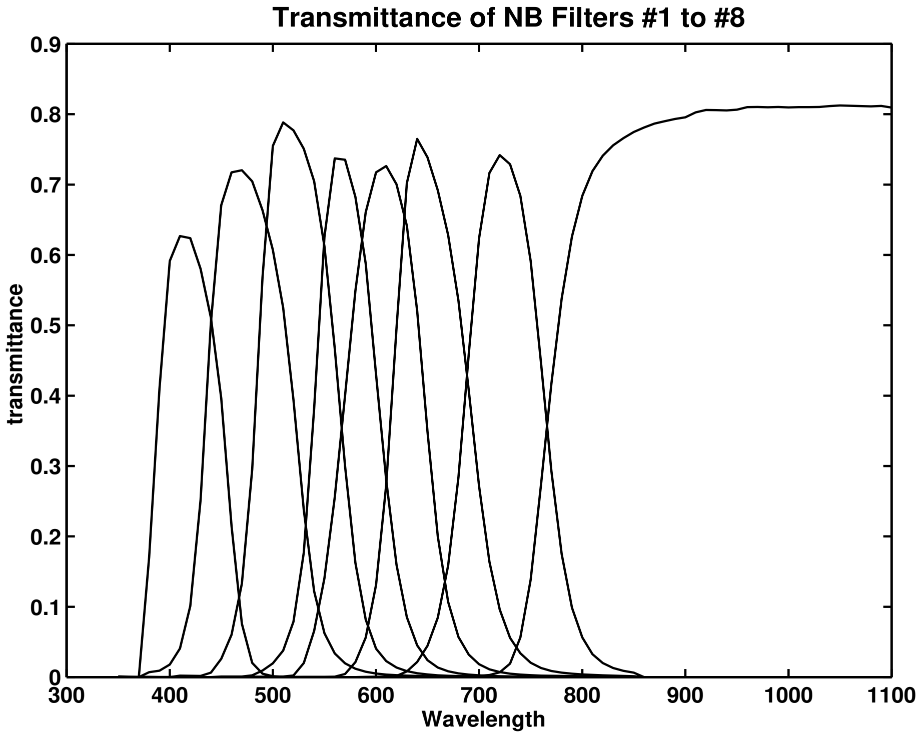

Figure 4.1.9 (Transmittance of NB Filters #1 to #8)

4.2 Neutral Density Filters

Neutral density filters were placed in front of the color filter and CCD camera lens to reduce the intensity of the incoming light, especially when a high intensity light source such as the integrating sphere was used during spectral calibration (see Setup #3 in Chapter 3). Because neutral density and color filters were highly reflective due to the metallic or chemical coating on either side of the filters, when used together the neutral density filter was placed 20 degrees off normal during an experiment with the CCD camera to avoid interreflections (see Setup #3 in Chapter 3).

The procedure for testing the transmittance of the neutral density (ND) filters was the same as for the narrow band (color) filters (*i.e.*, Setup #1 in Chapter 3). The difference between color and ND filters was that the neutral density filters were designed to uniformly attenuate an incident beam of radiation without spectrally altering the distribution. Neutral density filters are generally classified by their nominal optical densities, but measuring the actual transmittance of these filters over the spectrum range (350 nm – 1100 nm) was more appropriate for use with the CCD camera.

Filter transmittance may be expressed either as a simple % of the incident light or in terms of optical density. Optical density (OD) is defined as the negative logarithm to the base 10 of the transmittance which is the ratio of the power of the exiting beam to that of the incident beam. The transmittance, T, is

$$
\begin{aligned}
T &= \frac{I_T}{I_0} \\
\text{where} & \\
I_T &= \text{Transmitted power,} \\
I_0 &= \text{Incident power.}
\end{aligned}
$$

The optical density is then

$$\mathrm{OD} = log_{10}\frac{I_0}{I_T} = -log_{10}T$$

and it can be written as $T = 10^{-\mathrm{OD}}$.

The *nominal* optical densities of the seven neutral density filters that were tested are OD = 0.03, 0.1, 0.3, 0.5, 1.0, 2.0 and 3.0. The corresponding *nominal* percentage *transmittances* are shown in the table below:

Optical Density (nominal at 550 nm)	Percentage Transmittance (nominal at 550 nm)
0.03	93.32%
0.1	79.43%
0.3	50.12%
0.5	31.62%
1.0	10.00%
2.0	1.00%
3.0	0.1%

Neutral density filters can be stacked in series to produce higher densities. Theoretically, the total optical density of these combined neutral density filters is the sum of the individual densities.

$$\text{Total density} = \text{OD}_1 + \text{OD}_2 + \text{OD}_3 + \ldots$$

Therefore, the total transmittance of a stack of neutral density filters is the product of the transmittance of each filter.

$$\text{Total transmittance} = T_1.T_2.T_3\ldots.$$

When two filters are positioned in series with their surfaces perfectly parallel, the total transmittance can be increased due to multiple surface reflections between the filters. However, this is an undesired effect; thus a slight angle between surfaces was used to reduce the effect of the multiple surface reflections. When both color and ND filters were used with the CCD camera, the ND filters were placed 20 degrees off normal while the color filters were in their normal position, *i.e.*, they were normal to the path of the light beam. When a beam passed through a filter with an off normal angle, the traveling distance within the filter increased and the filter transmittance could decrease. On the other hand, the reflectance of the film itself could decrease at off-normal angles, thus leading to a higher value of filter transmittance. Therefore, we measured both the 20 degrees off normal transmittance and the normal transmittance. The following graphs (Figures 4.2.1-7) show the normal transmittance with solid lines and the 20 degrees transmittance with dotted lines. Appendix B tabulates the transmittance data for both normal and 20 degrees off normal orientations of the filters. When the ND filters are tilted at 20 degrees off normal, both increases and decreases in the filter transmittance are observed.

The last neutral density filter, OD = 3.0, had a lot of error in transmittance in the lower visible wavelength region. Therefore the OD = 3.0 neutral density filter was not used in the later experiments. In general, the neutral density transmittance values match the manufacturer's given (nominal) optical density values reasonably well within the visible range. For the various filters, the average *percentage* differences between the measured-normal and nominal *transmittances* are: OD = 0.03, -0.06%; OD = 0.1, -4.9%; OD = 0.3, -3.2%; OD = 0.5, +5.4%; OD = 1.0, + 1%; OD = 2.0, +10%. In the next chapter, the manufacturer's nominal optical density values are used for the linearity tests.

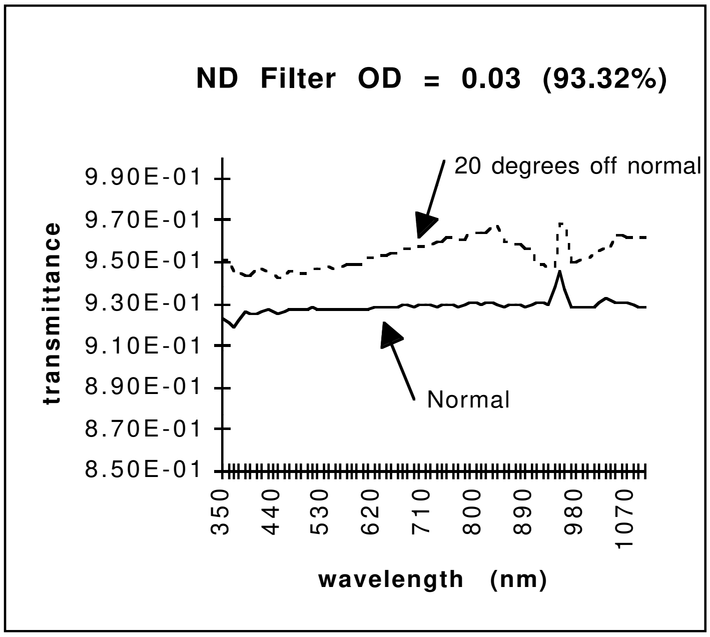

Figure 4.2.1 (OD = 0.03)

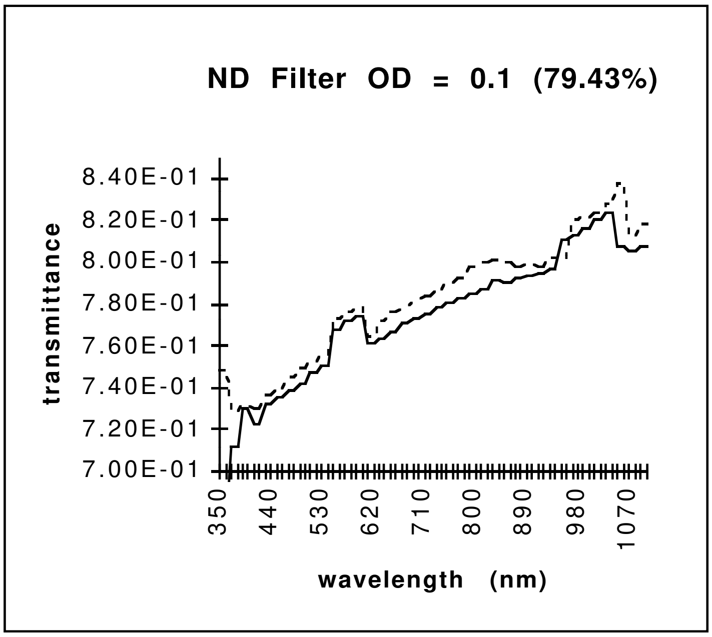

Figure 4.2.2 (OD = 0.1)

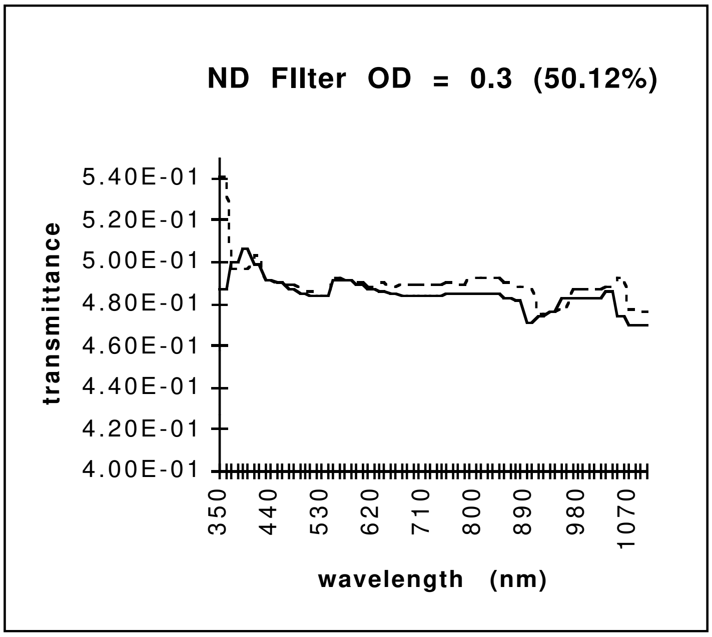

Figure 4.2.3 (OD = 0.3)

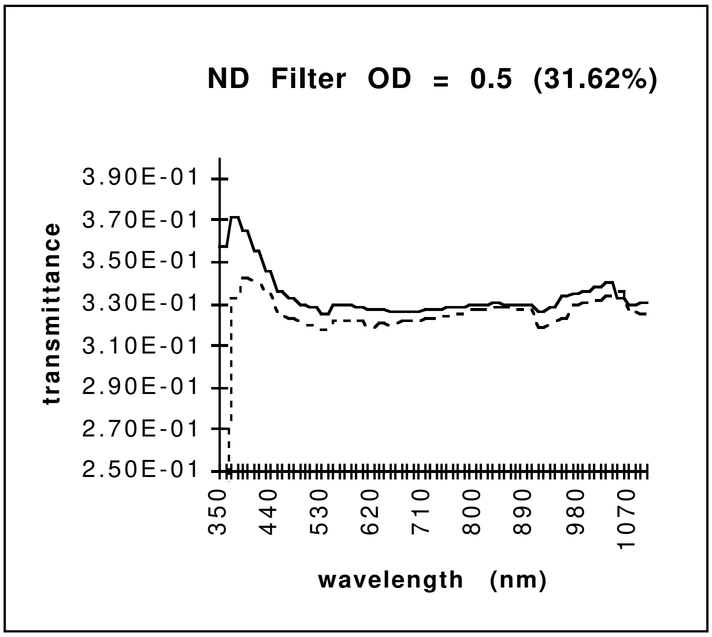

Figure 4.2.4 (OD = 0.5)

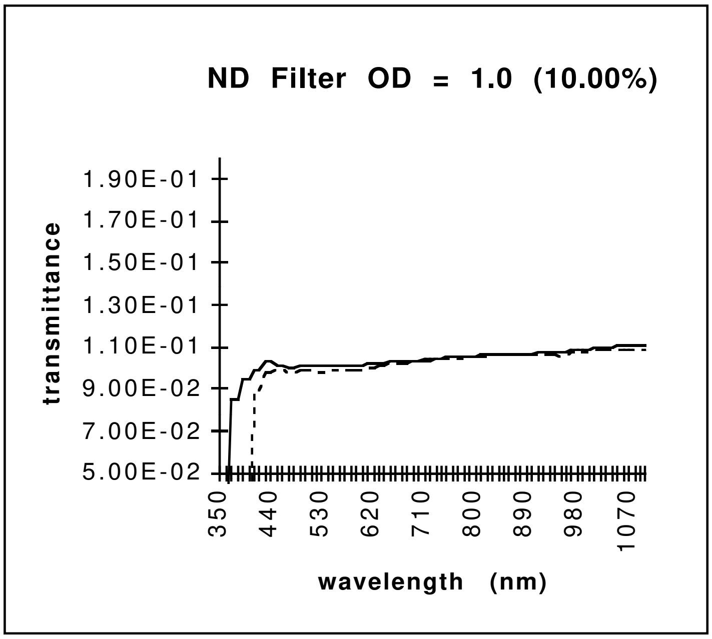

Figure 4.2.5 (OD = 1.0)

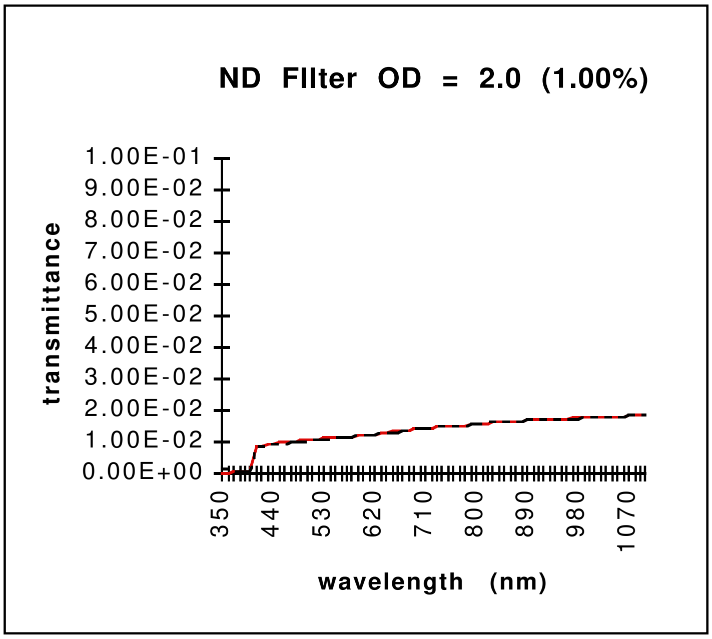

Figure 4.2.6 (OD = 2.0)

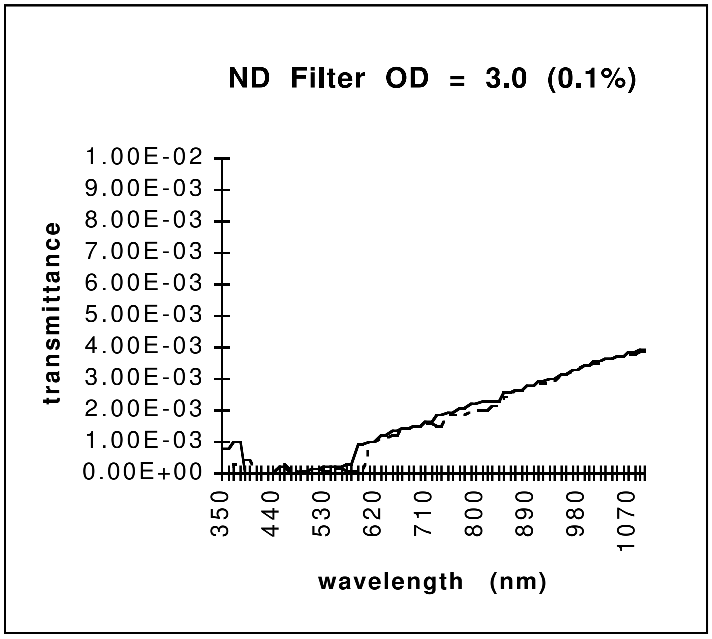

Figure 4.2.7 (OD = 3.0)

Chapter 5

CCD Camera Calibration

The calibration of the CCD camera includes a radiometric calibration and a system calibration. The former is to examine the linearity of the camera and the latter is to acquire the spectral response of the camera with respect to an incoming radiance spectrum. This chapter examines both calibration processes.

In general, the camera's radiometric and spectral calibrations depend on the wavelength spectrum of the viewed field and the camera's lens and shutter settings (*i.e.*, F-Stop, shutter speed and focal distance). This chapter considers a specific wide band light source and several narrow band, essentially monochromatic, light sources. The F-Stop, shutter speed and focal distance D (or camera position) are varied as appropriate. Unless otherwise stated, an F-Stop of F = 32 and a camera position of $D = 9.5''$ are employed.

The radiometric calibration of the camera is presented in Section 5.1, wherein the camera is shown to respond linearly to the incoming radiant energy or radiance. The spectral response calibration of the camera is described in Section 5.2, including a discussion of the mathematical inversion procedure (which uses basis functions) and a comparison with the manufacturer's published response curve. Section 5.3 provides preliminary statistical information on the performance of the 1024×1280 pixels in the CCD sensor array.

5.1 Radiometric Calibration

Before carrying out the spectral calibration of the camera, it is necessary to assure that the response of the camera varies linearly to changes in the incoming radiance. If the camera has a nonlinear response, the subsequent calibration will be very difficult. To examine the linearity response of the camera, a wide-band light source with different camera F-stops and various narrow band light sources with a constant camera F-stop were used. The general linear calibration of the camera with variations of F-stop and shutter speed is also examined.

5.1.1 Linearity Test Using Different F-Stops and a Wide Band Light Source

The first task was to study the linearity response using different camera F-stops. A constant wide-band light source (Lowel Tota 60 watts) was chosen. The setup is similar to that of Setup #2 in Chapter 3, except that the wide-band light source was substituted for the monochromator and the light source shown.

By cycling seven different neutral density filters in front of the CCD camera, the camera output signal was obtained as a function of the light energy transmitted through the filters. This procedure was repeated for 5 different F-stops. The camera responds to radiation over the 360nm to 1100nm wavelength range. Thus, an output signal represents a broadband, wavelength-integrated response over this wavelength range.

Data were taken in terms of the average pixel signal values over the CCD chip versus the manufacturer's optical density value for each filter. A proper shutter speed was chosen for each F-stop so that the average signal value of the pixels did not exceed 4095 (the value limit) when the highest transmittance filter (OD = 0.03) was used. Having maximum signal values as close to 4095 as possible meant better use of the 12 bit dynamic range of the camera. The corresponding dark current was subtracted from the signal values.

The dark current was found by shuttering the camera and measuring the signal from each pixel in the CCD array. The dark current did not increase with exposure time, as is normal for dark current. Therefore the measurement presumably represents amplifier and dark noise, which was essentially constant with time and may be regarded as a system bias. The low dark current and noise are a consequence of the low CCD chip temperature (-40^{o}C).

The following figures show the average pixel signal values as data points around a regression line. The percentage error is the average percentage difference between the data points (solid dots) and the regression line (dashed line). R-Square is the square of the Pearson product moment correlation which determines the correlation between the data and the straight regression line. An R-Square of one indicates that the data perfectly fit the straight regression line.

All the five graphs (Figures 5.1.1.1-5) indicate that the relation between signal strength and nominal transmittance is quite linear with only slight departures. This is due, in part, to the fact that two filters near the ends of the straight regression lines have nominal transmittances that are within 1% or less of their measured transmittances (*i.e.*, they are accurate ND filters). The average percentage difference between the data points and the regression line is less than 1% and the R-Square is close to 0.99. This establishes that the camera response is linear for the wide-band source over a range of F-stops. The signal values in the five tables and five graphs have no units, but may be cross compared quantitatively, since they are all proportional to radiant energy (in photons). A cross-comparison is presented in Section 5.1.3.

Neutral Density Filter	Signal
93.22% (OD = 0.03)	3883
79.43% (OD = 0.1)	3375
50.12% (OD = 0.3)	1999
31.62% (OD = 0.5)	1302
10% (OD = 1.0)	422
1% (OD = 2.0)	75
0.1% (OD = 3.0)	25
% Error	0.8128%
R-Square	0.9990

Table 5.1.1.1 (F-Stop = 22, S-Speed = 0.9 sec)

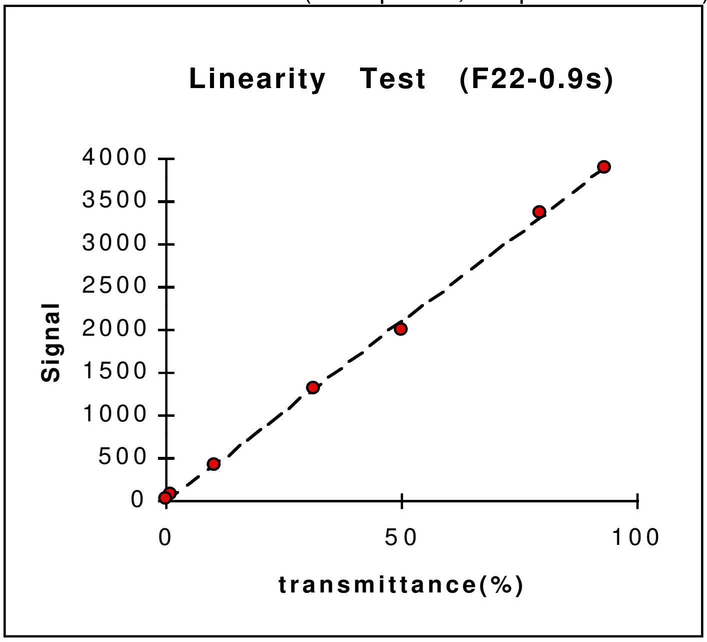

Figure 5.1.1.1 (F-Stop = 22, S-Speed = 0.9 sec)

Neutral Density Filter	Signal
93.22% (OD = 0.03)	3788
79.43% (OD = 0.1)	3293
50.12% (OD = 0.3)	1938
31.62% (OD = 0.5)	1288
10% (OD = 1.0)	417
1% (OD = 2.0)	74
0.1% (OD = 3.0)	27
% Error	0.7950%
R-Square	0.9989

Table 5.1.1.2 (F-Stop = 16, S-Speed = 0.4 sec)

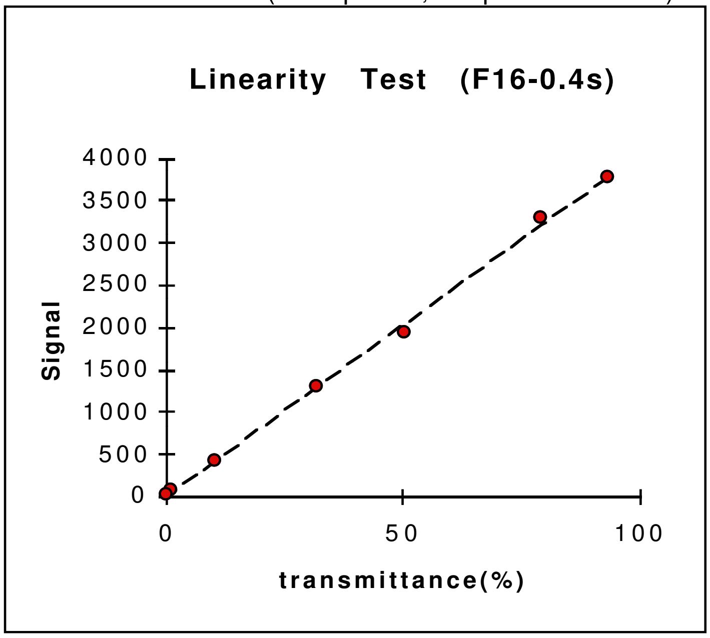

Figure 5.1.1.2 (F-Stop = 16, S-Speed = 0.4 sec)

Neutral Density Filter	Signal
93.22% (OD = 0.03)	3877
79.43% (OD = 0.1)	3376
50.12% (OD = 0.3)	1972
31.62% (OD = 0.5)	1304
10% (OD = 1.0)	434
1% (OD = 2.0)	75
0.1% (OD = 3.0)	26
% Error	0.9532%
R-Square	0.9987

Table 5.1.1.3 (F-Stop = 11, S-Speed = 0.18 sec)

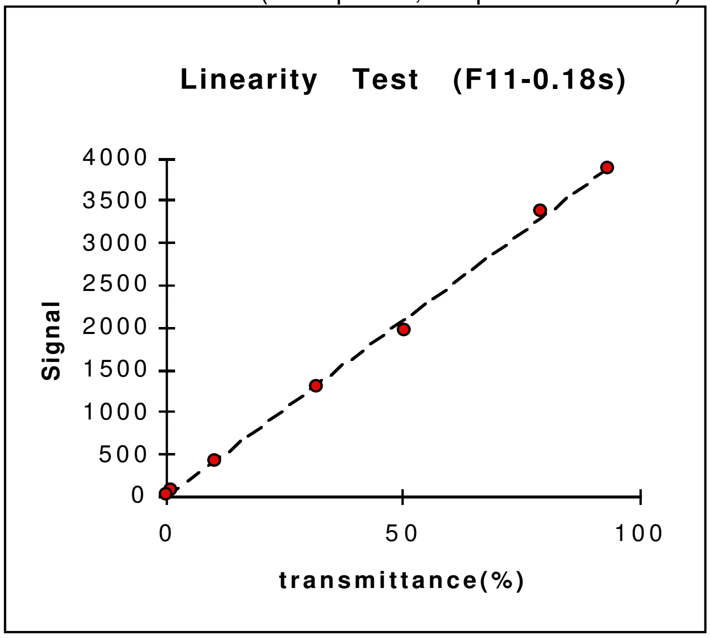

Figure 5.1.1.3 (F-Stop = 11, S-Speed = 0.18 sec)

Neutral Density Filter	Signal
93.22% (OD = 0.03)	3943
79.43% (OD = 0.1)	3426
50.12% (OD = 0.3)	2023
31.62% (OD = 0.5)	1334
10% (OD = 1.0)	436
1% (OD = 2.0)	74
0.1% (OD = 3.0)	25
% Error	0.7889%
R-Square	0.9990

Table 5.1.1.4 (F-Stop = 8, S-Speed = 0.07 sec)

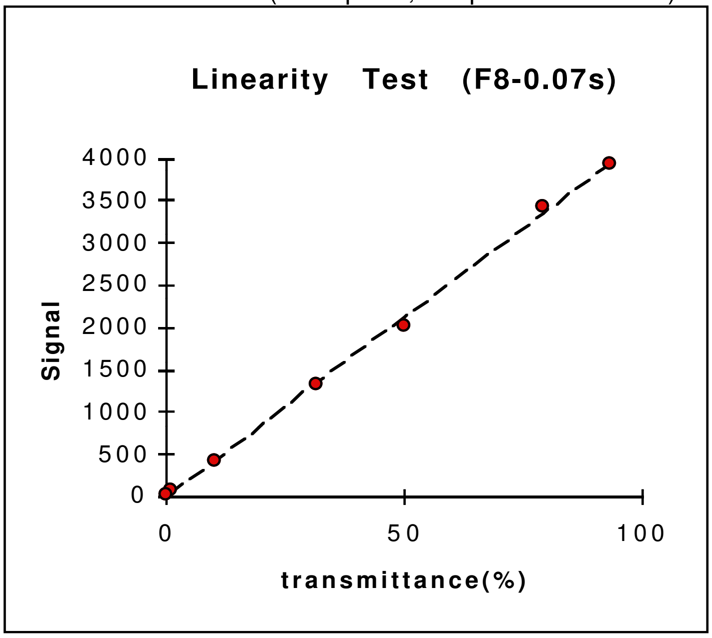

Figure 5.1.1.4 (F-Stop = 8, S-Speed = 0.07 sec)

Neutral Density Filter	Signal
93.22% (OD = 0.03)	3768
79.43% (OD = 0.1)	3248
50.12% (OD = 0.3)	1888
31.62% (OD = 0.5)	1252
10% (OD = 1.0)	412
1% (OD = 2.0)	72
0.1% (OD = 3.0)	25
% Error	1.0886%
R-Square	0.9984

Table 5.1.1.5 (F-Stop = 5.6, S-Speed = 0.015 sec)

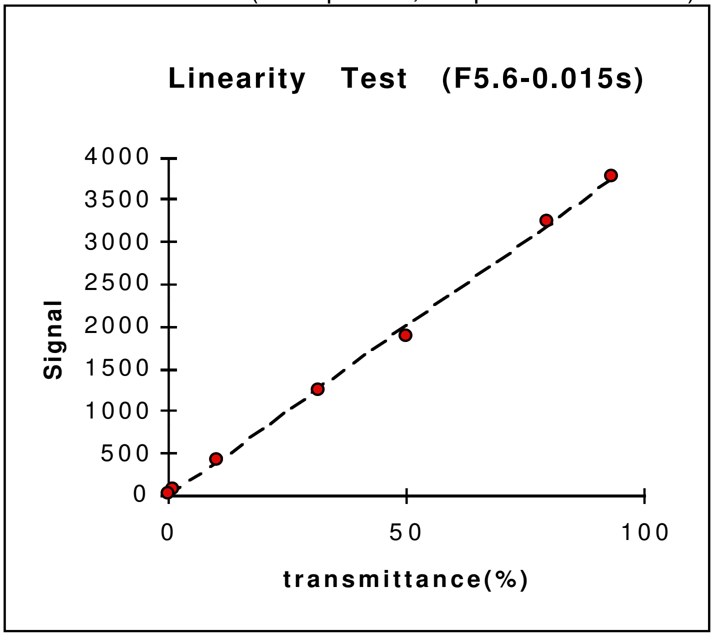

Figure 5.1.1.5 (F-Stop = 5.6, S-Speed = 0.015 sec)

5.1.2 Linearity Test Using a Fixed F-Stop and a Narrow-Band Monochromatic Light Source

Even though all seven neutral density filters have somewhat similar transmittance curves over the visible spectral region, slight errors may occur in the camera linearity check because the output of the wide-band light source (Lowel Tota 60 watts) varies spectrally and was not known. The use of a monochromatic, or narrow band, light source would provide a better test of the CCD camera's linearity.

The linearity was examined using nearly monochromatic light. Wavelengths of 600, 650, 700, 750 and 800 nm were chosen to cover the visible region. The test arrangement is shown in Setup #2 of Chapter 3. The monochromator emits a small band of wavelengths, and a half band width (HBW) resolution of 1 nm was maintained using 0.25 mm entrance and exit slits. Again, having the maximum signal value as close to 4095 as possible, when the OD = 0.03 neutral density filter was used, meant better use of the 12 bit dynamic range. This required long exposure times (*i.e.*, slow shutter speeds).

Figures 5.1.2.1 to 5.1.2.5 reveal that the relation between the signal level and transmittance is very linear for the wavelengths examined. All graphs have average percentage differences much smaller than 1% and R-Square much closer to 0.99 as compared to the previous section. Thus, the linearity of the CCD camera response with signal strength, at five specific wavelengths, was confirmed. A similar linear radiometric response of the CCD camera was established using other fixed F-stops for the camera lens.

Neutral Density Filter	Signal
93.22% (OD = 0.03)	3055
79.43% (OD = 0.1)	2602
50.12% (OD = 0.3)	1584
31.62% (OD = 0.5)	987
10% (OD = 1.0)	302
1% (OD = 2.0)	33
0.1% (OD = 3.0)	0.73
% Error	0.4164%
R-Square	0.9998

Table 5.1.2.1 (F-Stop = 32, wavelength = 600 nm)

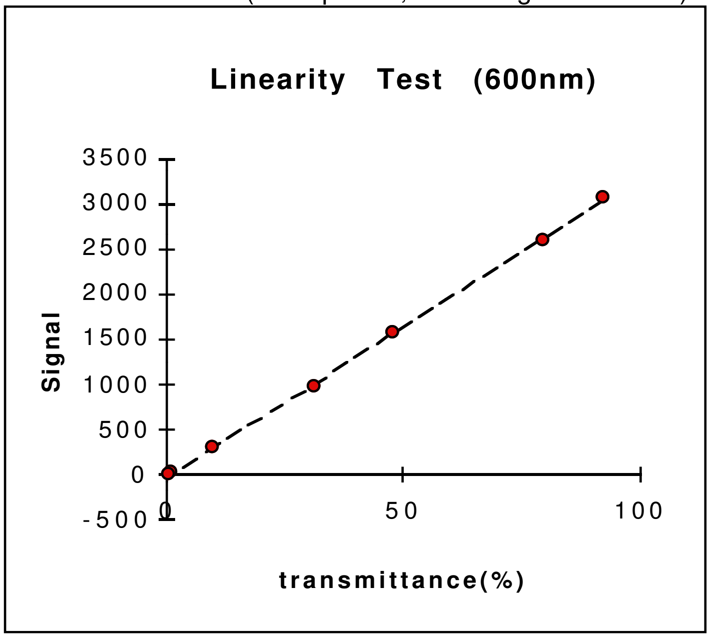

Figure 5.1.2.1 (F-Stop = 32, wavelength = 600 nm)

Neutral Density Filter	Signal
93.22% (OD = 0.03)	2921
79.43% (OD = 0.1)	2549
50.12% (OD = 0.3)	1504
31.62% (OD = 0.5)	382
10% (OD = 1.0)	307
1% (OD = 2.0)	36
0.1% (OD = 3.0)	1
% Error	0.2700%
R-Square	0.9999

Table 5.1.2.2 (F-Stop = 32, wavelength = 650 nm)

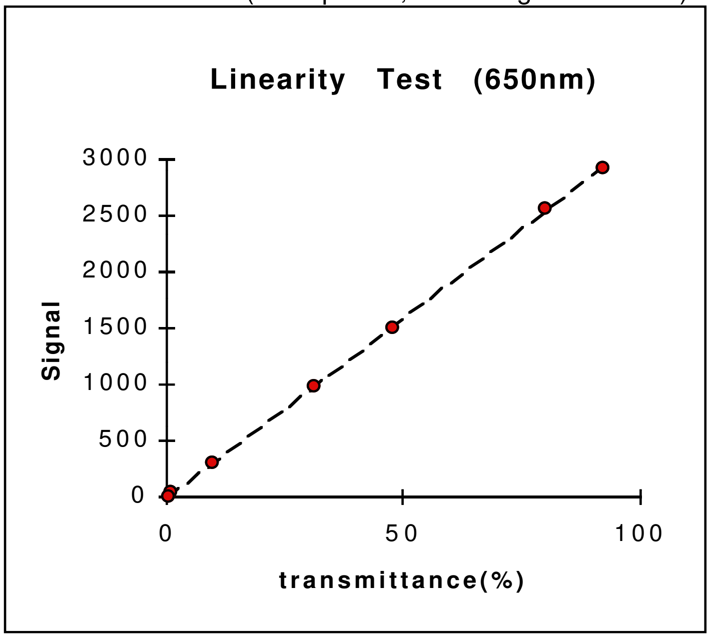

Figure 5.1.2.2 (F-Stop = 32, wavelength = 650 nm)

Neutral Density Filter	Signal
93.22% (OD = 0.03)	3029
79.43% (OD = 0.1)	2511
50.12% (OD = 0.3)	1514
31.62% (OD = 0.5)	947
10% (OD = 1.0)	299
1% (OD = 2.0)	38
0.1% (OD = 3.0)	2
% Error	0.9256%
R-Square	0.9989

Table 5.1.2.3 (F-Stop = 32, wavelength = 700 nm)

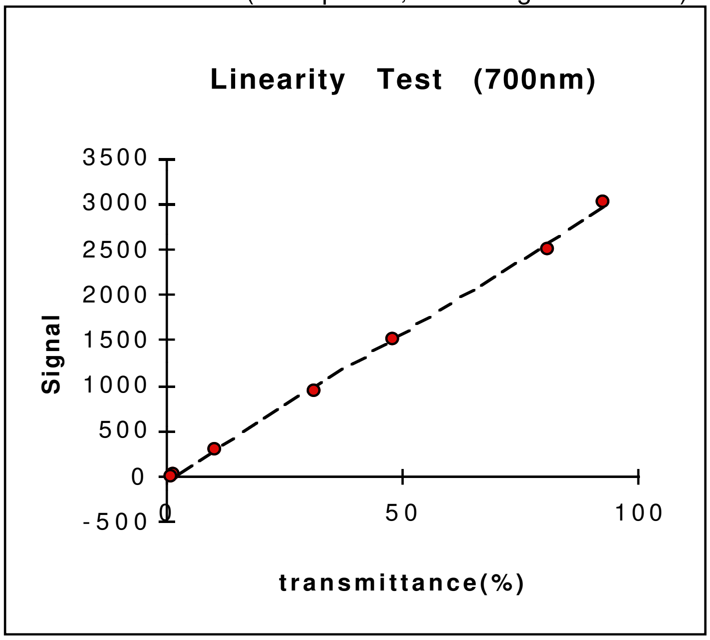

Figure 5.1.2.3 (F-Stop = 32, wavelength = 700 nm)

Neutral Density Filter	Signal
93.22% (OD = 0.03)	3117
79.43% (OD = 0.1)	2710
50.12% (OD = 0.3)	1564
31.62% (OD = 0.5)	1024
10% (OD = 1.0)	322
1% (OD = 2.0)	42
0.1% (OD = 3.0)	2.8
% Error	0.3986%
R-Square	0.9998

Table 5.1.2.4 (F-Stop = 32, wavelength = 750 nm)

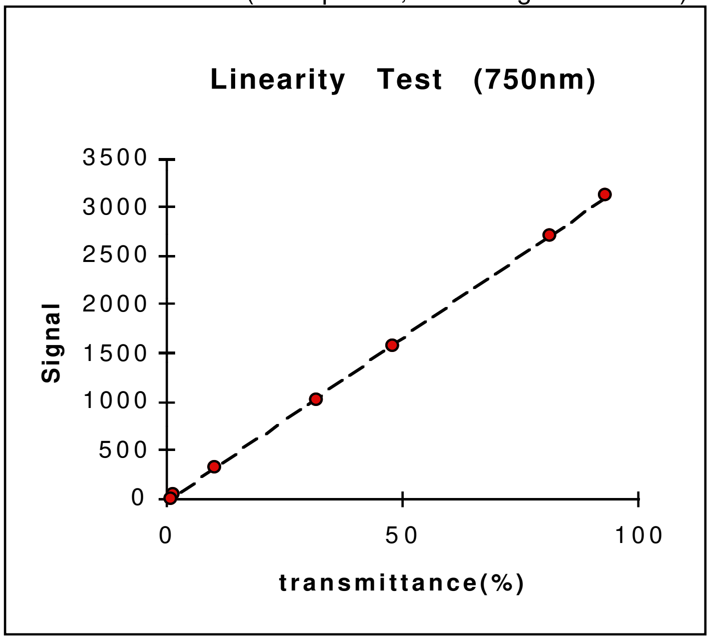

Figure 5.1.2.4 (F-Stop = 32, wavelength = 750 nm)

Neutral Density Filter	Signal
93.22% (OD = 0.03)	3269
79.43% (OD = 0.1)	2916
50.12% (OD = 0.3)	1640
31.62% (OD = 0.5)	1124
10% (OD = 1.0)	351
1% (OD = 2.0)	59
0.1% (OD = 3.0)	17
% Error	0.6406%
R-Square	0.9996

Table 5.1.2.5 (F-Stop = 32, wavelength = 800 nm)

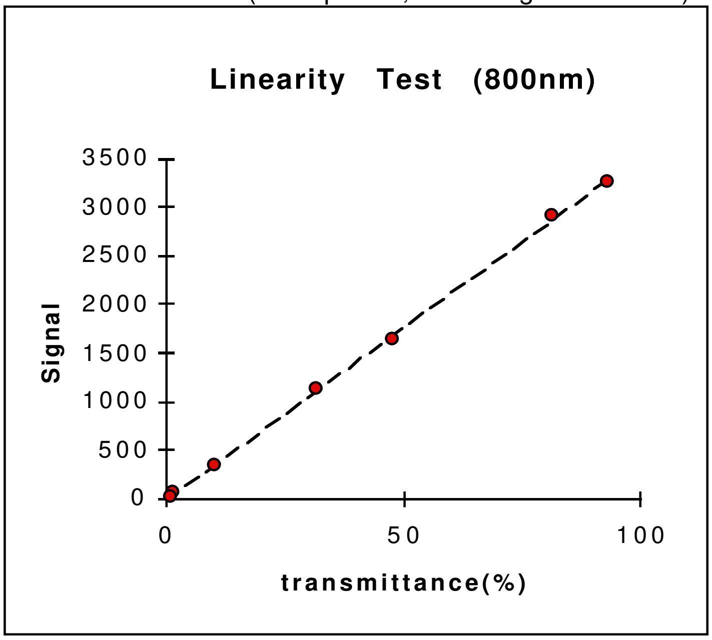

Figure 5.1.2.5 (F-Stop = 32, wavelength = 800 nm)

5.1.3 Comprehensive Linearity Tests vs. F-stop and Shutter Speed

In this section, the linearity of the camera response to incoming light from the wide band light source is established over a range of lens F-stop and camera shutter speed settings. The experimental arrangement is described in Section 5.1.1 and is similar to that shown in Setup #2 in Chapter 3.

The F-stop is set by dedents on the camera lens. The camera shutter speed is somewhat more complicated. The camera body employs a mechanical shutter, with finite delay and activation times which differ for opening and closing, but which seem to be repeatable. In addition, the CCD chip has its own electronic shutter, which activates when a bias voltage is applied to the MOS capacitors (sensors) on the chip, thus activating the capacitors. The electronic shutter is closed when the voltage is shut off. The accumulated charge (signal) of the capacitors is then read. The mechanical and electronic shutters are, in principle, controlled by the camera software, but the camera's instructions do not clearly spell this out. Instead, the user can employ delay times for the opening and closing of the mechanical shutter. It is not clear when the electronic shutter is opened with respect to these delay times. The present calibration provides some information on this.

Photons are absorbed in the silicon CCD chip and generate electrons by the photoelectric effect. These electrons are then stored in the MOS capacitors, which represent the active sensors. The signal read from the CCD chip is the accumulated charge of the capacitors, which is the photon count. The photon count is given by the following equation:

$$\text{Photon count} = C \cdot S \cdot F^{-2} \cdot T \cdot L'' \qquad (5.1)$$

where

C is a camera constant,

S is the camera shutter opening time (in seconds),

F is the F-stop setting of the lens,

T is the transmittance of the neutral density filter located between the light source and the camera lens, and

L'' is the wide-band light source power (watts/m^2) incident onto the neutral density filter.

The camera constant depends on the quantum efficiency and spectral range (roughly 360nm to 1100nm) of the CCD chip, the geometry and spectral transmittance (roughly 350nm to 900nm and beyond 1000nm) of the camera lens, and other factors. Since the signal is integrated over the response range of the chip, the coefficient C represents a wavelength-integrated value. The coefficient may be regarded as a constant in the present section.

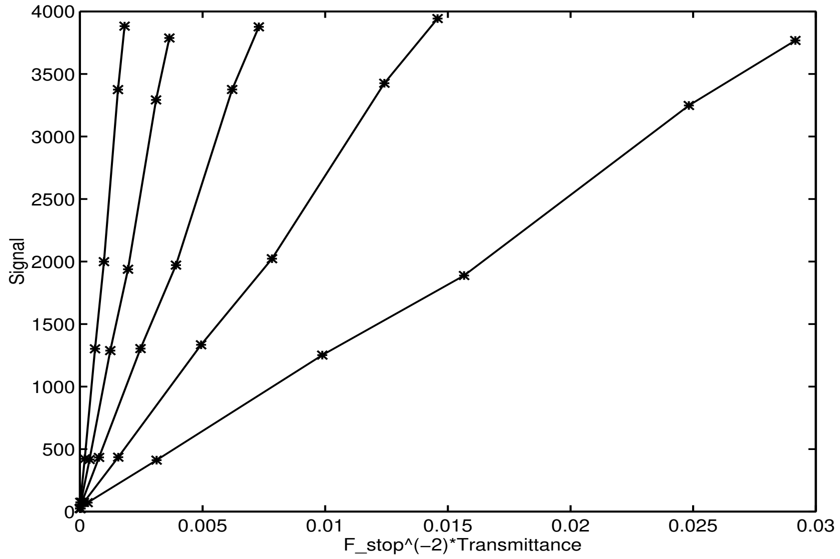

Figure 5.1.3.1 : CCD signal as a function of $F^{-2} \cdot T$.

Equation 5.1 suggests that the camera signal, or photon count, is proportional to the incident light power (L''), the neutral density filter transmittance (T), the lens-opening area ($1/F^2$), and the exposure time (S). We next convert the camera signal values reported in Figures 5.1.1.1-5 of Section 5.1.1 into the form of equation 5.1. Note that the signal values in those figures are graphed versus filter transmittance, T, with the lens (F, S) pair as the curve parameter. When graphed versus the $F^{-2} \cdot T$ product, the results are as shown in Figure 5.1.3.1 . (A graph versus $S \cdot T$ is very similar and is not shown.) Next, if we graph the results versus the product $S \cdot F^{-2} \cdot T$ we get the results shown in Figure 5.1.3.2, where error bars are shown which will be discussed later.

Clearly, there is an unexpected spread of the data in Figure 5.1.3.2 and the curves do not pass through the origin. Examination and further testing reveals that the spread is due to an offset in the shutter exposure time S. This is revealed in Figure 5.1.3.3, where the ordinate range has been expanded to show measured signals versus shutter speed S. The S-values were read as input to the controlling software for the camera. The delay times for the opening and closing of the mechanical shutter were both set to 0ms in the software control. The curves in Figure 5.1.3.3 for two different light source power settings suggest an intercept located to the left of the origin, with a value of 5ms or 11ms, depending upon whether the slope of the curves at large S or small S, respectively, is extrapolated to find the intercept. When the delays for the mechanical shutter were both changed to 10ms in the control software, results similar to Figure 5.1.3.3 were obtained, but with extrapolated intercepts of 27ms and 38ms instead of the 5ms and 11ms suggested in Figure 5.1.3.3. The difference between corresponding values is about 20ms, which is approximately

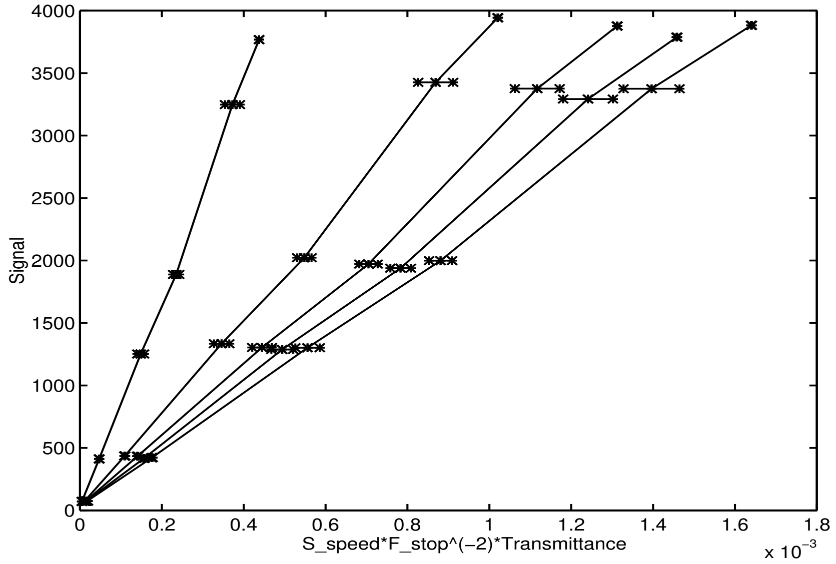

Figure 5.1.3.2 : CCD signal as a function of $S \cdot F^{-2} \cdot T$.

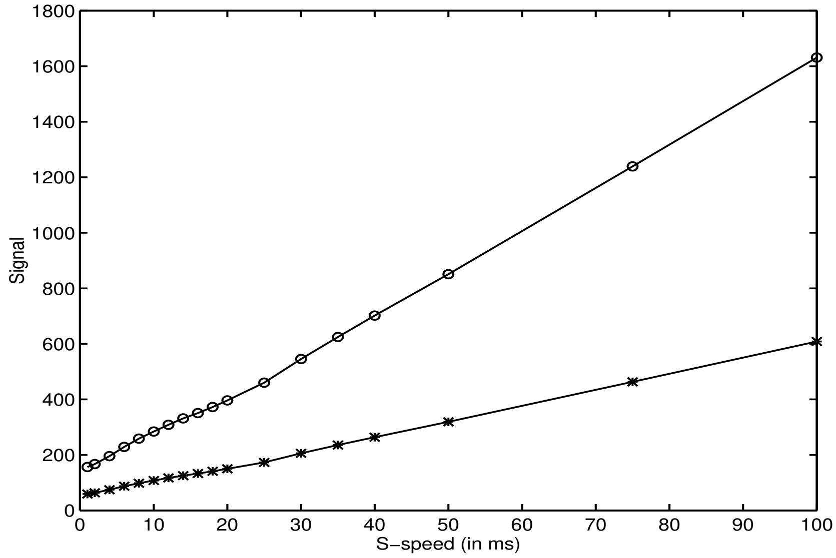

Figure 5.1.3.3 : CCD Signal as a function of Shutter speed measured with light sources of two different powers.

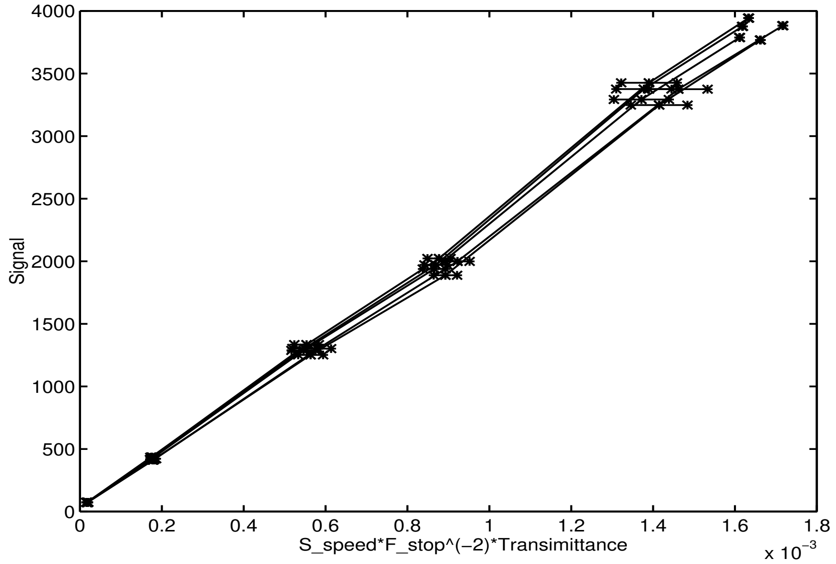

Figure 5.1.3.4 : CCD signal as a function of $S' \cdot F^{-2} \cdot T$.

the total of the front and back delay times.

For the results in Figure 5.1.3.2, the front and back delay times were 15ms and 30ms, respectively, corresponding to the recommended delay times for the camera and a total delay time of 45ms. By empirical testing, we find that an offset of 43ms will best collapse the curves in Figure 5.1.3.2. The collapsed results are shown in Figure 5.1.3.4, where the shutter speed S' in the abscissa is related to the set shutter speed S by $S' = S + 43\text{ms}$. Figure 5.1.3.4 appears to collapse the camera linearity calibration to a single curve in agreement with Equation 5.1.

From Equation 5.1 we may construct an estimate of the effect of errors in the input values on the right side of the equation. Taking the logarithm of the equation and differentiating, we obtain

$$\frac{\Delta \text{Photon count}}{\text{Photon count}} = \frac{\Delta S}{S} - 2\frac{\Delta F}{F} + \frac{\Delta T}{T}$$

where Δ denotes the error (uncertainty) in the indicated quantities. The effects of errors in the camera constant C and light source power L'' have been neglected. Using only the estimates of errors in the neutral density filter transmittances, ΔT , the error bars shown in Figures 5.1.3.2 and 5.1.3.4 are obtained. These appear sufficient to bracket the curves in Figure 5.1.3.4. These errors result because the manufacturer's *nominal* transmittance values were used in the abscissae of the figures shown, instead of weighted averages of the actual *measured* transmittances (Figures 4.2.1-7).

Although the linearity of the camera is demonstrated in Figure 5.1.3.4, the effects of camera focal distance, D, must be assessed in future work. Further work is also required to fully assess the effects of the shutter offset time, and its possible dependence on other camera parameters. After the linearity response of the camera was assured, the CCD camera response was calibrated spectrally. The spectral calibration is discussed in the following section.

5.2 Spectral Response Calibration

Basis functions are used to obtain the spectral response of the camera. This essentially means finding the camera coefficient $C(\lambda)$ in equation 5.1, or, in this section, the product $C \cdot S \cdot F^{-2}$ on the right side, where $S \cdot F^{-2}$ is held constant. The integrating sphere, which provides a wide-band light source with calibrated spectrum, a specific neutral density filter, and eight narrow band filters with known transmittance are used to do the spectral response calibration. The equipment and measurement setup is shown in Setup #3 of Chapter 3.

5.2.1 Use of Basis Functions To Obtain Average Camera Response

Because the calibrated spectrum of the Integrating Sphere has a wavelength range of 300 nm to 1100 nm, and the camera's CCD detector has a 360 nm to 1100 nm working range, the wavelength range for the camera response calibration was chosen to be 360 nm to 1100 nm.

Within this range, eight independent narrow band filters were selected to generate eight different images for computing the camera response. Since the light coming out of the Integrating Sphere had a very high spectral radiance, a neutral density filter was needed to attenuate the light source. The neutral density filters are reflective ND filters rather than absorptive ones, so the ND filter was placed at an angle of 20 degrees to avoid multiple reflections between the ND filter and the NB(narrow band) filters.

For the camera parameters, the exposure time was 0.1 second, the F-stop was 32, and the focal distance was $9.5''$. The reason for selecting such an exposure time and F-stop is that this combination limited the signal value to 4095. The use of another focal distance will be discussed later. Actually, the camera response should be calculated pixel by pixel, but here only the average data for certain Regions of Interest (ROI) are studied.

The signal value displayed on the monitor was the measured radiance which came out of the Integrating Sphere and passed through ND and NB filters. Therefore, a mathematical model could be constructed based on the equation

$$S = \int_{\lambda_1}^{\lambda_2} R_c(\lambda)\, I(\lambda)\, d\lambda$$

where

S is the signal value generated by the camera scenes and displayed on the monitor,

$R_c(\lambda)$ is the camera response,

$I(\lambda)$ is the spectral radiance of the light after passing through the ND and NB filters,

$\lambda_1 = 360$ nm and $\lambda_2 = 1100$ nm.

For numerical computation, a matrix form of the above equation was introduced. The continuous spectrum was broken into 38 intervals, 20 nm wide. However, orthogonal basis functions of the camera response had to be used to approach exact solutions of the camera response because there were 38 unknowns of the camera spectral response but only 8 equations were available due to the 8 nearly independent narrow band filters. The matrix form of the above equation was

$$[S]_8 = \left[I^t\right]_{8\times 38} \cdot [R_c]_{38}$$

where

S_i is the signal value from using the i-th NB filter after subtracting dark current measurement value for $i = 1$ to 8,

I^t_{ij} for $i = 1$ to 8 and $j = 1$ to 38, is the radiance of the jth discrete wavelength, passing through the ND filter and the ith NB filter. The jth discrete wavelength is $360 + (j-1) * 20$ nm,

R_{cj} is the camera response of the jth discrete wavelength.

The matrix $[I]$ could be formed by multiplying the diagonal matrix of spectral radiance $[SR]$ of the Integrating Sphere and the combined (ND and NB) filter transmittance matrix $[F]$.

$$\begin{aligned} [I] &= [SR]\cdot[F] \\ &= \begin{bmatrix} SR_1 & & & & \\ & \cdot & & & \\ & & SR_j & & \\ & & & \cdot & \\ & & & & SR_{38} \end{bmatrix} \cdot [f_1 \; \ldots \; f_8] \end{aligned}$$

where

SR_j is the spectral radiance of the jth discrete wavelength.

f_i is the combined ND and ith NB filter transmittance, $i = 1$ to 8.

In order to solve for the camera response, the camera response vector $[R_c]$ was assumed to be the product of an orthogonal basis function matrix $[B]$, which came from the combined filter transmittance function, and an unknown coefficient vector $[K]$, *i.e.*,

$$[R_c]_{38} = [B]_{38\times 8} \cdot [K]_8 \, .$$

The QR factorization method was used to get an orthogonal basis set. As mentioned before, orthogonal basis function matrix $[B]$ came from the combined filter transmittance function $[F]$ which has size 38×8. So the size of $[B]$ is 38×38 after QR factorization.

$$[F]_{38\times 8} \overset{\text{QR}}{=} [B]_{38\times 38} \cdot [T]_{38\times 8}$$

where $[T]_{38\times 8}$ is the upper triangular matrix produced produced by QR factorization.

Since the lower 30 rows of the matrix $[T]$ are all zeros due to the non-square characteristic of matrix $[F]$, the above equation can be rewritten as

$$[F]_{38\times 8} \overset{\text{QR}}{=} [B]_{38\times 8} \cdot [T]_{8\times 8}$$

This matrix $[B]$ with size 38 by 8 is exactly the basis function matrix used in this method. These basis function are shown in Figures 5.2.1.1 to 5.2.1.8.

From the equation

$$[S]_8 = \left[I^t\right]_{8\times 38} \cdot [R_c]_{38}$$

and

$$[R_c]_{38} = [B]_{38\times 8} \cdot [K]_8$$

the governing equation is

$$\begin{aligned} [S]_8 &= \left[I^t\right]_{8\times 38} \cdot [B]_{38\times 8} \cdot [K]_8 \\ &= [N]_{8\times 8} \cdot [K]_8 \end{aligned}$$

where, to simplify,

$$[N]_{8\times 8} = \left[I^t\right]_{8\times 38} \cdot [B]_{38\times 8}$$

Then the vector $[K]_8$ is given by

$$[K]_8 = [N]_{8\times 8}^{-1} \cdot [S]_8$$

After the coefficient vector $[K]_8$ was computed, the camera response could be found from the relationship $[R]_{38} = [B]_{38\times 8} \cdot [K]_8$ and is plotted in Figure 5.2.1.9.

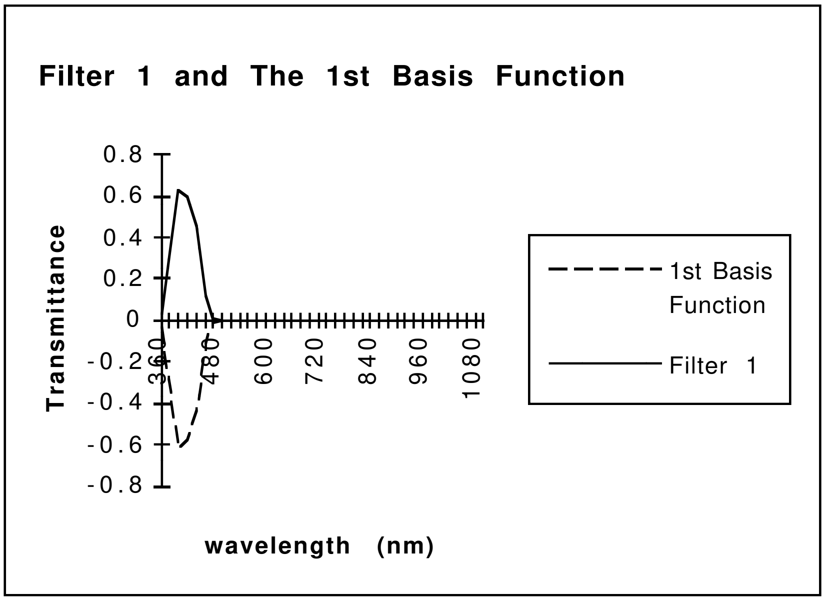

Figure 5.2.1.1 (filter 1 (peak 410 nm) with basis #1)

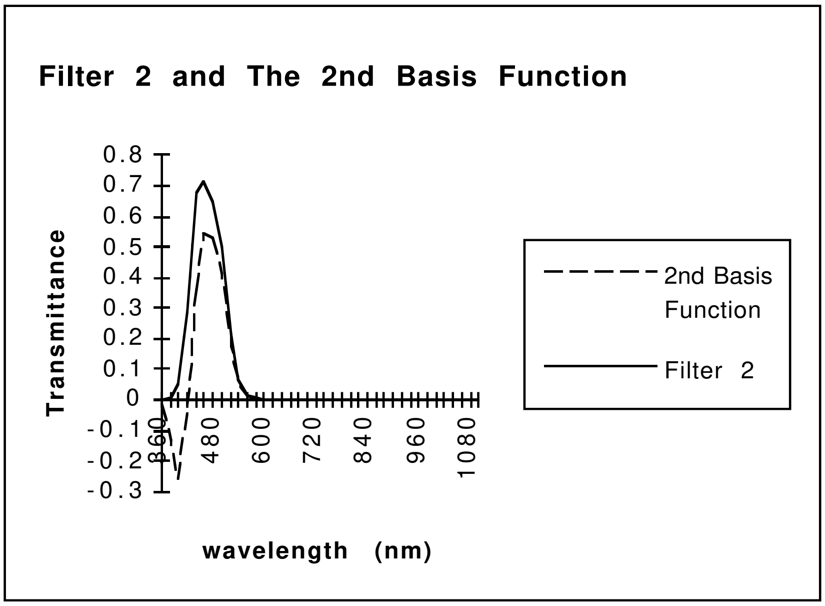

Figure 5.2.1.2 (filter 2 (peak 470 nm) with basis #2)

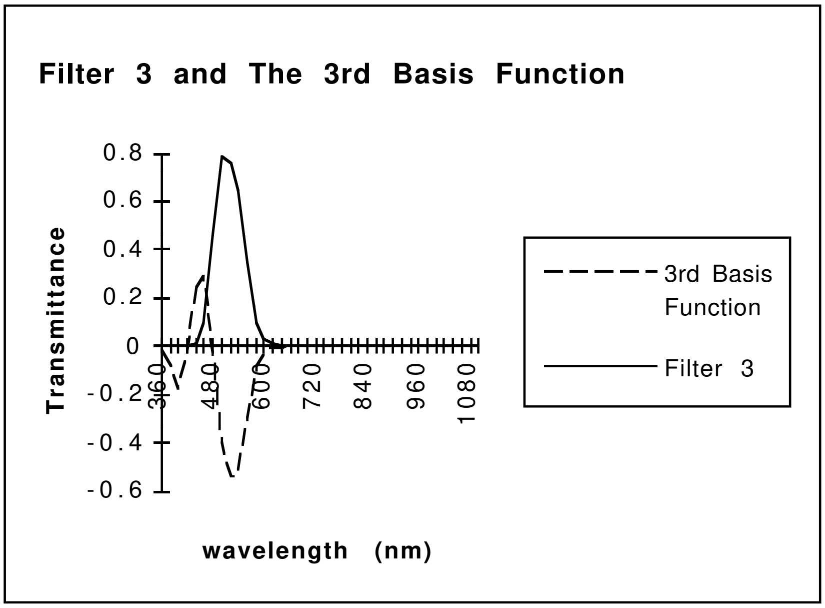

Figure 5.2.1.3 (filter 3 (peak 510 nm) with basis #3)

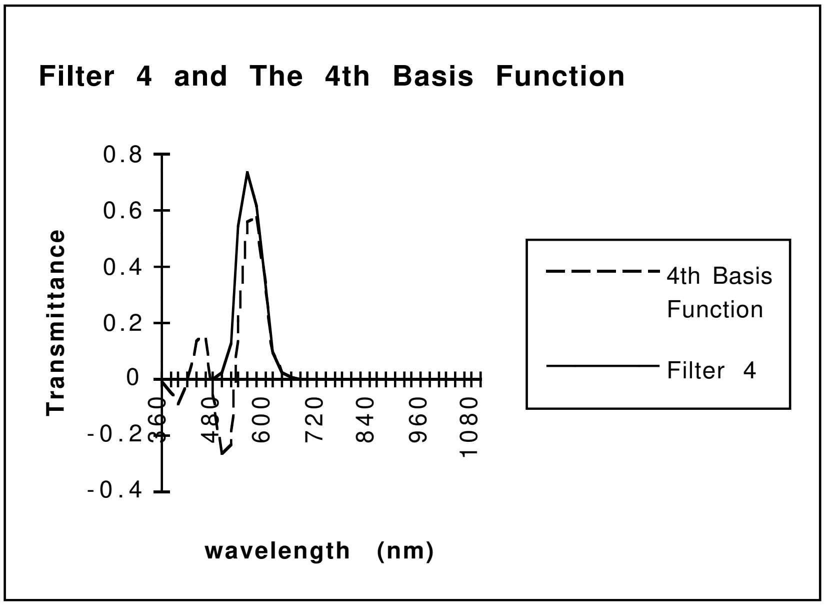

Figure 5.2.1.4 (filter 4 (peak 560 nm) with basis #4)

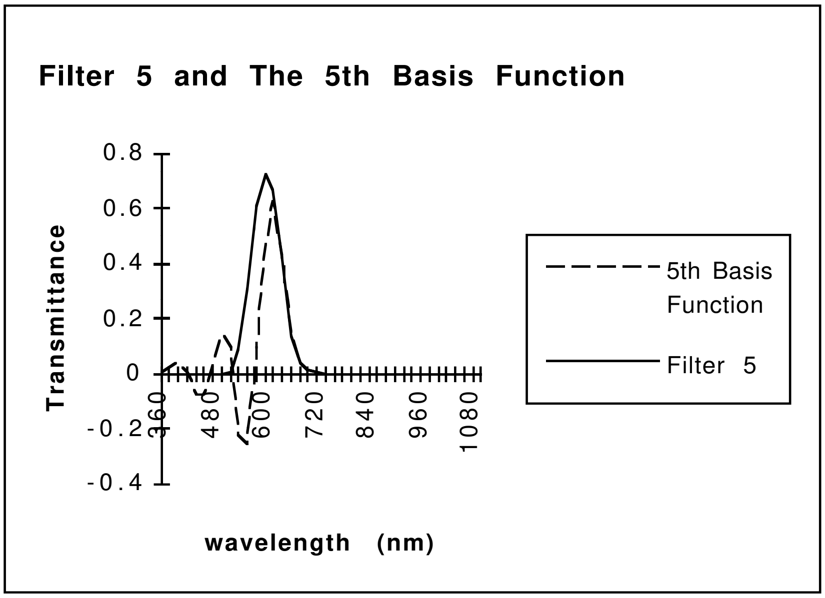

Figure 5.2.1.5 (filter 5 (peak 610 nm) with basis #5)

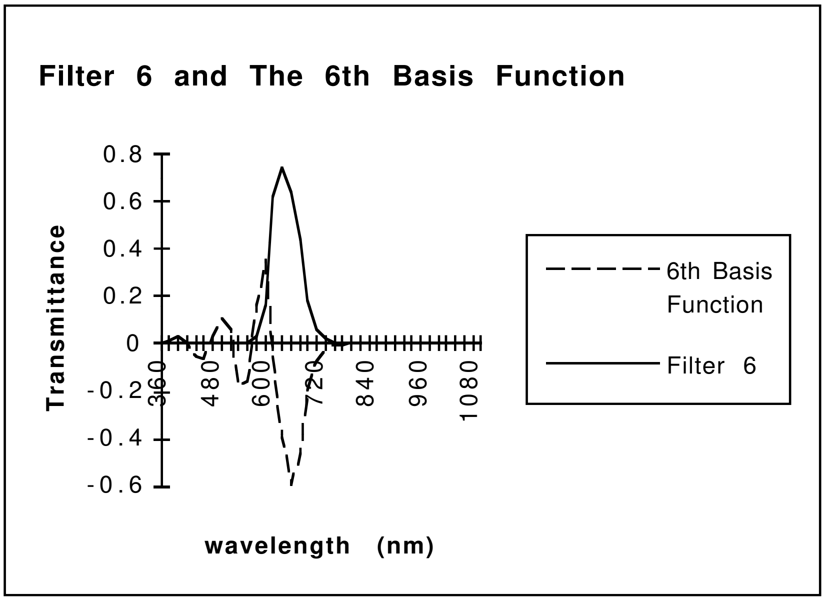

Figure 5.2.1.6 (filter 6 (peak 640 nm) with basis #6)

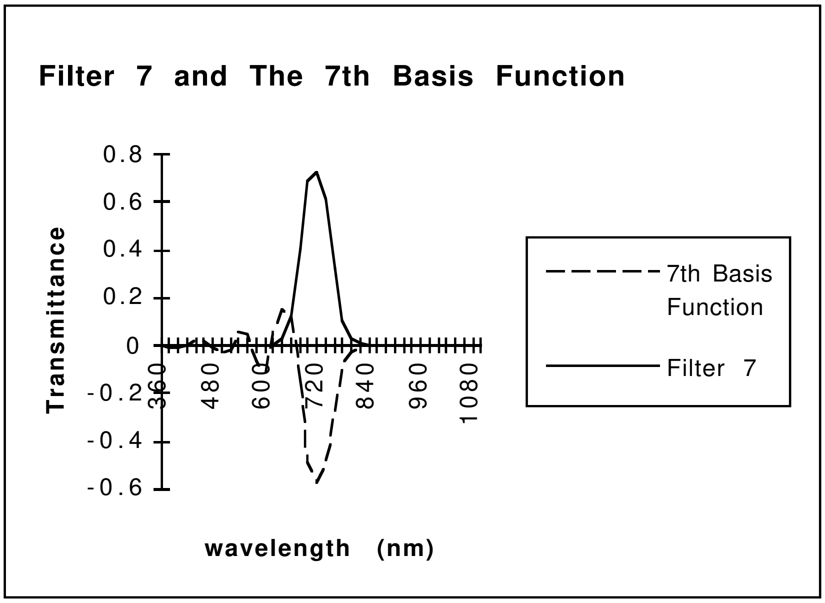

Figure 5.2.1.7 (filter 7 (peak 720 nm) with basis #7)

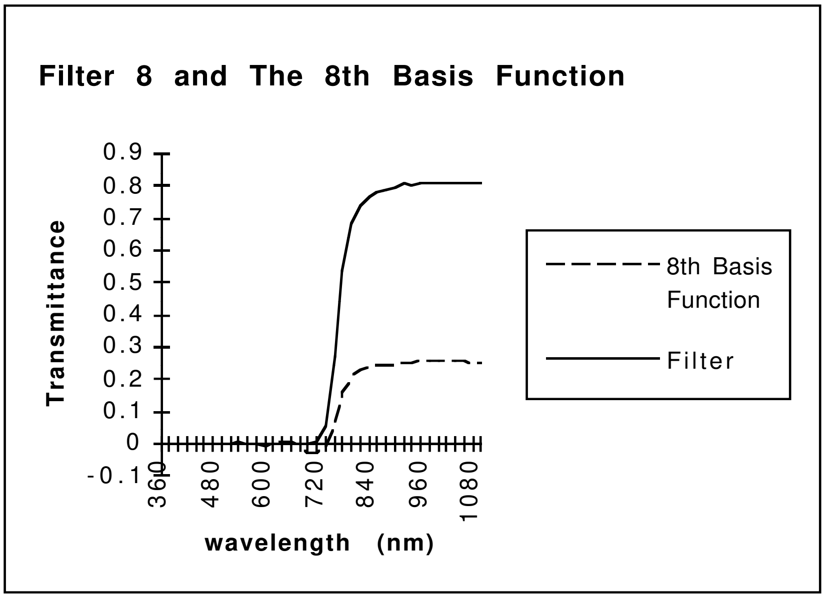

Figure 5.2.1.8 (filter 8 with basis #8)

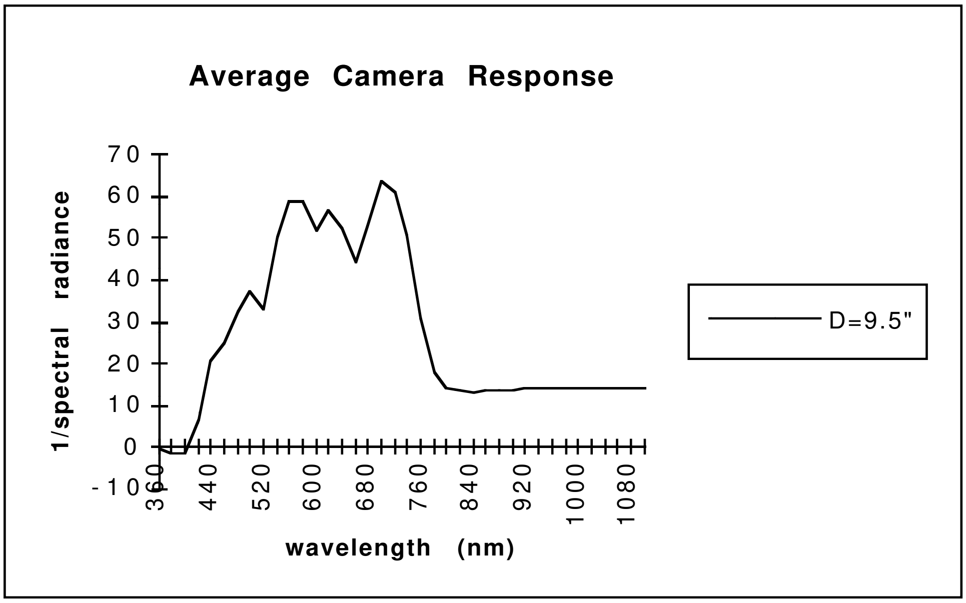

Figure 5.2.1.9 (camera response at D= 9.5”)

5.2.2 Camera Response for Different Positions of the Camera

Because the objects to be measured might have different distances to the camera, different focal distances were examined to understand whether the focal distance would change the camera response. Two focal distances of $D = 9.5''$ and $28''$ were selected. In order to improve the measurement accuracy during the experiment, five image shots were made for every filter. These were averaged. Then they were averaged over the Regions of Interest (ROI) used. The resulting grand averages for each of the eight filters were used to obtain the camera response calibration.

For a focal distance of $D = 9.5''$, the whole image of the exit port of the integrating sphere filled the active CCD port of the camera, so the ROI was the whole frame of the image. The corresponding average camera response is shown in Figure 5.2.1.9.

For a focal distance of $D = 28''$, the image of the exit port of the Integrating Sphere was so small that about 16 pictures would have been required to completely fill the CCD image frame of the camera. Instead, 4 representative ROI positions were selected. The image frame was divided into four quadrants (upper left, upper right, lower left, lower right). In the center of each quadrant, an ROI was placed of area equal to one-fourth of the quadrant area. Thus, there were 4 different ROI positions: upper left, upper right, lower left, and lower right, with each ROI having an area equal to one-sixteenth of the area of the total CCD image frame. The camera responses obtained by averaging over each of these ROIs are shown in Figure 5.2.2.1.

Since the 4 camera responses in Figure 5.2.2.1 are very similar, we use their average to represent the camera response for all, or any subset, of sensors in an image taken at a focal distance of $28''$. This is an important assumption when using a small light source. For example, when using the monochromator as a light source, the image of the monochromator's exit slit only appears as a small ROI on the image frame of the camera.

Once the camera response for each focal distance was found, they were plotted together in Figure 5.2.2.2 for comparison. The figure also shows the manufacturer's published response curve for the CCD chip KAF1300L [13] as a solid line. This is a quantum efficiency curve for the CCD chip, uncorrected for the CCD camera lens transmittance or for actual energy (*i.e.* energy $= \frac{h\mathcal{C}}{\lambda}$ where h is Plank's constant, $\mathcal{C}$ is the speed of light and λ is the wavelength).

The KAF 1300L response curve in Figure 5.2.2.2 was arbitrarily scaled vertically to fit into the figure. Within the visible range, all three curves have similar shapes. However, the use of the basis function approach contributes to differences between the calculated camera response curves and the manufacturer's CCD chip response curve. In particular, the filters provide no spectral resolution beyond about 800 nm, where an almost uniform-transmittance long pass filter was used (see Figure 4.1.8). Thus, the calculated camera response curves beyond 800 nm provide only an estimate of the *average* of the true camera response. The infrared cutoff of the camera lens also may contribute to the differences.

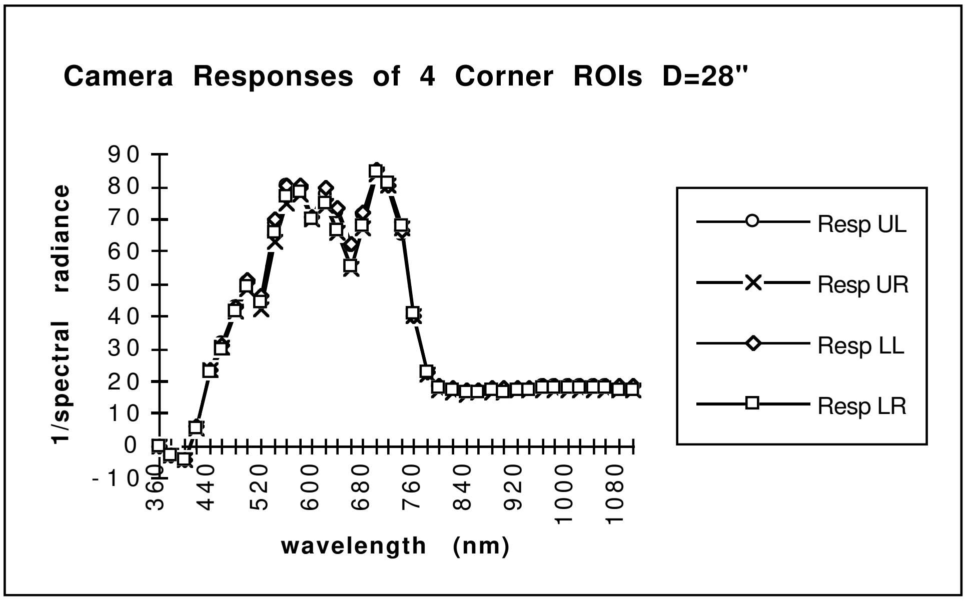

Figure 5.2.2.1 (D=28”, camera response for four corner shots)

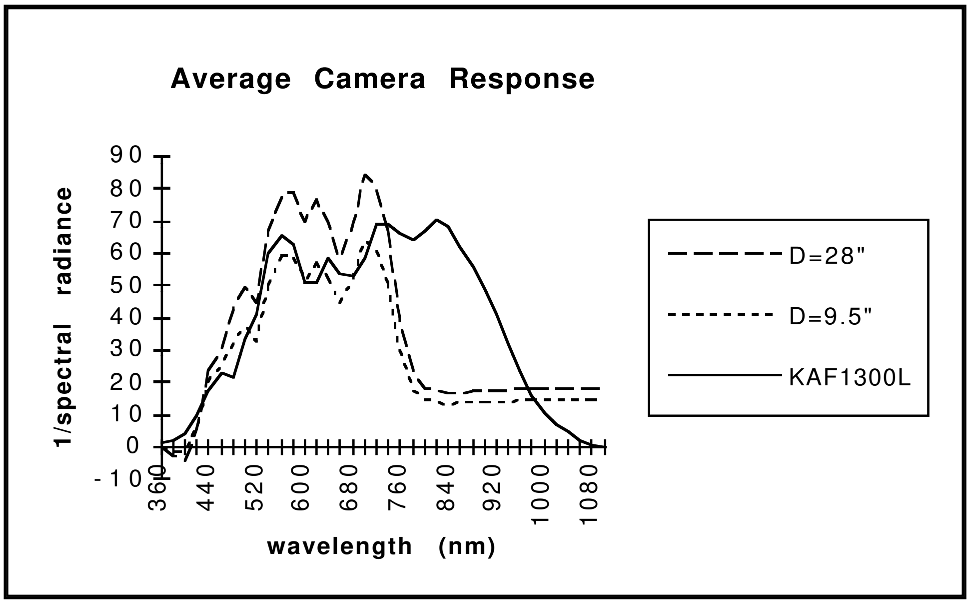

Figure 5.2.2.2

From Figure 5.2.2.2, the two calculated camera responses have the same shape but different amplitudes. The camera response at $D = 28''$ has a higher gain than at $D = 9.5''$. In an ideal case, assuming that all of the CCD sensors in the 2D array have uniform response, the responses calculated above should, in theory, be identical. However, the responses have been averaged over different sensors (*i.e.*, different ROIs). Furthermore, there may be significant differences in defining the receiving solid angles of the camera for $D = 28''$ and $9.5''$; the ratios between the receiving aperture of the camera, the radiating area, and the distance between the camera and the source, are different. Therefore, the camera response depends on focal distance, and this must be factored in when using the camera as a radiometer. When factored in, source spectra can be recreated radiometrically. This is demonstrated in Section 6.1.2.

5.3 Pixel Response Variation

In order to make sure all sensors, or pixels, are normal and transform the radiance to signals well, all the 1024×1280 pixels of an image were examined. Because the Integrating Sphere emits very uniform radiance out of the exit port, it is a proper tool for examining the pixel response variation. The wide-band source light was used, and a picture was taken by using a ND filter (OD = 0.1) and the 8th or long-pass NB filter. A camera distance of $9.5''$ was used. The measurement setup is shown in Setup #3 of Chapter 3. Because the whole image was covered by a presumed constant light source, all the pixels should have the same values. The histogram of pixel responses for this image is shown in Figure 5.3.1 to display the pixel variation.

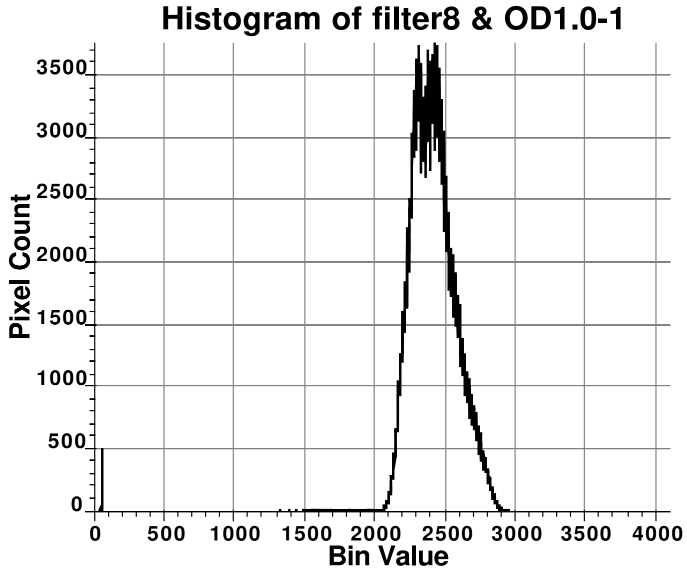

Figure 5.3.1

Figure 5.3.1 shows that most pixels had a signal value between 2100 and 2900. However, 1024 pixels have unusual signal values around 50. These extra-low-value pixels are located in the first left column of pixels in an image, and this situation happened in every image acquired. These pixels may be shadowed or somehow shielded by the optical system, or may be electronically shorted. Therefore, when doing pixel by pixel calibration, these pixels would not give reasonable camera response, and this effect needs to be considered when using the camera.

For a more quantitative analysis of the pixel variation, the average signal value of the a whole image was calculated and the numbers of pixels with more than 5%, 10% and 15% deviation from the average value were counted. Table 5.3.1 shows the distribution of the signal values.

	Number of counts
5% below mean	296,919
5% above mean	280,114
10% below mean	41,297
10% above mean	101,536
20% below mean	2,187
20% above mean	109

Table 5.3.1

Since there is a total of 1024×1280 pixels in a whole image, it may be concluded from Table 5.3.1 that 0.2% and 0.01% of the total pixels are lower and higher than the 20% deviation of the average signal value, 3.1% and 7.7% of the total pixels are lower and higher than the 10% deviation of the average signal value, and 22.6% and 21.4% of the total pixels are lower and higher than the 5% deviation of the average signal value.

The reasons for the existence of the statistical spread of pixel values might be flaws of the CCD chip for those pixels with lower or higher signal values, *i.e.*, variance due to manufacturing, and the possible reflection of environmental radiation into the image by the filters for some pixels with higher signal values. Unfortunately, although the ND filter was set at an angle of 20 degrees to avoid reflections between filters, some reflection errors, and possible ambient reflections, still existed.

Chapter 6

Spectrum Recreation and Sensitivity Analysis

In this chapter, we describe a method for the spectral recreation of a wide-band light source using the camera response function found in Chapter 5. We also verify the method by recreating narrow band light sources generated by a monochromator. The recreated wide-band and narrow band spectra using different discrete intervals are studied in Sections 6.2 and 6.3. The signal value sensitivity and an error analysis are discussed in Section 6.4.

6.1 Wide Band Light Source Recreation

Since the camera response function had already been found, the first thing for examining the accuracy of the camera responses was to recreate the wide-band light source to see if the recreated spectrum could effectively represent the light source. Recreations were also carried out for different regions of interest (ROI) on the CCD chip and for different focal distances. The experimental arrangement is shown in Setup #3 of Chapter 3.

6.1.1 Use of Basis Functions to Recreate a Wide Band Light Source Spectrum

The method of recreation is similar to the method of computing the camera response. First of all, the discrete forms of the 8 total response function R_{mi}'s were used to form a 38×8 matrix, $[R_m]_{38\times 8}$. (Total response function was the product of combined ND and i-th NB filter transmittance function and the camera response function. Discretization was done at 20 nm intervals in the wavelength range 360 nm to 1100 nm.) The basis function matrix $[O]$ for spectrum recreation was extracted from $[R_m]_{38\times 8}$ by using QR factorization method. $[O]_{38\times 8}$ contained 8 basis functions, each at 38 wavelength intervals. Note that the basis functions in $[O]$ are different from the basis functions used in camera response calibration. The difference is due to the fact that the basis functions for camera response computation were derived from the eight narrow-band filter functions only, whereas the basis functions used here are derived from the product of the eight narrow band filter functions with the camera response function. Figures 6.1.1.1 to 6.1.1.8 show the resulting basis functions $[O]$.

Like the procedure for the camera calibration, the unknown spectrum $[I_R]_{38}$ was expressed as a linear combination of the basis functions. Since the governing equation of the spectrum recreation is :

$$[S_m]_8 = \left[R^t_m\right]_{8\times 38} \cdot [I_R]_{38}$$

where

$S_{m\,i}$ is the signal value from using the ith NB filter after subtracting dark current measurement value, $i = 1$ to 8,

$R^t_{m\,ij}$ is the total response of the camera at j-th discrete wavelength and i-th NB filter in combination with a ND filter of OD = 1. The jth discrete wavelength is $360 + (j-1) * 20$ nm for $j = 1$ to 38.

I_{Rj} is the unknown radiance at the jth discrete wavelength.

Using the expression for $[I_R]$ in terms of the basis functions in $[O]$:

$$[I_R]_{38} = [O]_{38\times 8} \cdot [C]_8$$

where $[C]_8$ is a coefficient vector. The governing equation can be rewritten as:

$$\begin{aligned} [S_m]_8 &= \left[R^t_m\right]_{8\times 38} \cdot [O]_{38\times 8} \cdot [C]_8 \\ &= [M]_{8\times 8} \cdot [C]_8 \end{aligned}$$

where, for convenience,

$$[M]_{8\times 8} = \left[R^t_m\right]_{8\times 38} \cdot [O]_{38\times 8}\,.$$

Therefore, the coefficient vector $[C]_8$ is given by

$$[C]_8 = [M]^{-1}_{8\times 8} \cdot [S_m]_8$$

and a recreated spectrum $[I_R]$ is computed from the expression

$$[I_R]_{38} = [O]_{38\times 8} \cdot [C]_8\,.$$

For a focal distance of $D = 9.5''$, the wide-band radiance spectrum from the integrating sphere light source is recreated using this method and is shown in Figure 6.1.1.9 along with the spectral radiance of the integrating sphere (SR).

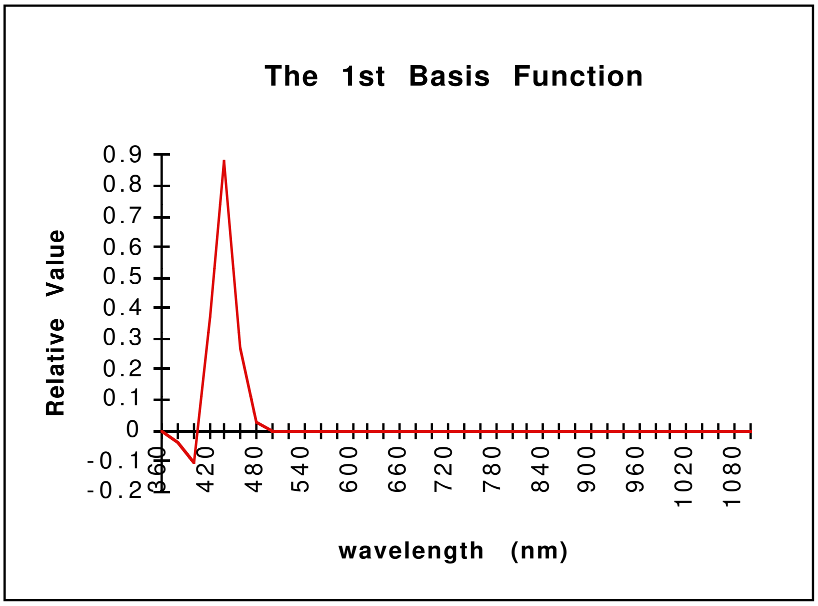

Figure 6.1.1.1 (Basis function #1 for recreation)

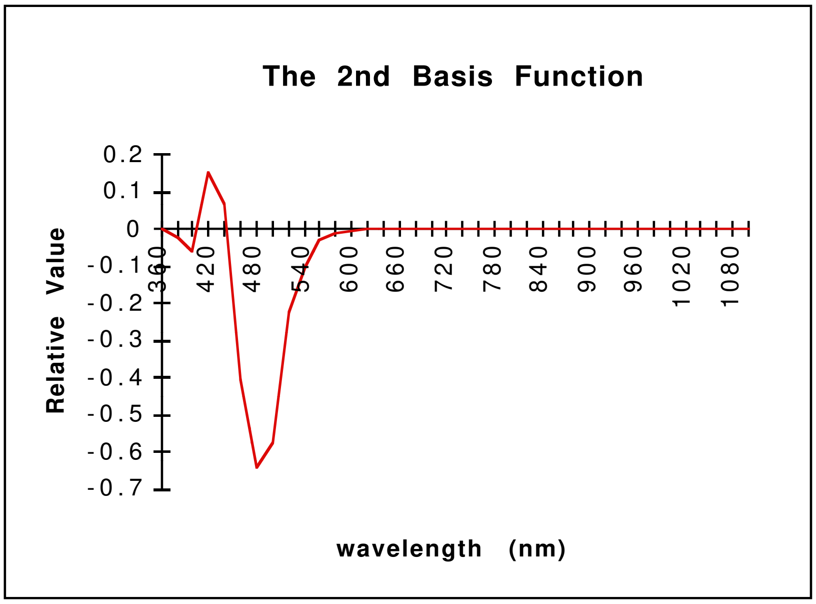

Figure 6.1.1.2 (Basis function #2 for recreation)

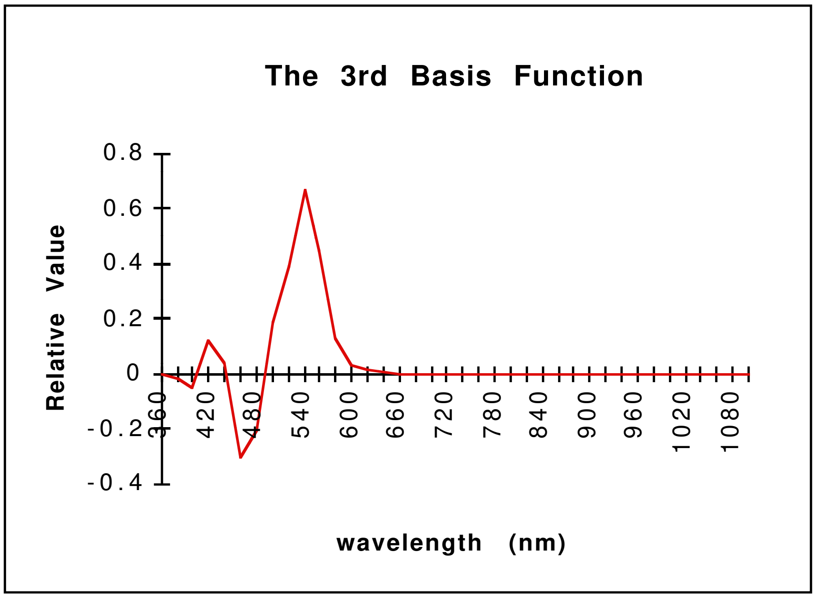

Figure 6.1.1.3 (Basis function #3 for recreation)

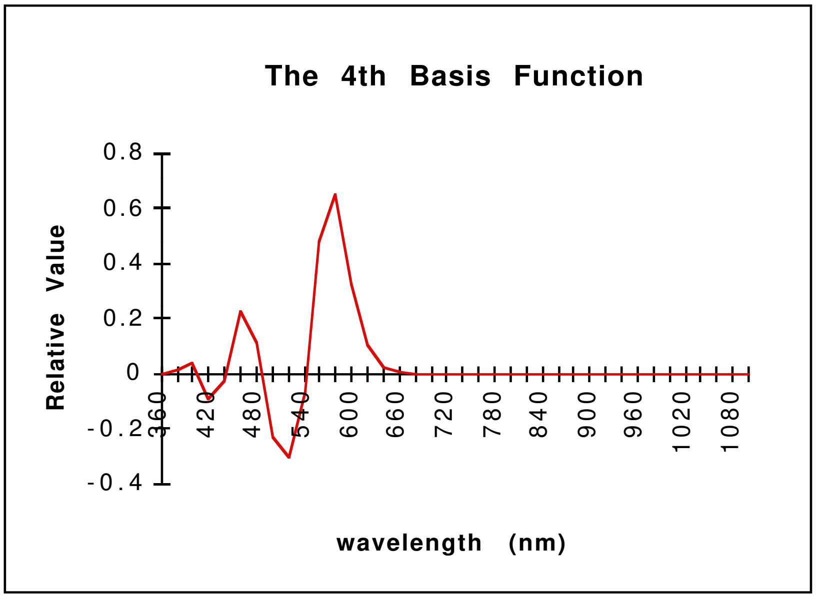

Figure 6.1.1.4 (Basis function #4 for recreation)

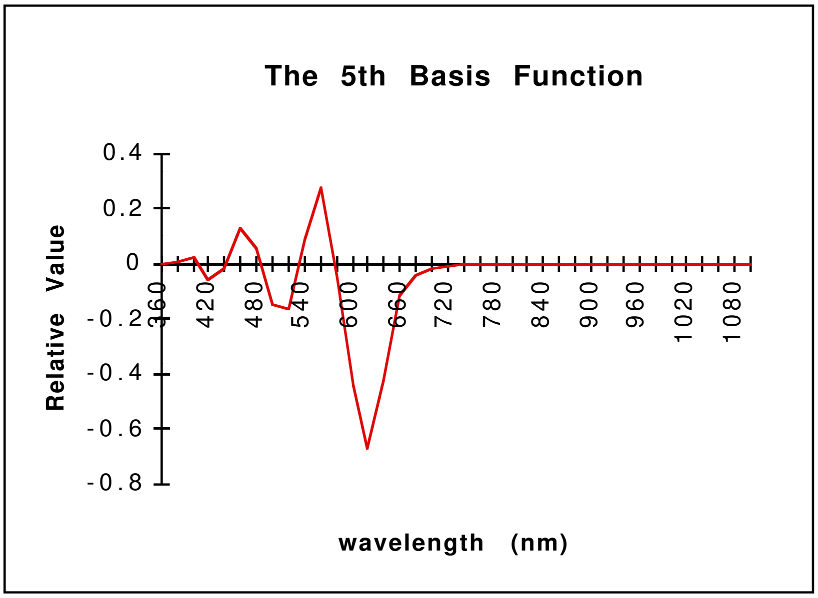

Figure 6.1.1.5 (Basis function #5 for recreation)

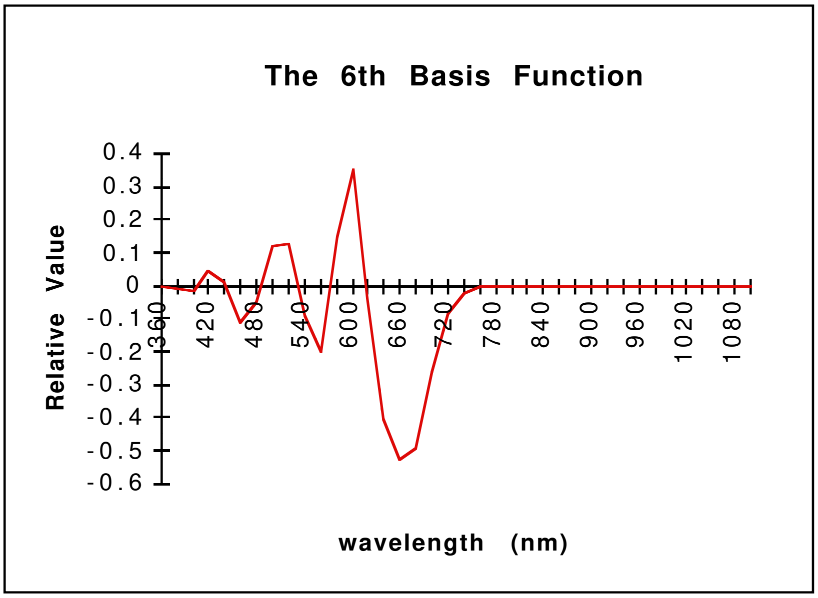

Figure 6.1.1.6 (Basis function #6 for recreation)

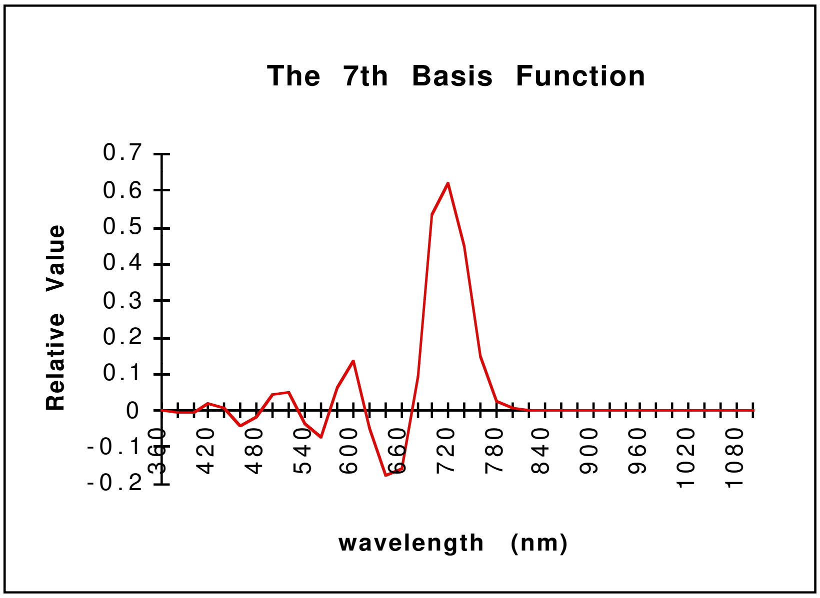

Figure 6.1.1.7 (Basis function #7 for recreation)

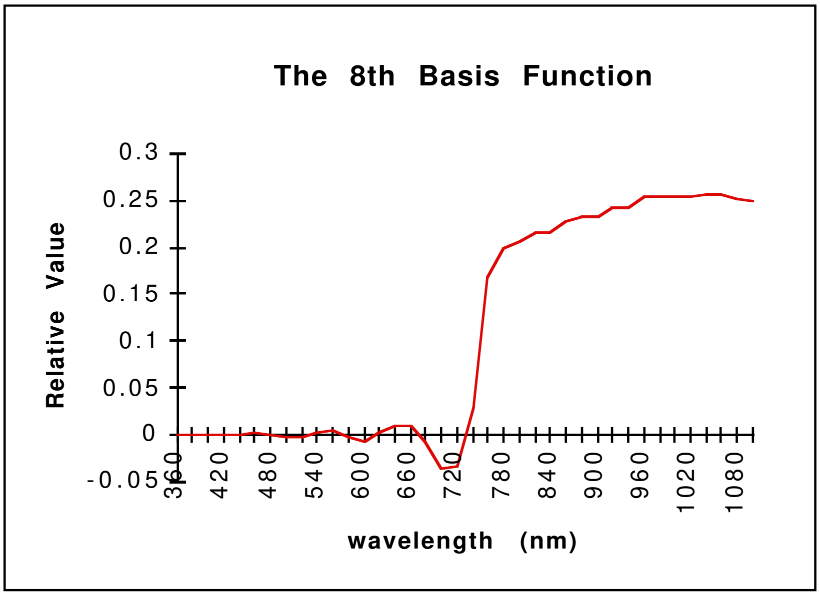

Figure 6.1.1.8 (Basis function #8 for recreation)

6.1.2 Recreated Wide Band Source Spectra Using Different Regions Of Interest and Camera Positions

When taking the same image into the camera over a period of time during either calibration or spectral recreation procedures, it is necessary to assure the stability of the camera over that period of time. Five sets of shots were taken 4 to 5 minutes apart at focal distance of $9.5''$, and from the resulting images spectra were recreated. Figure 6.1.2.1 shows the recreated spectra. The five recreated spectra were identical which assured that the camera was steady over a reasonable period of time.

For a focal distance of $28''$, four spectra were created, each corresponding to an image taken in such a way that the integrating sphere light source occupied an ROI located in the center of one corner quadrant of the image. The spectra were created by averaging images from five shots. Figure 6.1.2.2 shows these recreated spectra. These 4 spectra were identical, which assured that the spectral reconstruction was independent of the position of image registration on the CCD chip.

Further, the superposition of the spectra reconstructed from measurements at $D = 28''$ and at $D = 9.5''$ (Figure 6.1.2.3) showed that they were identical and hence indicated that the variation in the focal distance did not affect the reconstruction. Different camera responses for the two focal distances were, however, used.

Figures 6.1.2.1-3 show that the recreated spectrum simulated the smooth wide band light source spectrum only approximately at different focal distances and ROIs. The lack of a very good agreement between the recreated spectrum and the actual spectrum may be attributed to the fact that the basis functions used were not sufficient both for representing the camera response and the recreated source spectrum. Further investigation on the recreation of narrow band spectra using the above method is reported in the next section.

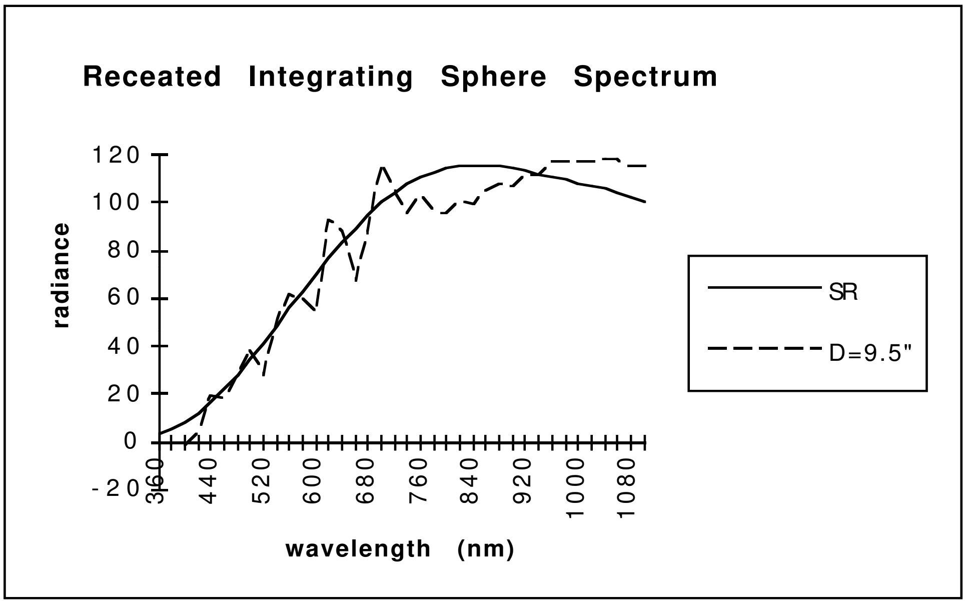

Figure 6.1.1.9 (Recreated spectrum using D =9.5”)

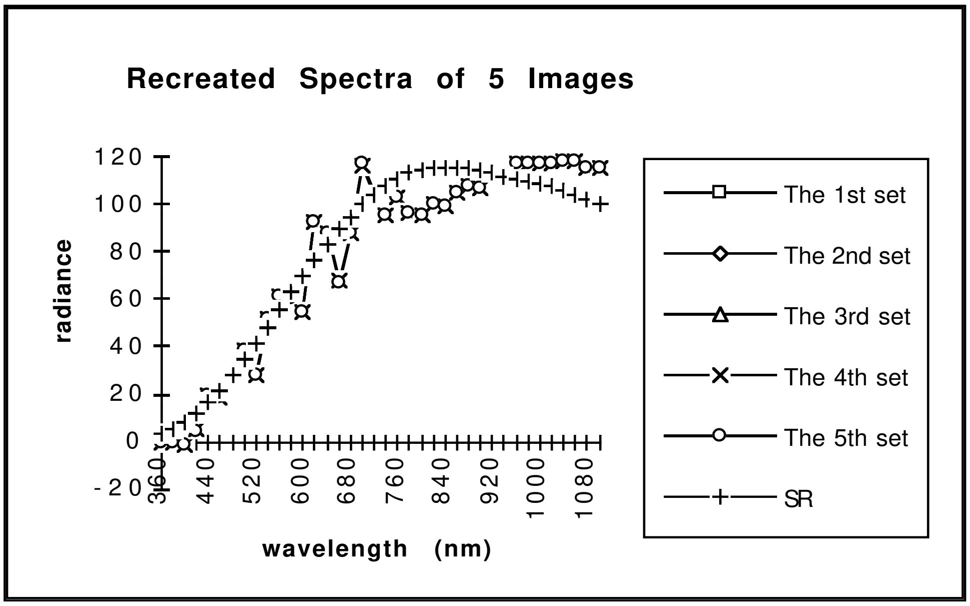

Figure 6.1.2.1 (5 sets of the same image taking over period of 4 - 5 minutes apart)

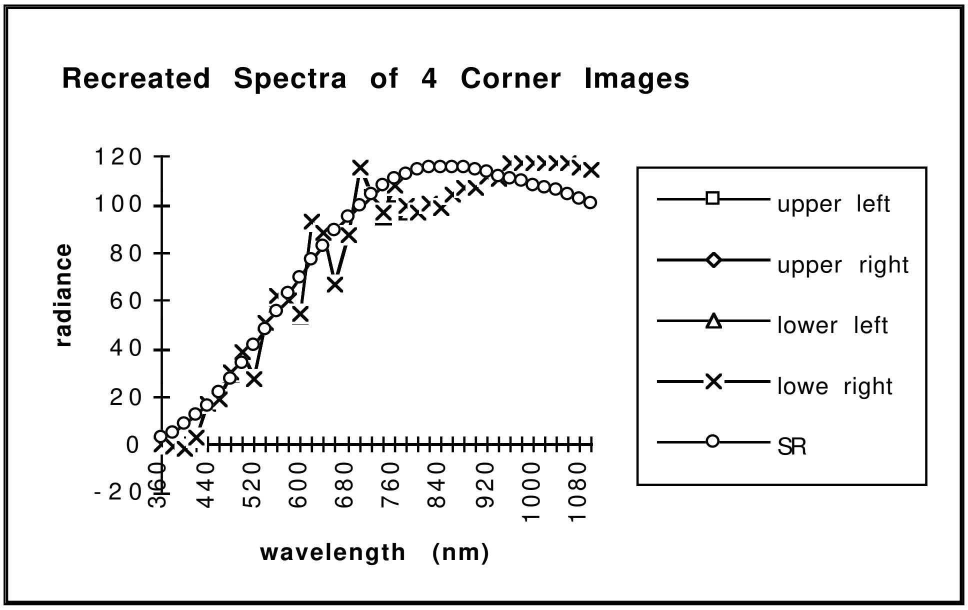

Figure 6.1.2.2 (Recreated Spectra of 4 corner images)

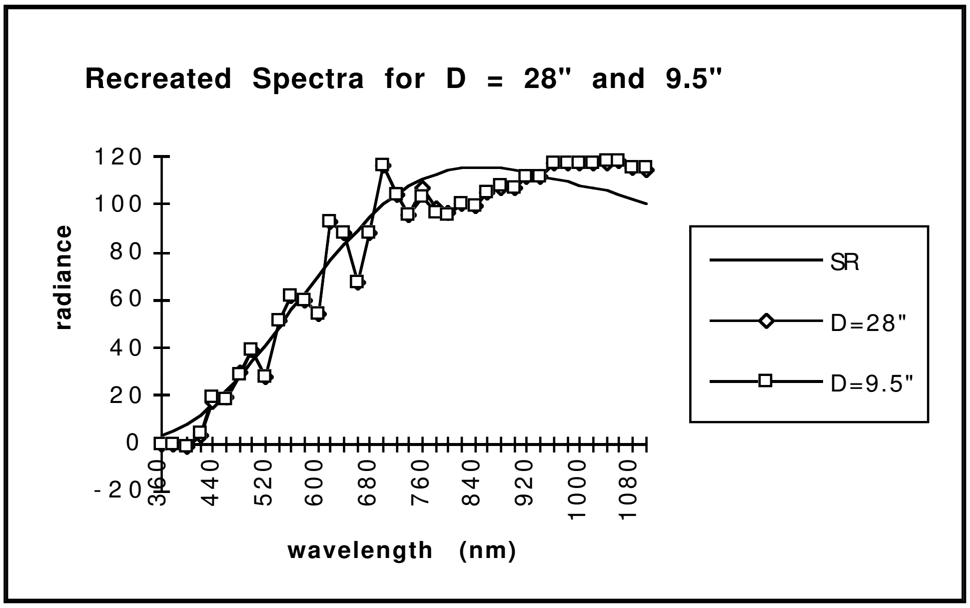

Figure 6.1.2.3 (Recreated Spectra for D =28” and D = 9.5”)

6.2 Narrow Band Light Source Recreation Using Basis Functions

In addition to the recreation of the wide-band light source, specific narrow wavelength band sources generated by a monochromator were also recreated to understand the performance of the CCD camera. The recreated spectra were expected to peak at the specified source wavelengths and have zero spectral radiance outside the source bandwidth. The method of light source recreation described in the previous section was used, and the measurement arrangement is shown in Setup #2 of Chapter 3.

By adjusting the entrance and exit slits of the monochromator the half bandwidth (HBW) of the exit radiation was varied. Table 6.2.1 shows the slit sizes used and the corresponding HBWs of the monochromatic source light.

HBW (nm)	Slit (mm)
0.5	0.125
1	0.25
2	0.5
5	1.25
10	2.5
20	5.0

Table 6.2.1 : HBW resolution of monochromatic light sources.

To begin, a 550 nm wavelength from the monochromator was selected. Figure 6.2.1 shows the corresponding recreated spectra for different monochromator slit widths. The peaks of the recreated spectra were precisely located at a wavelength of 550 nm. As the slit width increased, the amplitude of the spectra increased because more light passed through the slits. Figure 6.2.1 shows that the bandwidth was slightly wider when using larger slits. However, the HBWs of the 6 recreated spectra as listed in Table 6.2.2 are significantly larger than the HBWs of the light source.

The low wavelength resolution of the recreated spectra may be attributed to the present set of eight basis functions. Indeed, the five central oscillatory peaks appearing in Figure 6.2.1 may be attributed to peaks appearing in the basis function representation (*i.e.*, Figures 6.1.1.1 to 6.1.1.6, approximately). Note that the peak of the 550 nm narrow band light source happens to fall near the peak of one of the narrow band filters (filter #4, peak at 560 nm) used to construct the basis set. The appearance of negative radiances in Figure 6.2.1 is also a consequence of using the present basis function approach.

Slit Size	0.125 mm	0.25 mm	0.5 mm	1.25 mm	2.5 mm	5.0 mm
HBW	44.87 nm	49.44 nm	49.30 nm	50.00 nm	51.21 nm	51.10 nm

Table 6.2.2 : HBW resolution of 550 nm recreations.

In addition to 550 nm, two other wavelengths in the visible range, one shorter at 450 nm and one longer wavelength at 650 nm, were studied, and were generated with slits of 0.125, 0.5 and 2.5 nm. Figures 6.2.2 and 6.2.3 show the recreated spectra of the source radiance for these wavelengths.

The figures show that the peak of each recreated spectrum occurred at exactly the wavelength that the monochromator generated. Table 6.2.3 illustrates the HBW of the recreated spectra for the three different slits for wavelengths of 450 and 650 nm. Again, the extracted HBWs were much larger than the monochromator HBWs (shown in Table 6.2.1), but were almost independent of the increasing slit width.

	450 nm	650 nm
0.125 mm slit	46.19 nm	69.42 nm
0.5 mm slit	45.86 nm	69.02 nm
2.5 mm slit	44.51 nm	70.00 nm

Table 6.2.3: HBW resolution of 450 and 650 nm recreations.

The oscillatory behavior in Figures 6.2.2 and 6.2.3 is again due to the present choice of basis functions (Figures 6.1.1.1-7, approximately). The match in the peaks of the recreated sources with the actual 450 nm and 650 nm sources was probably incidental because the peaks of the light sources were nearby that of NB filter #2 (peak 470 nm) and filter #6 (peak 640 nm), respectively, which were used, in part, to construct the basis set.

In conclusion, the spectral recreation procedure appears to have worked relatively better for a wide-band, smooth light source spectrum (Figures 6.1.2.1-3) than for narrow band spectra (Figures 6.2.1-3). For the latter, the location of the peaks appears to be well resolved, but this is probably fortuitous, and the wavelength resolution of the spectra away from the peaks is poor. For the wide-band, smooth spectrum, the recreation is still somewhat rough and this is considered further in the next section.

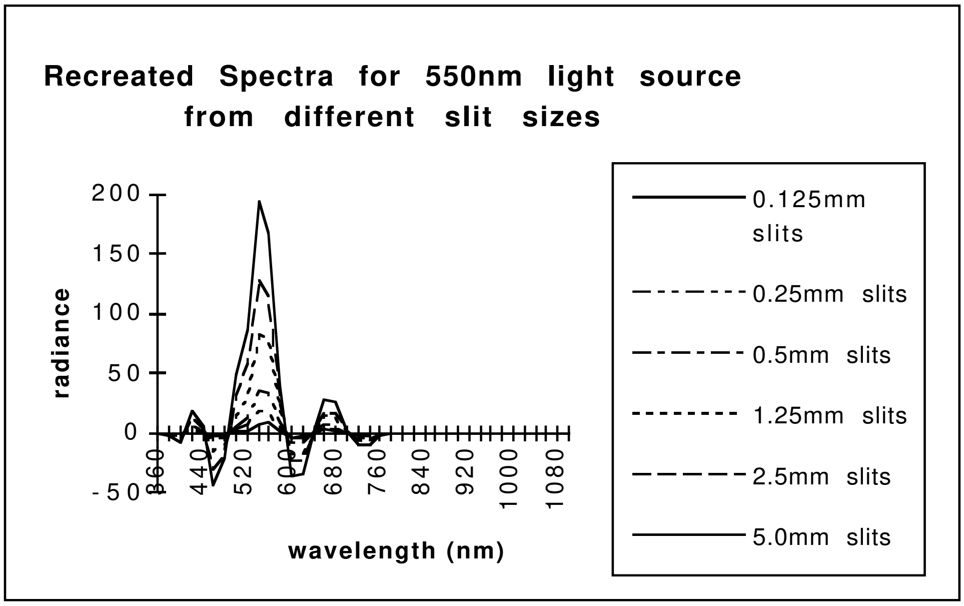

Figure 6.2.1 (550 nm wavelength recreation w/ different slit sizes)

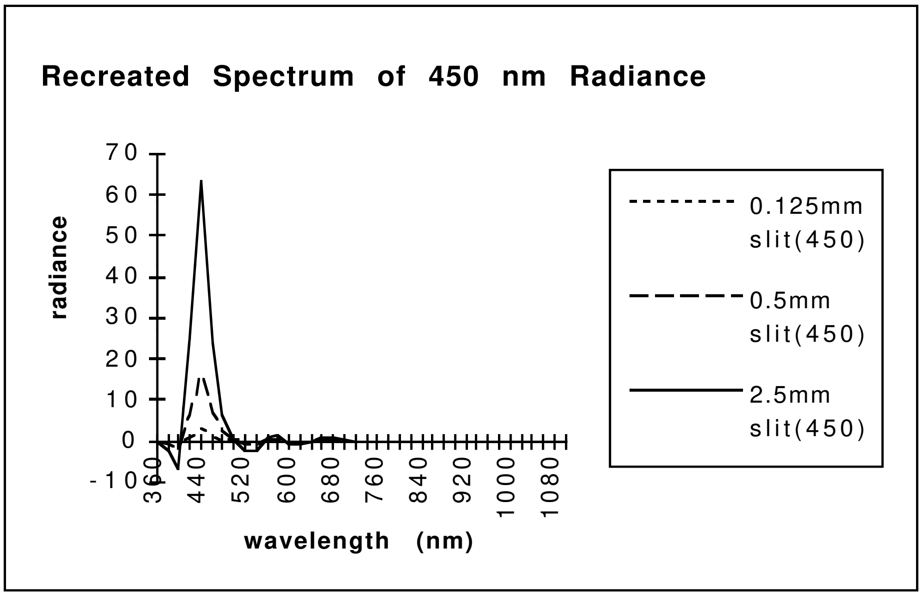

Figure 6.2.2 (450 nm recreation w/ 3 slit sizes)

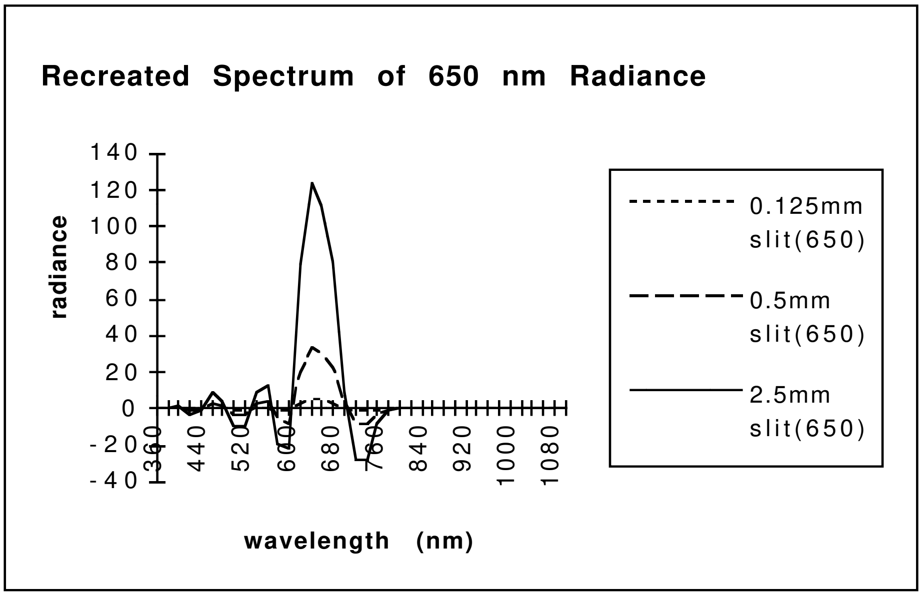

Figure 6.2.3 (650 nm recreation w/ 3 slit sizes)

6.3 Effect of the Wavelength Reconstruction Interval on Recreated Spectra

All the numerical computations discussed above employed a 20 nm wavelength interval for reconstruction. In this section, different wavelength intervals for reconstruction are considered, with a view to improving the reconstruction. Constant wavelength intervals of 10 nm and 40 nm, as well as nonuniform intervals which match the peaks (to within 20 nm) of the narrow band (NB) filter transmittances (*i.e.*, peak intervals), are considered. The wide-band and three narrow band (peaks at 450 nm, 550 nm and 650 nm) light source spectra were recreated using these intervals.

6.3.1 Wide Band Light Source Spectrum

The recreation of the wide-band light source spectrum of the Integrating Sphere was done for intervals of 10 nm, 20 nm, 40 nm and peak intervals. The peak intervals are spaced at approximately 50 nm, on average, neglecting filter #8 (which has an ill-defined peak, arbitrarily placed by us at 800 nm). The peak intervals recreation was graphed at eight wavelength locations (400 nm, 450 nm, 500 nm, 560 nm, 600 nm, 640 nm, 710 nm and 800 nm). Figures 6.3.1 to 6.3.4 display the recreated spectra.

By overlaying Figures 6.3.1.1, 6.3.1.2 and 6.3.1.3, it was clear that all of the information in the 20 nm interval reconstruction was contained in the 10 nm reconstruction. The additional in-between points in the 10 nm reconstruction could be found by linear interpolation of the 20 nm data points. Therefore, there was no additional information in the 10 nm interval reconstruction, at least for the wide-band source spectrum. Further, the 20 nm and 40 nm reconstructions were very close at their shared reconstruction points.

Using the peak intervals, Figure 6.3.1.4, the recreated spectrum gave the best fit to the wide-band Integrating Sphere light source spectrum. The 40 nm and 20 nm reconstructions were not as good, and, of these, the 20 nm reconstruction was the worst. The peak interval reconstruction in Figure 6.3.1.4 was exactly located on the wide-band light source spectrum. However, this did not mean that using the peak intervals is always better. The required wavelength resolution of a recreated spectrum also has to be taken into account.

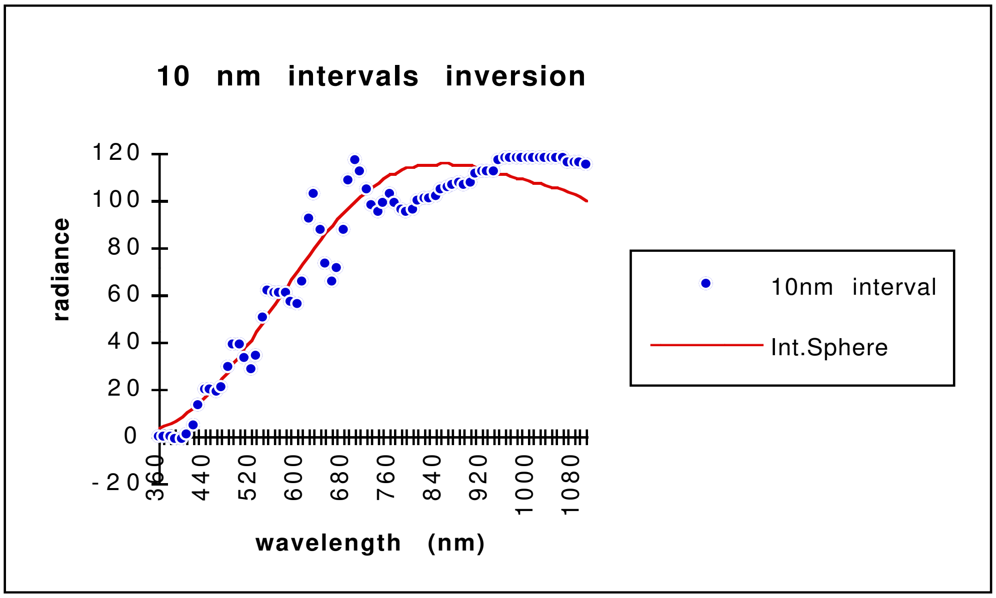

Figure 6.3.1.1 (10 nm intervals recreation)

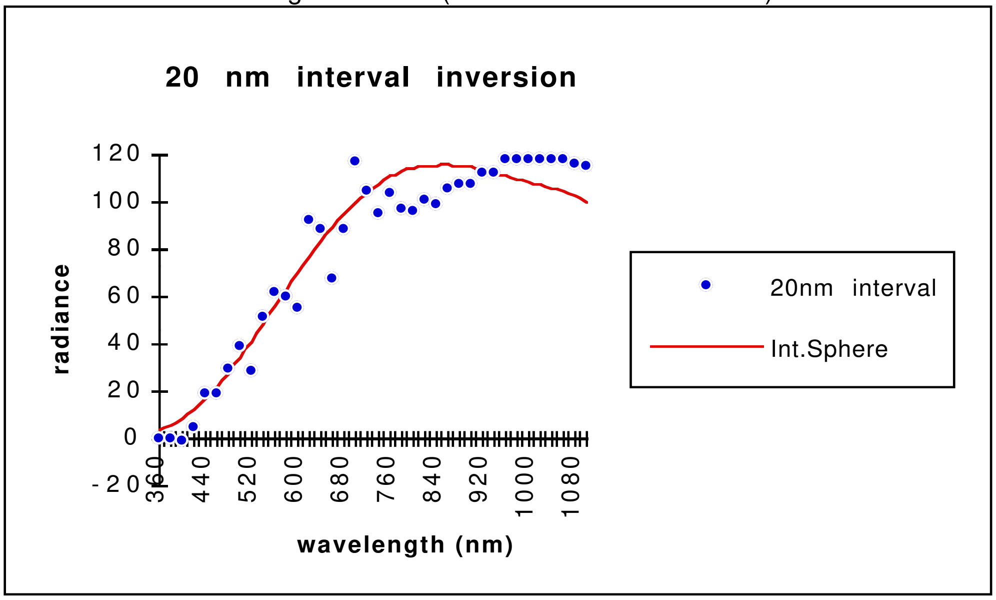

Figure 6.3.1.2 (20 nm intervals recreation)

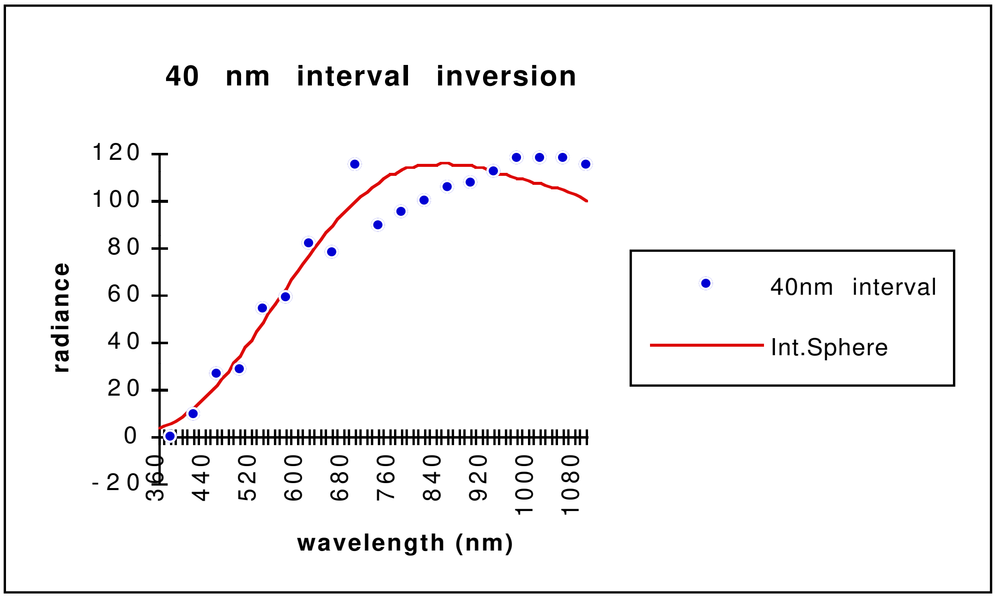

Figure 6.3.1.3 (40 nm intervals recreation)

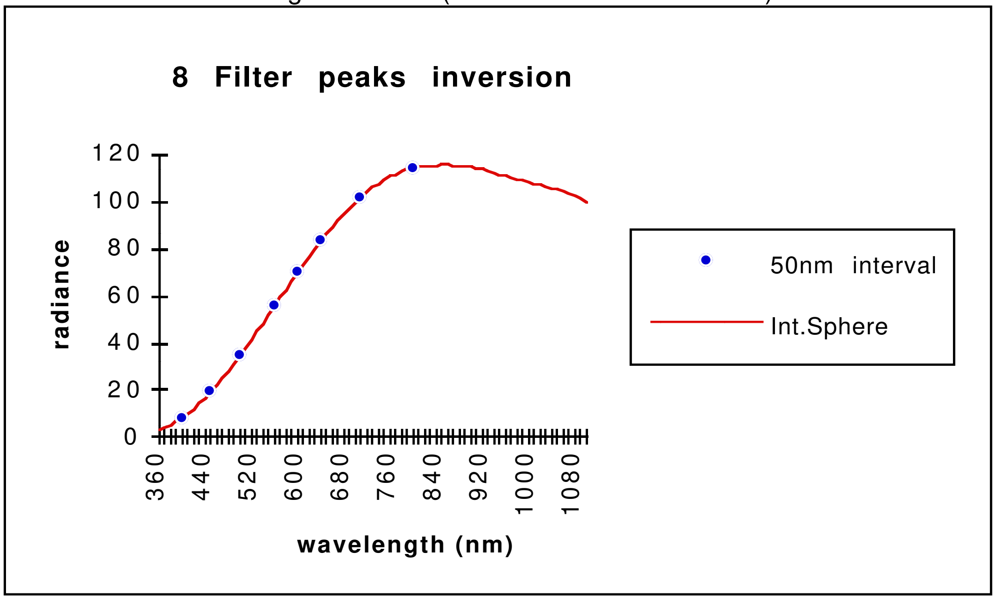

Figure 6.3.1.4 (filter peaks recreation)

6.3.2 Narrow Band Monochromatic Light Source Spectra

In order to examine the resolution of recreated narrow band spectra by using different reconstruction intervals, the monochromator data from Section 6.2 was used. Wavelengths of 450, 550 and 650 nm were selected using the 2.5 mm slits, and the HBW of these wavelength bands was 10 nm. Figures 6.3.2.1 to 6.3.2.4 show the recreated spectra of these specific light sources by using intervals of 10 nm, 20 nm, 40 nm and peak intervals.

By comparing the HBWs of these recreated spectra with the HBW (10 nm) of the source beam generated by the monochromator, the difference in resolution could be determined. Table 6.3.2.1 illustrates the HBWs of these recreated spectra.

	450 nm	550 nm	650 nm
10 nm interval	41.54 nm	42.94 nm	68.90 nm
20 nm interval	44.51 nm	51.22 nm	70.00 nm
40 nm interval	80.91 nm	61.11 nm	68.72 nm
peak interval	51.56 nm	194.19 nm	59.21 nm

Table 6.3.2.1 : HBW resolution of three recreated narrow band light sources using four different reconstruction intervals.

Table 6.3.2.1 and Figures 6.3.2.1-4 show that there is slightly better peak resolution when narrower reconstruction intervals are used, at least for source light of 450 nm and 550 nm wavelengths. The resolution by using peak intervals was the worst, even though when used for a wide-band smooth spectrum, the reconstruction was the best. Thus, for non-smooth, or spiky, spectra, reconstruction using narrower wavelength intervals, such as 20 nm, should be considered and may have some advantages in improving the wavelength resolution. Note, however, that all the recreations in Figures 6.3.2.1-4 continue to display regions of negative reconstructions, which are nonphysical and due to the choice of basis functions.

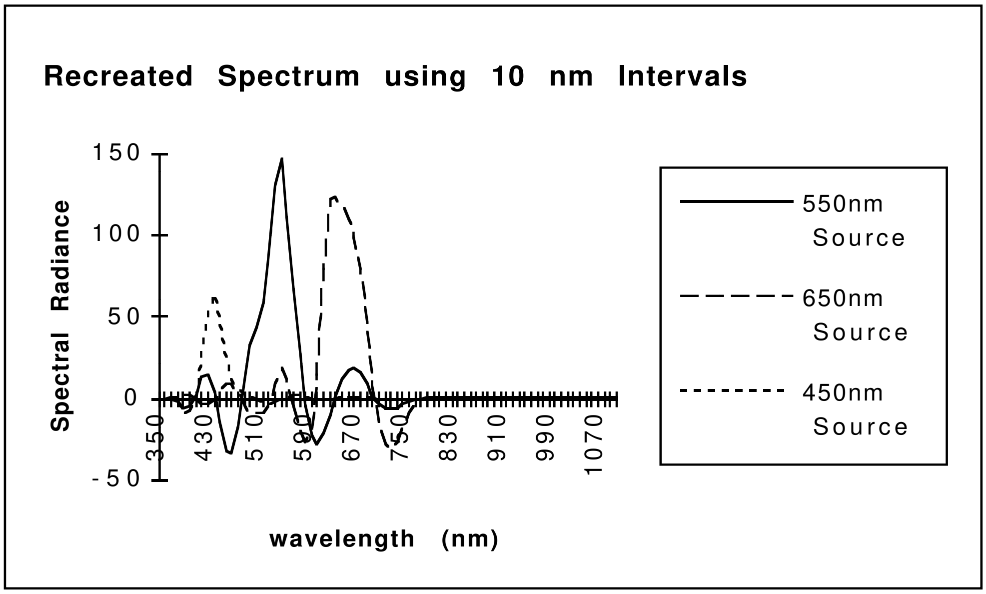

Figure 6.3.2.1 (10 nm intervals recreation)

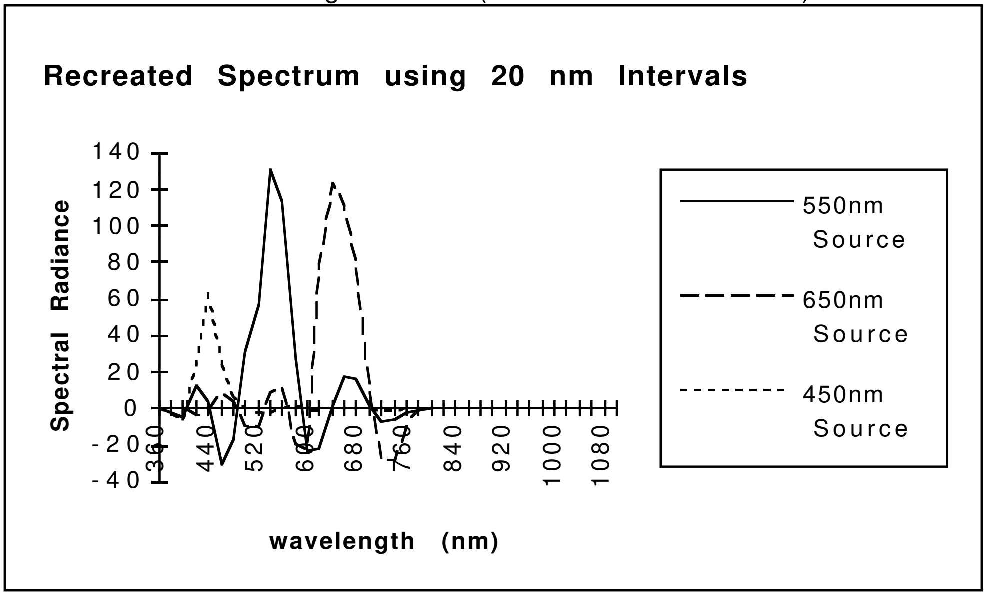

Figure 6.3.2.2 (20 nm intervals recreation)

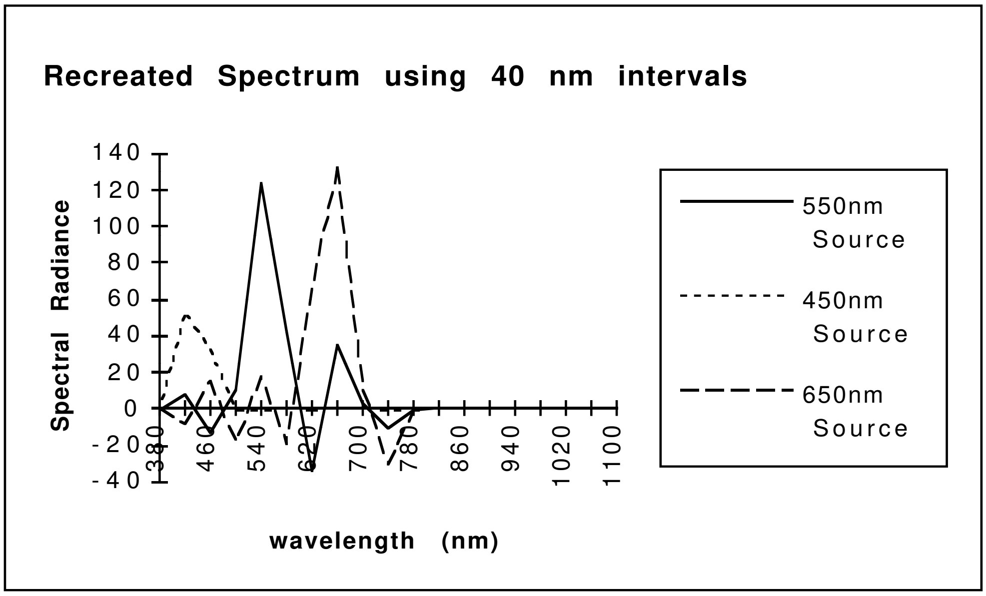

Figure 6.3.2.3 (40 nm intervals recreation)

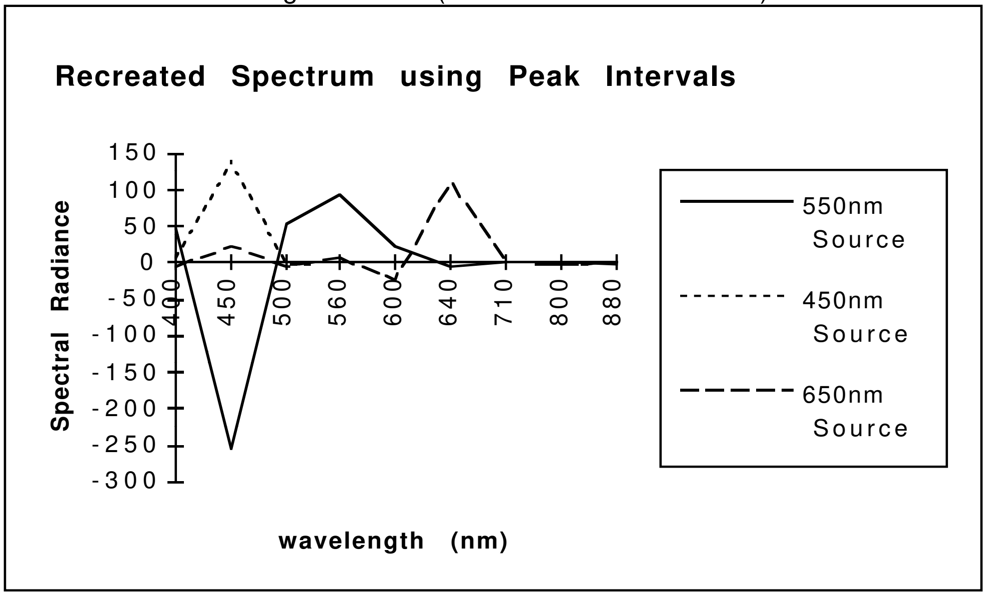

Figure 6.3.2.4 (filter peaks recreation)

6.4 Error Estimates for Wide Band Source Recreations

6.4.1 Signal Value Sensitivity

The spectrum recreation method discussed so far was based on eight camera response signals where each signal corresponded to the camera response in the presence of a particular NB filter. In this section investigations are described to find how a variation in each of these eight signals affects the reconstruction of a wide band source spectrum.

The wide-band spectrum of the Integrating Sphere light source was used as a standard spectrum to be examined. The experimental arrangement is as shown in Setup #3 of Chapter 3. One of the signals corresponding to either a NB filter or to the dark current of the camera was increased by 1% of its original value and the signal was reconstructed. Separate increases were carried out with each of the signals in turn and the results were analyzed. Figures 6.4.1-9 show the fractional change in the spectral amplitude due to the change in the signal. In the figures, $S_{m1} \ldots S_{m8}$ represent the signal values obtained by using the eight filters (i-th NB filter +ND filter) and S_{md} is the average dark current of the camera. A constant reconstruction interval of 20 nm was employed.

The percentage change in a spectrum was found to be within $\pm 5\%$ for most of the wavelength range except below 440 nm, no matter which of the signals from S_{m1} to S_{m8} was changed. However, it also indicated that the input signal was at places amplified by 5 times in the reconstruction process. Further, for the spectrum below 440 nm the amplification was found to be much larger. The source signal in this region was also much weaker.

Figure 6.4.9 shows the sensitivity of the dark current measurement. The sensitivity of this measurement was also extremely large below wavelength 440 nm as with the other sensitivity reconstructions.

The results obtained in this section are used in Section 6.5 for estimating the wavelength distribution of the error when different wavelength reconstruction intervals are employed.

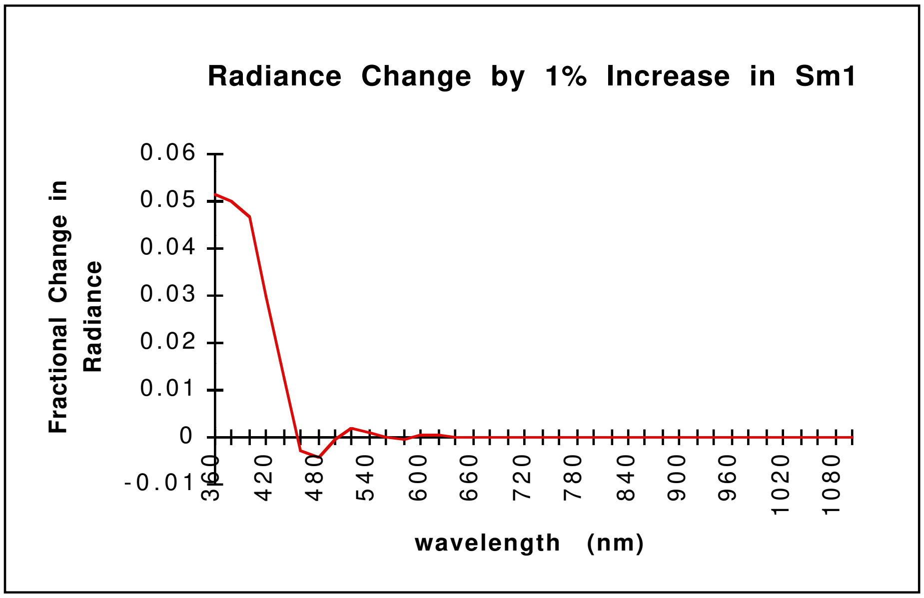

Figure 6.4.1 (First input signal increased by 1%)

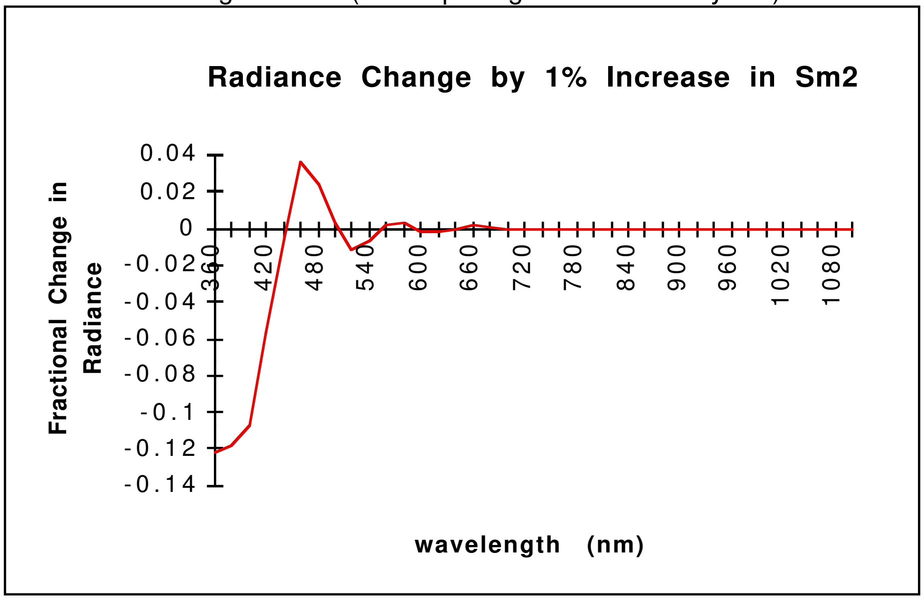

Figure 6.4.2 (Second input signal increased by 1%)

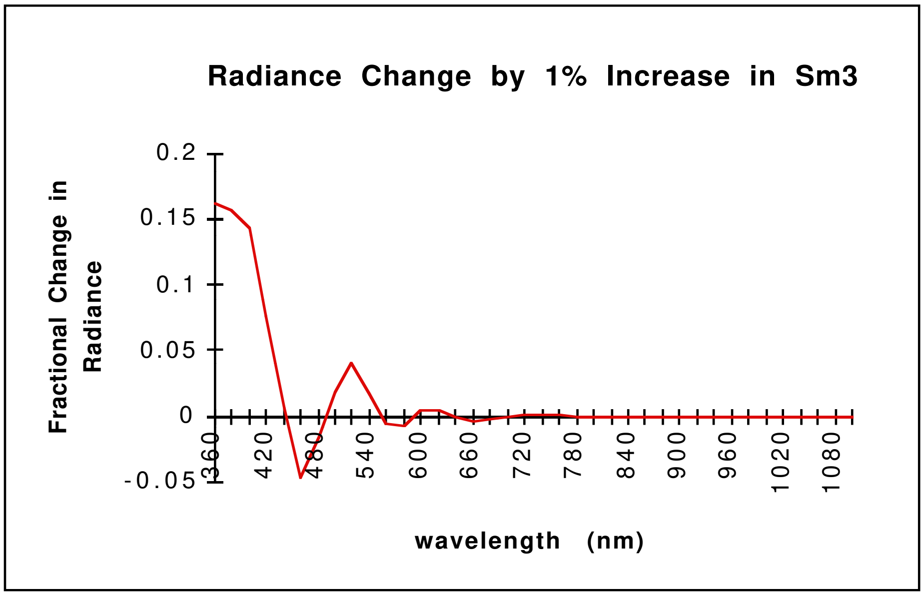

Figure 6.4.3 (Third input signal increased by 1%)

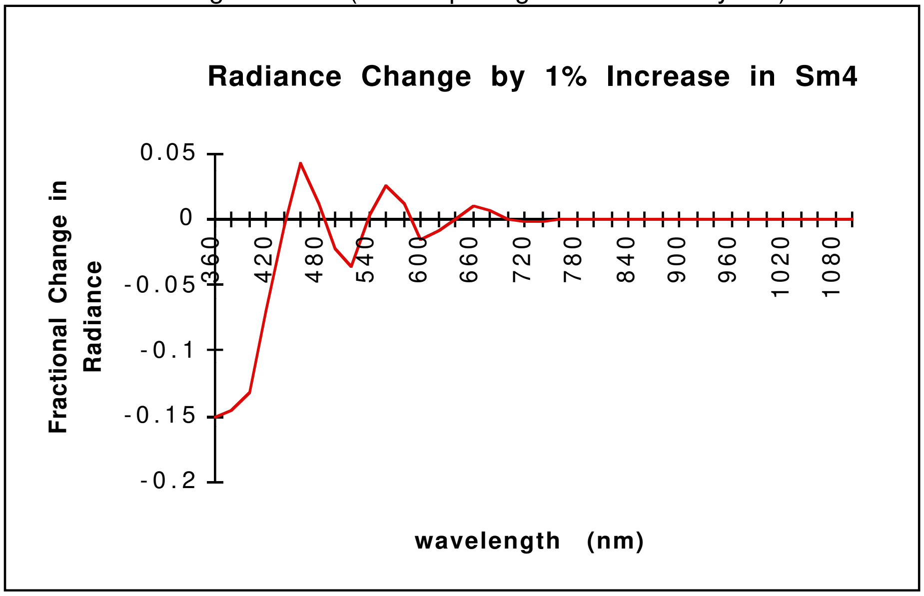

Figure 6.4.4 (Fourth input signal increased by 1%)

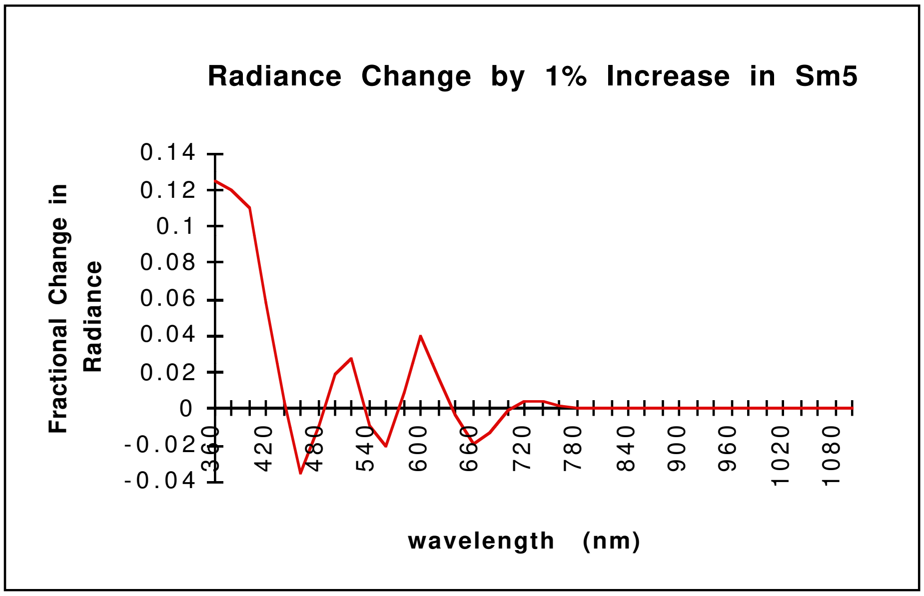

Figure 6.4.5 (Fifth input signal increased by 1%)

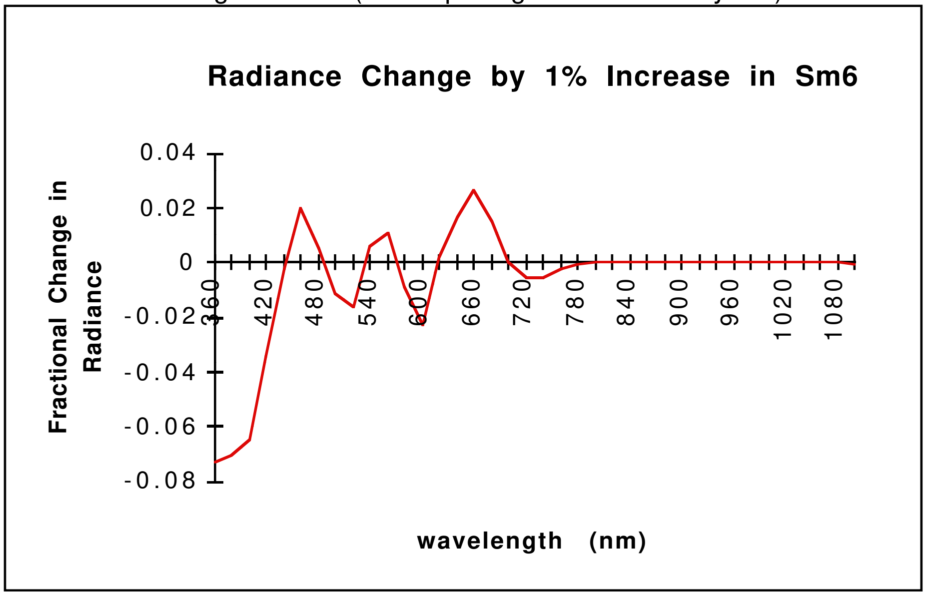

Figure 6.4.6 (Sixth input signal increased by 1%)

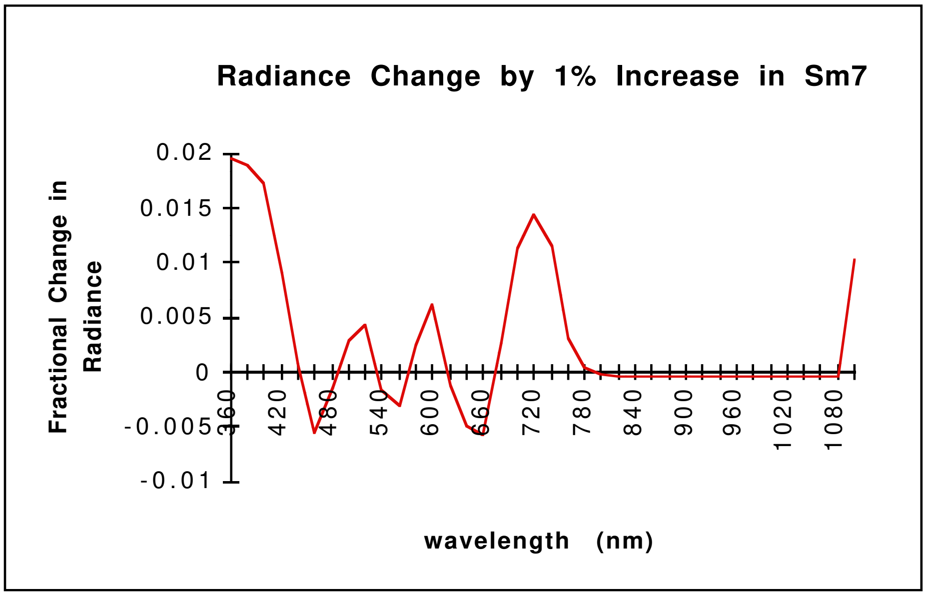

Figure 6.4.7 (Seventh input signal increased by 1%)

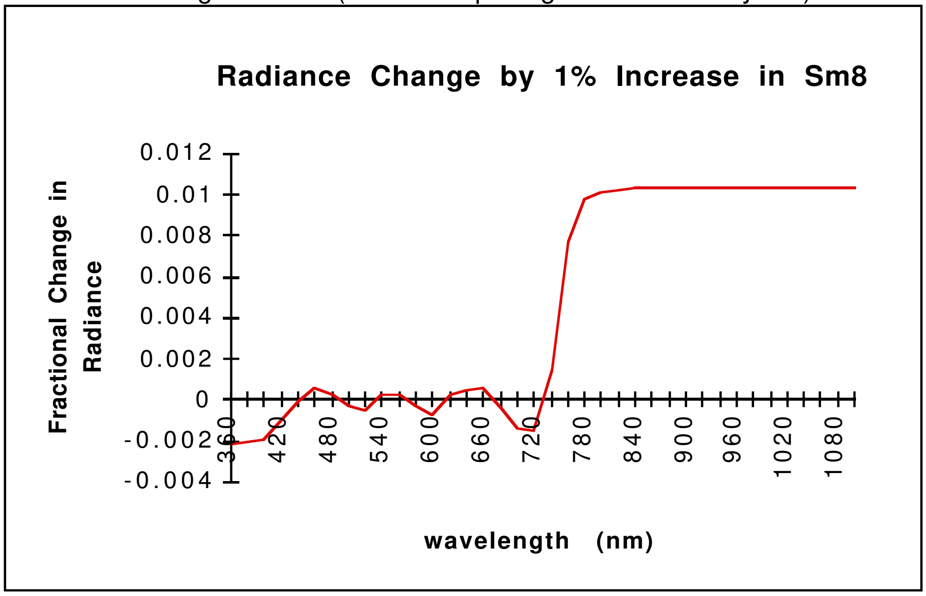

Figure 6.4.8 (Eighth input signal increased by 1%)

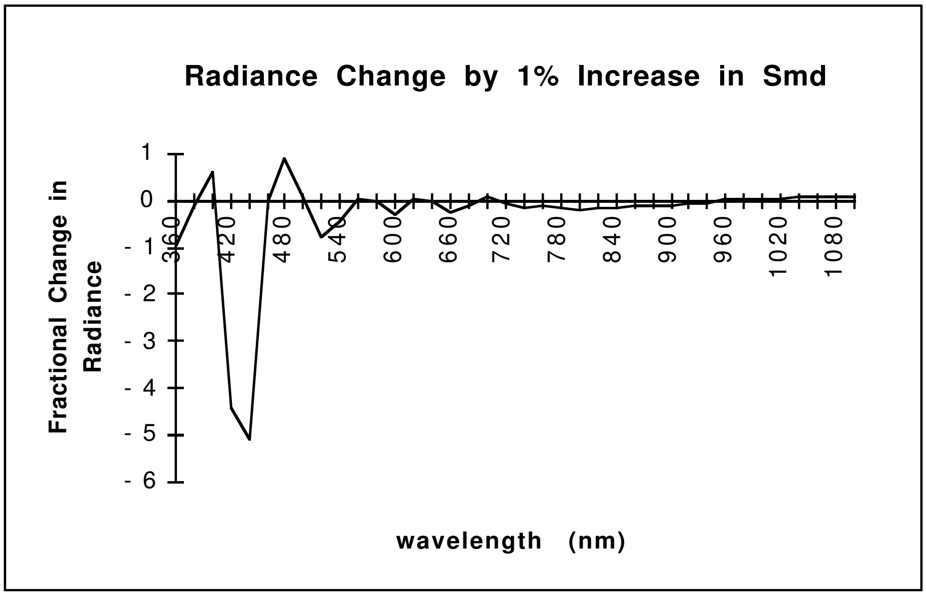

Figure 6.4.9 (Dark current signal increased by 1%)

6.4.2 Effect of Measurement Errors

In this section, an attempt is made to estimate the effect of measurement errors on the spectral reconstruction of the wide band light source (the experiment shown in Setup #3 of Chapter 3). The analysis employs sensitivity data as described in, but additional to, Section 6.4.1. The estimation provides error estimates as a function of wavelength, and for different wavelength reconstruction intervals.

The effect of measurement errors on a recreated spectral radiance distribution, $I(\lambda)$, can be estimated. As I is computed from the measured signals in the presence of the filters and dark current, it may be written as a function of such signals, *i.e.*,

$$I(\lambda, S_{m1}, S_{m2}, \ldots S_{m8}, S_{md}).$$

Then a formal expression for the rms error or rms standard deviation, dI, of a spectral reconstruction is

$$dI_j = \left(\left(\frac{\delta I_j}{\delta S_{m1}} \sigma_1 \right)^2 + \left(\frac{\delta I_j}{\delta S_{m2}} \sigma_2 \right)^2 + \ldots + \left(\frac{\delta I_j}{\delta S_{m8}} \sigma_8 \right)^2 + \left(\frac{\delta I_j}{\delta S_{md}} \sigma_d \right)^2 \right)^{\frac{1}{2}}$$

where

I_j is the recreated spectral source radiance at the jth discrete wavelength,

S_{mi} is the signal value obtained by using filter i, $i = 1$ to 8,

S_{md} is the signal value of the dark current measurement,

σ_i is the standard deviation (or other error estimate) of the uncertainty in the signal value, and

$\frac{\delta I_j}{\delta S_{mi}}$ is the percentage change in the recreated radiance at the jth wavelength due to a 1% increase in the CCD signal obtained with the i-th filter.

Estimates of the standard deviation, or error, σ_i, in a signal were obtained from the laboratory experiment. Using 10 measurements (*i.e.*, repetitions) taken for each of the eight filters, the average standard deviations of the pixel signals were found. By blocking the lens of the camera with a shutter, the average standard deviation of the dark current was similarly found from 10 repetitions. We use these standard deviations as a measure of σ_i for $i = 1$ to 8 and d. Other errors, primarily systematic, that might contribute to the σ_i have been neglected. The σ_i estimates are tabulated in Table 6.4.2.1.

σ_1	σ_2	σ_3	σ_4	σ_5	σ_6	σ_7	σ_8	σ_d
0.39	0.21	0.61	0.46	0.40	0.71	1.88	2.61	0.09

Table 6.4.2.1 : Estimates of standard deviation of the error in a measured signal.

The spectral recreation procedure for $I(\lambda)$ is carried out by using specific wavelength reconstruction intervals (*e.g.*, 10 nm, 20 nm, 40 nm or nonuniform peak intervals). The sensitivity coefficient $\frac{\delta I_j}{\delta S_{mi}}$ depends on the particular reconstruction intervals that are used. Data for this coefficient are shown in Figures 6.4.1 to 6.4.9 for a 20 nm interval reconstruction. Similar data, not shown, were generated for 10 nm, 40 nm and peak intervals reconstructions.

Using the computed dI_j values we constructed upper and lower bounds for a recreated wide-band light source spectrum. One would expect that the actual spectrum would lie between these bounds. The upper bound is calculated by adding dI_j to a recreated spectrum while the lower bound is calculated by subtracting dI_j from a recreated spectrum. The error range in the spectra is shown in Figures 6.4.2.1 to 6.4.2.4. The figures correspond to different wavelength reconstruction intervals.

Figures 6.4.2.1 to 6.4.2.4 show that a 10 nm wavelength reconstruction interval had the largest upper and lower bound errors when compared with 20 nm, 40 nm and peak intervals. This results from the 10 nm reconstruction having much larger values of the signal sensitivity coefficients $\frac{\delta I_j}{\delta S_{mi}}$. The peak intervals reconstruction is the only one for which the upper and lower error bounds are both *close* to one another and *bound* the original light source spectrum. However, the peak interval approach does not work well with non smooth light source spectra. Therefore, 20 nm interval reconstruction may be better, in general, for such reconstructions.

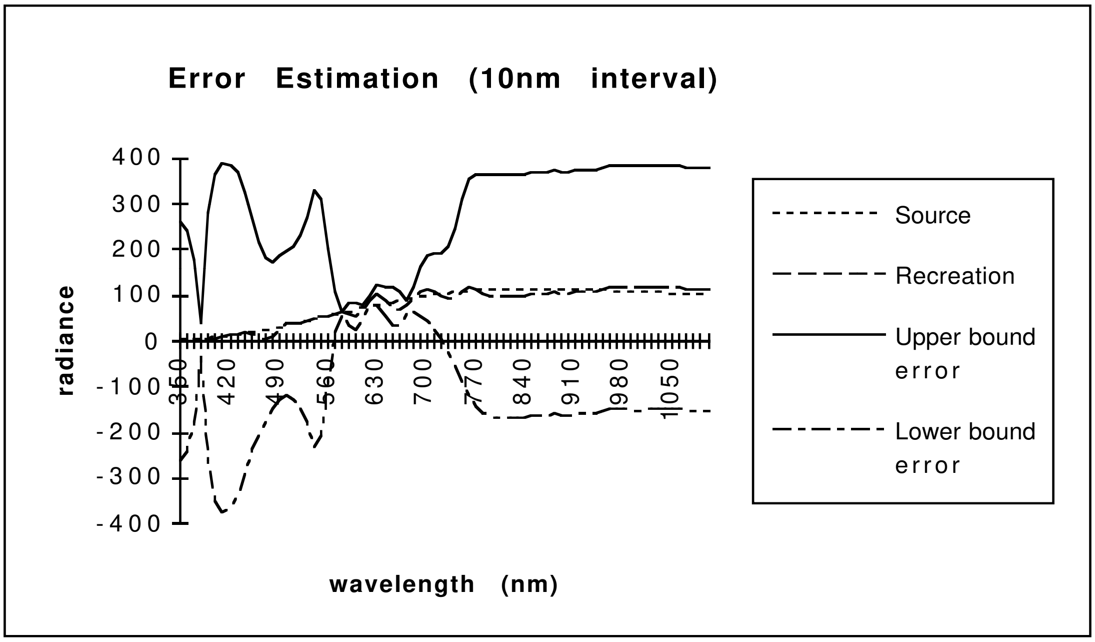

Figure 6.4.2.1 (76 discrete wavelength)

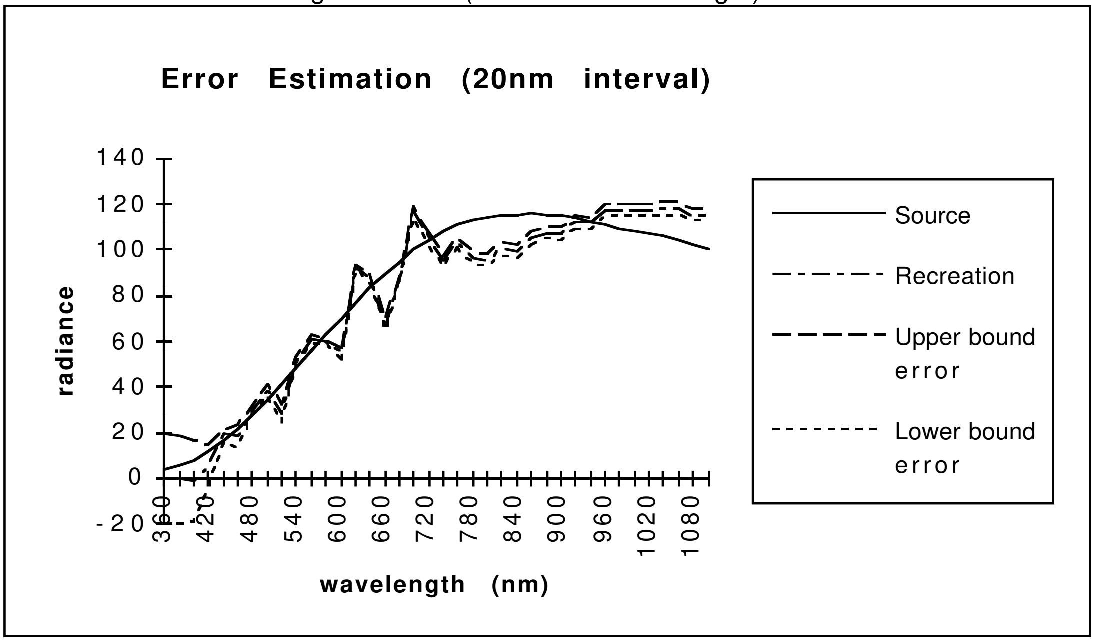

Figure 6.4.2.2 (38 discrete wavelength)

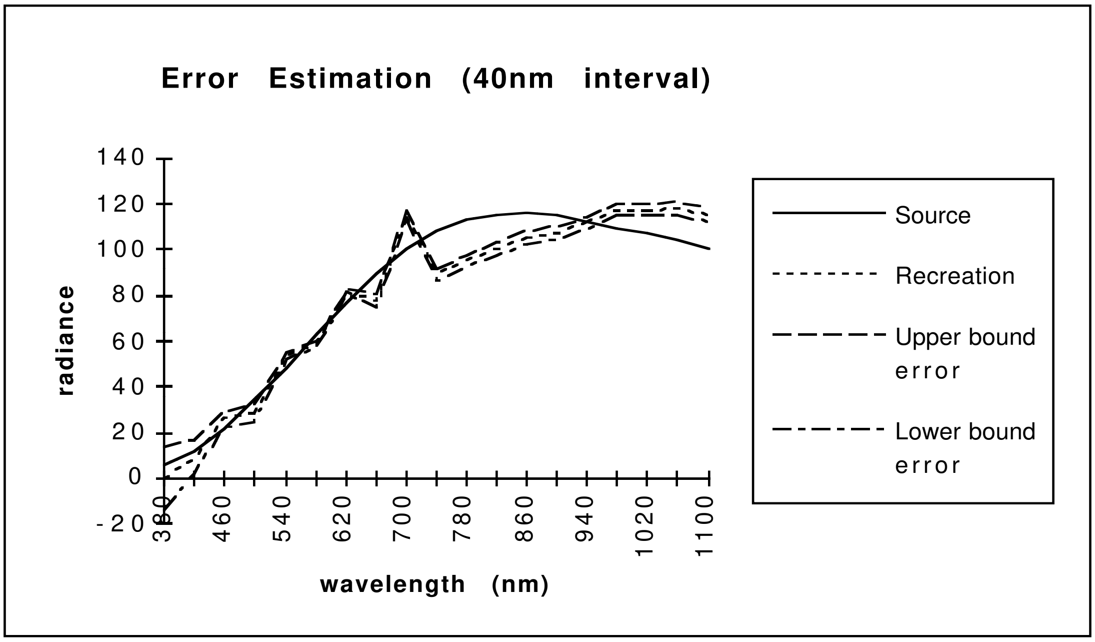

Figure 6.4.2.3 (19 discrete wavelength)

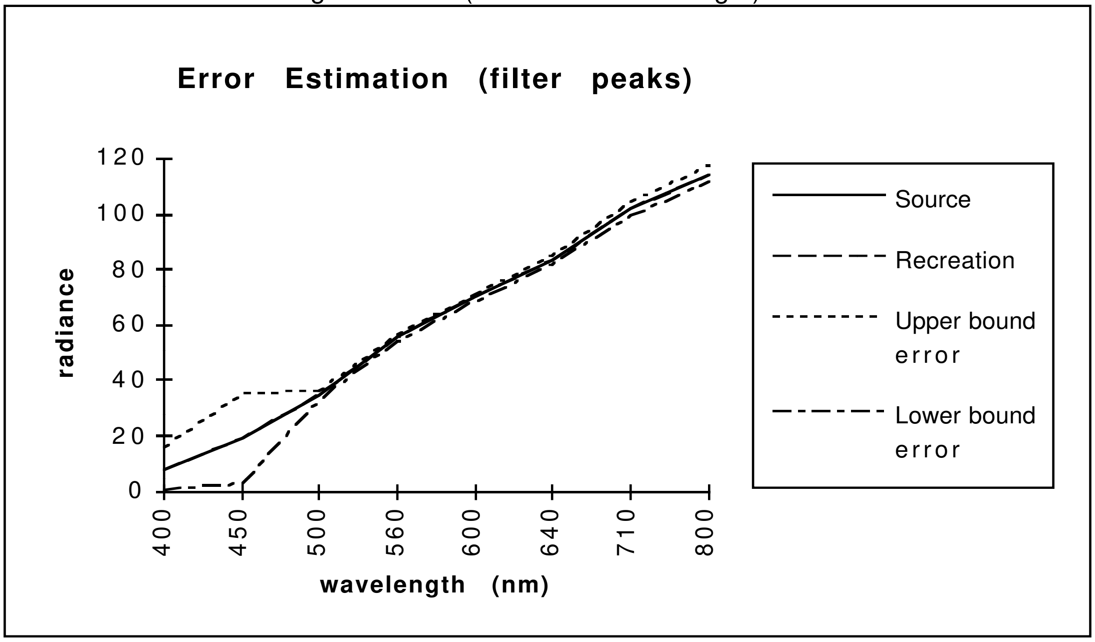

Figure 6.4.2.4 (8 discrete wavelength)

6.4.3 Effect of Calculation Errors

In this section we estimate the integral errors arising in the spectral recreation of several wide band sources. This is essentially a check on calculation errors that might arise during the reconstruction process. Wide-band, unfiltered source signals are measured and compared with estimates of the same signal obtained by integrating the recreated spectral signal over all wavelengths.

A reflecting surface (a picture in MATLAB User's Guide - Plate 7 [19]) composed of eight regions of different reflection characteristics (*i.e.*, different colors) was illuminated by the Lowel Tota 60 watt light source, and was imaged using the CCD camera. These regions, R, were selected for spectral recreation. The measured signals and apparent colors of these regions are listed in Table 6.4.3.1.

	R_1 (Red)	R_2 (Orange)	R_3 (Yellow)	R_4 (Green)	R_5 (Blue)	R_6 (Indigo)	R_7 (Purple)	R_8 (Black)
S_{m0}	1471	1478	1299	731	736	719	735	159
S_{md}	95	93	94	93	95	94	93	96
S_{m1}	91	95	93	93	95	91	92	90
S_{m2}	95	101	99	100	109	106	95	92
S_{m3}	106	126	143	116	120	119	94	97
S_{m4}	121	158	191	108	110	108	99	100
S_{m5}	211	251	218	108	107	104	109	101
S_{m6}	310	306	274	109	107	109	129	101
S_{m7}	388	390	284	148	151	151	180	107
S_{m8}	594	555	514	482	498	486	458	125

Table 6.4.3.1

Note : R_j is the j-th region of the light-reflecting surface,
S_{m0} is the corresponding CCD signal measured without any filter,
S_{mi} is the CCD signal obtained by using the ith NB filter, and
S_{md} is the dark current signal.

For each region R_j, spectral reconstruction was carried out by using the method described in Section 6.1. A 20 nm reconstruction interval was used. The unfiltered wide band pixel signal was then estimated from the dark current value plus the product of the recreated spectrum row vector and the camera response column vector. The product represents a numerical integration over wavelengths of the recreated signal. The recreated wide-band signals, and the percentage errors for the eight regions, are listed in Table 6.4.3.2.

	R_1	R_2	R_3	R_4	R_5	R_6	R_7	R_8
Computed Signal	1429.8	1468.9	1252.5	732.70	757.46	739.69	734.43	151.27
Error	-2.80%	-6.20%	-3.58%	2.30%	2.92%	2.88%	-0.07%	-4.68%

Table 6.4.3.2 Recreated integral signals and errors.

The errors listed in Table 6.4.3.2 arise from the particular basis function set used and the numerical errors in the computation of the spectral recreations. Of course, the degree of independence of the NB filters also affects the accuracy of the recreations as does the spectral response range of the camera. Although the camera was observed to respond out to 1500 nm, albeit very weakly, the calibrated response range was out to only 1100 nm. For the wide-band recreations in Table 6.4.3.2, it would appear that the errors arising from the mismatch of the calibration range and the camera's response range are small.

Chapter 7

Summary and Conclusions

This report presents preliminary calibration data for the use of the Photometrics PXL1300L as a spectroradiometric CCD camera. Through the use of basis functions, the CCD camera response was found. Using the equipment setup and the method described in this report, which also uses basis functions, it is now possible to obtain the spectral radiance of all pixels of a viewed scene. The resulting spectral reconstructions can be used for validating Computer Graphics simulations.

The inversion procedure employed narrow band and neutral density filters. The spectral transmission data for these filters are included in this report, and in a separate $3\frac{1}{2}''$ floppy disk.

The camera was found to have a nearly perfect linear radiometric response to incident light throughout the visible region. Based on this linearity, the basis function approach could be adopted successfully. The radiometric calibration was extended to include the effects of lens F-stop setting and camera shutter speed, S, the latter being set both electronically and by a mechanical shutter through the control software. A shutter-speed offset is required for accurate calibration. The spectral response calibration of the camera was carried out by using basis functions and shows good qualitative agreement with the manufacturer's published response curve.

Recreations of wide band and narrow band light sources were carried out using the basis function inversion methodology. Some problems remained unsolved. The recreated spectrum of the narrow band light source had regions of negative radiance which resulted in unnatural spectra. In addition, the recreated spectrum of the wide-band light source was not very smooth as compared to the manufacturer's data, except when the peak intervals reconstruction method was employed. Further work on basis functions is required. Filter and environmental interreflections also can occur in the experiment, leading to errors.

Other tasks remaining are summarized by the points below.

1. **Camera linearity:** The camera linearity needs to be measured as a function of lens focal distance, D, to complement the measurements in

this report. This should include further studies of the effect of the shutter speed offset on the calibration.

2. **Camera spectral response:** The dependence of the camera's spectral response calibration on lens parameters, *e.g.*, the F-Stop and focal distance (D) settings, needs to be measured.

3. **Individual sensor calibration:** All sensors in the CCD camera should be individually calibrated to get high quality radiometric images. The calibration should include statistical data on the spread of the sensors, and ways to efficiently use the calibrations and to correct for dead sensors.

4. **Quicker spectral reconstruction:** Procedures for simplifying the initial calibration of the sensors are required. For the spectral reconstructions, a simple way to include the F-Stop and focal distance (D) dependences of the calibration is needed, as are procedures that would allow the relative shape (but not amplitude) of a reconstruction to be found quickly.

5. **Basis sets:** Better basis sets are needed for both camera calibration and spectral reconstruction. For wide-band signals,

    - are eight narrow band filters appropriate?,
    - do we need additional wide band filters?,
    - should we use only the filter peaks method?

    For narrow band signals,

    - how can we get good spectral resolution and still avoid the negative reconstructions?

    Can we get better least square representations, and smoother reconstructions, by adding more (linearly dependent) filters?

6. **Inversion Range:** Was our basis set and calibration applied to too wide a spectral range? What would happen if we used a narrower wavelength window, *e.g.,* 400 nm to 700 nm, for reconstruction, by perhaps adding a longwave cutoff filter that would be used for all measurements?

Acknowledgments

We acknowledge the significant and generous help of Sing-Choong Foo, our fellow graduate student in the Program of Computer Graphics. It would have been difficult to complete this work without Sing-Choong. We also acknowledge helpful discussions with Will Vodra during the initial stage of this project. The equipment described in this report was funded by the National Science Foundation Thermal Systems Program, under Grant CTS-9213183, "Engineering Equipment Grant: A Request for Thermal Radiation Measurement Equipment" and with matching funds from the Program of Computer Graphics and Cornell University. The Program of Computer Graphics at Cornell is one of the five sites of the NSF/ARPA Science and Technology Center for Computer Graphics and Scientific Visualization (Grant ASC-8920219). The Program of Computer Graphics and Light Measurement Laboratory host equipment provided by the Hewlett-Packard, IBM and Digital Equipment Corporations.

Bibliography

[1] T. H. Himlan, *Design of a Light Measurement Laboratory for the Program of Computer Graphics*, M.Eng report, School of Mechanical and Aerospace Engineering, Cornell University, August 1987.

[2] T. H. Himlan, *Spectroradiometric 2D imaging and physical property measurements for validating and improving global illumination simulations*, Master's thesis, school of Architecture, Arts & Planning, Cornell University, August 1991.

[3] S.-C. Foo and K.E. Torrance, *Equipment Acquisition for the Light Measurement Laboratory of the Cornell Program of Computer Graphics*, Report PCG-95-5, Program of Computer Graphics, Cornell University, Ithaca, NY, 135 pages,1995.

[4] C. Buil, *CCD Astronomy*, Willman-Belle, 1991.

[5] G.E.Healey, *Radiometric CCD Camera Calibration and Noise Estimation*, IEEE Trans. on Pattern Analysis and Machine Intelligence, Vol 16, No 3, pp 267-276, 1994.

[6] J.R. Janesick, T. Elliott, S. Collins, M.M. Blouke and J. Freeman, *Scientific charge-coupled devices*, Optical Engineering, Vol 26, No 8, pp 692-714, 1987.

[7] A. Rose and P.K. Weimer, *Physical Limits to the Performance of Imaging Systems*, Physics Today, pp 24-32, September 1989.

[8] S.A. Shafer, *The Calibrated Imaging Lab under Construction at CMU*, DARPA Image Understanding Workshop, pp 509-515, 1985.

[9] L.B. Wolff and T.A. Mancini, *Liquid Crystal Polarization Camera*, IEEE Workshop on Applications of Computer Vision, Palm Springs, CA, pp120-127, 1992.

[10] B.W. Tansley and Associates, *IQCam: Image Analysis System*, Manotick, Ontario, 1995.

[11] *Melles Griot Catalog: Optics Guide 5*, Milles Griot, Inc., 1994.

[12] *Oriel Catalog: Optics & Filters Vol 3*, Oriel Corp., 1990.

[13] *KAF-1300L 1280(H) × 1024(V) pixel Full-Frame CCD Image Sensor Performance Specification*, Revision 0, April 21, 1992, Eastman Kodak Company, Microelectronics Technology Division, Rochester, New York, 14650.

[14] *Charge-Coupled Devices for Quantitative Electronic Imaging*, Photometrics Ltd., 1991.

[15] *Optronic OL750 Operating Manual*, Optronic Laboratory, Inc., 1994.

[16] *IPLab Spectrum: User's Guide version 2.5*, Signal Analytics Corp., 1994.

[17] *PXL System Manual*, Photometrics Ltd., 1994.

[18] *SC-5000 Integrating Sphere System: General Instruction*, Labsphere Inc., 1993.

[19] *MATLAB: User's Guide*, The Math Works Inc., 1994.

Appendix A

Transmittance Data of the Narrow Band (NB) Color Filters

λ	NB#1	NB#2	NB#3	NB#4	NB#5	NB#6	NB#7	NB#8
350	0	0	0	0	0	0	0	0
360	0.035932	0	0	0	0	0	0	0
370	0.059163	0	0	0	0	0	0	0
380	0.170386	0	0	0	0	0	0	0
390	0.409746	0.006938	0	0	0	0	0	0
400	0.591559	0.017938	0	0	0	0	0	0
410	0.626919	0.040649	0	0	0	0	0	0
420	0.623953	0.100956	0	0	0	0	0	0
430	0.580177	0.25205	0.001769	0	0	0	0	0
440	0.510721	0.504158	0.006487	0	0	0	0	0
450	0.396265	0.67066	0.025938	0.000844	0	0	0	0
460	0.214565	0.717474	0.060271	0.000839	0	0	0	0
470	0.075895	0.720404	0.132859	0.000914	0	0	0	0
480	0.020192	0.704699	0.295301	0.002454	0	0	0	0
490	0.004856	0.663545	0.568344	0.009307	0.00073	0	0	0
500	0.001259	0.607196	0.754852	0.019549	0.000784	0	0	0

510	0.000372	0.525035	0.788411	0.037624	0.000852	0	0	0
520	0.000117	0.393859	0.777118	0.078818	0.002407	0.000312	0	0
530	5.32E-05	0.237475	0.750835	0.177104	0.020048	0.000343	0	0
540	3.68E-05	0.122179	0.704869	0.381376	0.06568	0.000407	0	0
550	3.63E-05	0.062394	0.612145	0.625751	0.140552	0.000481	0	0
560	4.91E-05	0.03362	0.467006	0.737219	0.255694	0.000648	0	0
570	6.87E-05	0.019582	0.299635	0.73539	0.400597	0.004393	0.00009	0
580	9.26E-05	0.01196	0.162323	0.682484	0.549008	0.021367	0.0000964	0
590	0.000118	0.007702	0.081911	0.587675	0.660828	0.056205	0.000111	0
600	0	0.005068	0.040453	0.430156	0.717394	0.130984	0.000595	7.5253E-05
610	0	0.003647	0.022801	0.280229	0.726341	0.273206	0.000571	0.00080516
620	0	0.002721	0.013578	0.159687	0.700331	0.496138	0.001658	0.00076988
630	5.09E-09	0.002104	0.008498	0.085237	0.641564	0.702109	0.008017	0.00073344
640	7.02E-09	0.001643	0.005574	0.045064	0.520458	0.764835	0.021466	0.00071797
650	0	0.00131	0.003746	0.024005	0.349074	0.738611	0.04463	0.0006999
660	1.23E-08	0.001075	0.002653	0.013706	0.199829	0.691774	0.084576	0.00074335
670	2.52E-08	0.000905	0.001965	0.00839	0.10693	0.62834	0.158548	0.00088387
680	1.71E-07	0.000776	0.001499	0.005366	0.057054	0.535002	0.28403	0.00112024
690	1.07E-06	0.000669	0.001166	0.003623	0.031902	0.407415	0.459112	0.00141914
700	3.21E-06	0.000584	0.000923	0.002485	0.018296	0.271276	0.623801	0.00188866
710	5.05E-06	0.000518	0.000748	0.001774	0.01115	0.164009	0.716564	0.00306645
720	5.72E-06	0.000473	0.00062	0.001318	0.007213	0.096038	0.741849	0.00678346
730	5.64E-06	0.00043	0.000533	0.00101	0.005001	0.055902	0.728942	0.0191181
740	5.31E-06	0.000394	0.000461	0.000822	0.003567	0.033844	0.684032	0.05651266
750	4.95E-06	0.000364	0.000407	0.000736	0.002715	0.020532	0.591163	0.1386759
760	4.69E-06	0.000338	0.000364	0.000688	0.002237	0.012977	0.44651	0.2735501
770	4.51E-06	0.000318	0.000326	0.000635	0.001976	0.008754	0.293595	0.4164122
780	4.41E-06	0.000299	0.000291	0.000537	0.001777	0.006419	0.175061	0.5377319
790	4.37E-06	0.000283	0.00026	0.000426	0.001569	0.004884	0.098636	0.6262389
800	4.43E-06	0.000268	0.000234	0.000333	0.001328	0.003871	0.056376	0.6839475
810	4.57E-06	0.000255	0.000212	0.000266	0.001057	0.00314	0.03255	0.719199
820	4.74E-06	0.000244	0.000195	0.000224	0.00083	0.002598	0.020101	0.7410306
830	5.04E-06	0.000235	0.000182	0.000195	0.000638	0.002146	0.01304	0.755732
840	5.4E-06	0.000227	0.000169	0.000172	0.0005	0.00174	0.009015	0.7658772

850	5.83E-06	0.000219	0.000158	0.000154	0.00041	0.00137	0.006484	0.7747403
860	0	0	0	0	0	0	0	0.7811601
870	0	0	0	0	0	0	0	0.7867228
880	0	0	0	0	0	0	0	0.7901527
890	0	0	0	0	0	0	0	0.7933423
900	0	0	0	0	0	0	0	0.7956543
910	0	0	0	0	0	0	0	0.802637
920	0	0	0	0	0	0	0	0.8060698
930	0	0	0	0	0	0	0	0.8058788
940	0	0	0	0	0	0	0	0.805488
950	0	0	0	0	0	0	0	0.8065279
960	0	0	0	0	0	0	0	0.8100982
970	0	0	0	0	0	0	0	0.8102957
980	0	0	0	0	0	0	0	0.8099367
990	0	0	0	0	0	0	0	0.8102619
1000	0	0	0	0	0	0	0	0.8096515
1010	0	0	0	0	0	0	0	0.8100472
1020	0	0	0	0	0	0	0	0.8100019
1030	0	0	0	0	0	0	0	0.8103695
1040	0	0	0	0	0	0	0	0.8114999
1050	0	0	0	0	0	0	0	0.8123985
1060	0	0	0	0	0	0	0	0.8120344
1070	0	0	0	0	0	0	0	0.8115987
1080	0	0	0	0	0	0	0	0.8111969
1090	0	0	0	0	0	0	0	0.8118606
1100	0	0	0	0	0	0	0	0.8093725

Appendix B

Transmittance Data of the Neutral Density (ND) Filters

B.1 ND Transmittance at Normal Position

λ	ND1(0.03)	ND2(0.1)	ND3(0.3)	ND4(0.5)	ND5(1.0)	ND6(2.0)	ND7(3.0)
350	9.23E-01	6.77E-01	4.87E-01	3.58E-01	1.61E-02	0.00E+00	7.53E-04
360	9.21E-01	6.77E-01	4.87E-01	3.58E-01	1.61E-02	0.00E+00	7.53E-04
370	9.19E-01	7.12E-01	5.00E-01	3.71E-01	8.46E-02	3.23E-04	9.79E-04
380	9.23E-01	7.12E-01	5.00E-01	3.71E-01	8.46E-02	3.23E-04	9.79E-04
390	9.26E-01	7.30E-01	5.06E-01	3.65E-01	9.43E-02	6.33E-04	0.00E+00
400	9.26E-01	7.30E-01	5.06E-01	3.65E-01	9.43E-02	6.33E-04	0.00E+00
410	9.25E-01	7.22E-01	4.99E-01	3.55E-01	9.91E-02	8.23E-03	0.00E+00
420	9.26E-01	7.22E-01	4.99E-01	3.55E-01	9.91E-02	8.23E-03	0.00E+00
430	9.27E-01	7.32E-01	4.91E-01	3.46E-01	1.03E-01	9.37E-03	0.00E+00
440	9.26E-01	7.32E-01	4.91E-01	3.46E-01	1.03E-01	9.37E-03	0.00E+00
450	9.25E-01	7.35E-01	4.90E-01	3.36E-01	1.01E-01	9.96E-03	2.19E-04
460	9.26E-01	7.35E-01	4.90E-01	3.36E-01	1.01E-01	9.96E-03	2.19E-04
470	9.27E-01	7.39E-01	4.87E-01	3.33E-01	1.00E-01	1.00E-02	0.00E+00
480	9.27E-01	7.39E-01	4.87E-01	3.33E-01	1.00E-01	1.00E-02	0.00E+00
490	9.27E-01	7.42E-01	4.85E-01	3.30E-01	1.01E-01	1.05E-02	4.55E-05
500	9.28E-01	7.42E-01	4.85E-01	3.30E-01	1.01E-01	1.05E-02	4.55E-05

510	9.28E-01	7.47E-01	4.84E-01	3.28E-01	1.01E-01	1.07E-02	1.34E-04
520	9.28E-01	7.47E-01	4.84E-01	3.28E-01	1.01E-01	1.07E-02	1.34E-04
530	9.27E-01	7.51E-01	4.84E-01	3.25E-01	1.01E-01	1.10E-02	1.98E-04
540	9.27E-01	7.51E-01	4.84E-01	3.25E-01	1.01E-01	1.10E-02	1.98E-04
550	9.27E-01	7.68E-01	4.91E-01	3.30E-01	1.01E-01	1.13E-02	1.74E-04
560	9.27E-01	7.68E-01	4.91E-01	3.30E-01	1.01E-01	1.13E-02	1.74E-04
570	9.27E-01	7.72E-01	4.91E-01	3.30E-01	1.01E-01	1.16E-02	2.40E-04
580	9.27E-01	7.72E-01	4.91E-01	3.30E-01	1.01E-01	1.16E-02	2.40E-04
590	9.27E-01	7.74E-01	4.89E-01	3.29E-01	1.01E-01	1.20E-02	9.21E-04
600	9.27E-01	7.74E-01	4.89E-01	3.29E-01	1.01E-01	1.20E-02	9.21E-04
610	9.27E-01	7.61E-01	4.87E-01	3.27E-01	1.02E-01	1.22E-02	1.02E-03
620	9.28E-01	7.61E-01	4.87E-01	3.27E-01	1.02E-01	1.22E-02	1.02E-03
630	9.29E-01	7.63E-01	4.86E-01	3.27E-01	1.02E-01	1.26E-02	1.22E-03
640	9.29E-01	7.63E-01	4.86E-01	3.27E-01	1.02E-01	1.26E-02	1.22E-03
650	9.28E-01	7.67E-01	4.85E-01	3.26E-01	1.03E-01	1.32E-02	1.37E-03
660	9.29E-01	7.67E-01	4.85E-01	3.26E-01	1.03E-01	1.32E-02	1.37E-03
670	9.30E-01	7.71E-01	4.84E-01	3.26E-01	1.03E-01	1.35E-02	1.41E-03
680	9.30E-01	7.71E-01	4.84E-01	3.26E-01	1.03E-01	1.35E-02	1.41E-03
690	9.29E-01	7.73E-01	4.84E-01	3.26E-01	1.03E-01	1.38E-02	1.48E-03
700	9.30E-01	7.73E-01	4.84E-01	3.26E-01	1.03E-01	1.38E-02	1.48E-03
710	9.30E-01	7.75E-01	4.84E-01	3.27E-01	1.04E-01	1.42E-02	1.66E-03
720	9.30E-01	7.75E-01	4.84E-01	3.27E-01	1.04E-01	1.42E-02	1.66E-03
730	9.29E-01	7.78E-01	4.84E-01	3.27E-01	1.04E-01	1.45E-02	1.85E-03
740	9.30E-01	7.78E-01	4.84E-01	3.27E-01	1.04E-01	1.45E-02	1.85E-03
750	9.30E-01	7.81E-01	4.85E-01	3.29E-01	1.05E-01	1.48E-02	1.93E-03
760	9.30E-01	7.81E-01	4.85E-01	3.29E-01	1.05E-01	1.48E-02	1.93E-03
770	9.29E-01	7.83E-01	4.85E-01	3.29E-01	1.05E-01	1.51E-02	2.03E-03
780	9.30E-01	7.83E-01	4.85E-01	3.29E-01	1.05E-01	1.51E-02	2.03E-03
790	9.31E-01	7.85E-01	4.85E-01	3.30E-01	1.05E-01	1.55E-02	2.18E-03
800	9.31E-01	7.85E-01	4.85E-01	3.30E-01	1.05E-01	1.55E-02	2.18E-03
810	9.30E-01	7.87E-01	4.85E-01	3.30E-01	1.06E-01	1.57E-02	2.28E-03
820	9.31E-01	7.87E-01	4.85E-01	3.30E-01	1.06E-01	1.57E-02	2.28E-03
830	9.31E-01	7.91E-01	4.85E-01	3.31E-01	1.06E-01	1.60E-02	2.28E-03

840	9.30E-01	7.91E-01	4.85E-01	3.31E-01	1.06E-01	1.60E-02	2.28E-03
850	9.29E-01	7.90E-01	4.83E-01	3.30E-01	1.06E-01	1.64E-02	2.57E-03
860	9.30E-01	7.90E-01	4.83E-01	3.30E-01	1.06E-01	1.64E-02	2.57E-03
870	9.30E-01	7.93E-01	4.82E-01	3.30E-01	1.07E-01	1.66E-02	2.63E-03
880	9.30E-01	7.93E-01	4.82E-01	3.30E-01	1.07E-01	1.66E-02	2.63E-03
890	9.29E-01	7.94E-01	4.71E-01	3.30E-01	1.07E-01	1.68E-02	2.76E-03
900	9.30E-01	7.94E-01	4.71E-01	3.30E-01	1.07E-01	1.68E-02	2.76E-03
910	9.31E-01	7.95E-01	4.74E-01	3.26E-01	1.08E-01	1.70E-02	2.91E-03
920	9.31E-01	7.95E-01	4.74E-01	3.26E-01	1.08E-01	1.70E-02	2.91E-03
930	9.30E-01	7.97E-01	4.76E-01	3.28E-01	1.08E-01	1.72E-02	3.00E-03
940	9.38E-01	7.97E-01	4.76E-01	3.28E-01	1.08E-01	1.72E-02	3.00E-03
950	9.46E-01	8.11E-01	4.83E-01	3.34E-01	1.08E-01	1.71E-02	3.15E-03
960	9.38E-01	8.11E-01	4.83E-01	3.34E-01	1.08E-01	1.71E-02	3.15E-03
970	9.29E-01	8.13E-01	4.83E-01	3.35E-01	1.09E-01	1.74E-02	3.28E-03
980	9.29E-01	8.13E-01	4.83E-01	3.35E-01	1.09E-01	1.74E-02	3.28E-03
990	9.29E-01	8.16E-01	4.83E-01	3.36E-01	1.09E-01	1.76E-02	3.40E-03
1000	9.29E-01	8.16E-01	4.83E-01	3.36E-01	1.09E-01	1.76E-02	3.40E-03
1010	9.28E-01	8.20E-01	4.83E-01	3.38E-01	1.10E-01	1.77E-02	3.52E-03
1020	9.31E-01	8.20E-01	4.83E-01	3.38E-01	1.10E-01	1.77E-02	3.52E-03
1030	9.33E-01	8.24E-01	4.86E-01	3.40E-01	1.10E-01	1.78E-02	3.65E-03
1040	9.32E-01	8.24E-01	4.86E-01	3.40E-01	1.10E-01	1.78E-02	3.65E-03
1050	9.31E-01	8.07E-01	4.74E-01	3.33E-01	1.11E-01	1.78E-02	3.73E-03
1060	9.31E-01	8.07E-01	4.74E-01	3.33E-01	1.11E-01	1.78E-02	3.73E-03
1070	9.31E-01	8.05E-01	4.70E-01	3.30E-01	1.11E-01	1.85E-02	3.84E-03
1080	9.30E-01	8.05E-01	4.70E-01	3.30E-01	1.11E-01	1.85E-02	3.84E-03
1090	9.29E-01	8.08E-01	4.70E-01	3.31E-01	1.11E-01	1.87E-02	3.93E-03
1100	9.29E-01	8.08E-01	4.70E-01	3.31E-01	1.11E-01	1.87E-02	3.93E-03

B.2 ND Transmittance at 20 degrees Off-Normal Position

λ	ND1-20 (0.03)	ND2-20 (0.1)	ND3-20 (0.3)	ND4-20 (0.5)	ND5-20 (1.0)	ND6-20 (2.0)	ND7-20 (3.0)
350	9.51E-01	7.48E-01	5.41E-01	9.10E-02	2.34E-02	1.26E-03	0.00E+00
360	9.51E-01	7.48E-01	5.41E-01	9.10E-02	2.34E-02	1.26E-03	0.00E+00
370	9.45E-01	7.29E-01	4.97E-01	3.33E-01	1.34E-02	4.61E-04	2.98E-04
380	9.45E-01	7.29E-01	4.97E-01	3.33E-01	1.34E-02	4.61E-04	2.98E-04
390	9.44E-01	7.32E-01	4.97E-01	3.42E-01	1.48E-02	2.17E-04	3.88E-04
400	9.44E-01	7.32E-01	4.97E-01	3.42E-01	1.48E-02	2.17E-04	3.88E-04
410	9.47E-01	7.30E-01	5.03E-01	3.40E-01	8.81E-02	8.08E-03	0.00E+00
420	9.47E-01	7.30E-01	5.03E-01	3.40E-01	8.81E-02	8.08E-03	0.00E+00
430	9.45E-01	7.36E-01	4.91E-01	3.35E-01	9.79E-02	9.01E-03	0.00E+00
440	9.45E-01	7.36E-01	4.91E-01	3.35E-01	9.79E-02	9.01E-03	0.00E+00
450	9.43E-01	7.40E-01	4.89E-01	3.25E-01	1.00E-01	9.34E-03	2.61E-04
460	9.43E-01	7.40E-01	4.89E-01	3.25E-01	1.00E-01	9.34E-03	2.61E-04
470	9.46E-01	7.45E-01	4.89E-01	3.23E-01	9.71E-02	9.67E-03	5.00E-05
480	9.46E-01	7.45E-01	4.89E-01	3.23E-01	9.71E-02	9.67E-03	5.00E-05
490	9.45E-01	7.49E-01	4.87E-01	3.21E-01	9.95E-02	1.02E-02	1.91E-05
500	9.45E-01	7.49E-01	4.87E-01	3.21E-01	9.95E-02	1.02E-02	1.91E-05
510	9.47E-01	7.53E-01	4.86E-01	3.20E-01	9.94E-02	1.06E-02	1.15E-04
520	9.47E-01	7.53E-01	4.86E-01	3.20E-01	9.94E-02	1.06E-02	1.15E-04
530	9.48E-01	7.56E-01	4.84E-01	3.18E-01	9.85E-02	1.08E-02	5.31E-05
540	9.48E-01	7.56E-01	4.84E-01	3.18E-01	9.85E-02	1.08E-02	5.31E-05
550	9.47E-01	7.73E-01	4.92E-01	3.22E-01	9.94E-02	1.11E-02	1.14E-04
560	9.47E-01	7.73E-01	4.92E-01	3.22E-01	9.94E-02	1.11E-02	1.14E-04
570	9.49E-01	7.76E-01	4.91E-01	3.22E-01	9.94E-02	1.15E-02	9.19E-05
580	9.49E-01	7.76E-01	4.91E-01	3.22E-01	9.94E-02	1.15E-02	9.19E-05
590	9.49E-01	7.79E-01	4.90E-01	3.22E-01	9.95E-02	1.18E-02	8.10E-05
600	9.49E-01	7.79E-01	4.90E-01	3.22E-01	9.95E-02	1.18E-02	8.10E-05

610	9.52E-01	7.65E-01	4.88E-01	3.19E-01	1.00E-01	1.21E-02	9.61E-04
620	9.52E-01	7.65E-01	4.88E-01	3.19E-01	1.00E-01	1.21E-02	9.61E-04
630	9.53E-01	7.72E-01	4.90E-01	3.21E-01	1.01E-01	1.24E-02	1.05E-03
640	9.53E-01	7.72E-01	4.90E-01	3.21E-01	1.01E-01	1.24E-02	1.05E-03
650	9.54E-01	7.76E-01	4.88E-01	3.20E-01	1.02E-01	1.30E-02	1.18E-03
660	9.54E-01	7.76E-01	4.88E-01	3.20E-01	1.02E-01	1.30E-02	1.18E-03
670	9.56E-01	7.79E-01	4.89E-01	3.22E-01	1.02E-01	1.34E-02	1.41E-03
680	9.56E-01	7.79E-01	4.89E-01	3.22E-01	1.02E-01	1.34E-02	1.41E-03
690	9.58E-01	7.82E-01	4.89E-01	3.22E-01	1.03E-01	1.38E-02	1.50E-03
700	9.58E-01	7.82E-01	4.89E-01	3.22E-01	1.03E-01	1.38E-02	1.50E-03
710	9.57E-01	7.84E-01	4.89E-01	3.23E-01	1.03E-01	1.40E-02	1.56E-03
720	9.57E-01	7.84E-01	4.89E-01	3.23E-01	1.03E-01	1.40E-02	1.56E-03
730	9.60E-01	7.87E-01	4.89E-01	3.23E-01	1.04E-01	1.45E-02	1.52E-03
740	9.60E-01	7.87E-01	4.89E-01	3.23E-01	1.04E-01	1.45E-02	1.52E-03
750	9.62E-01	7.90E-01	4.90E-01	3.24E-01	1.04E-01	1.48E-02	1.87E-03
760	9.62E-01	7.90E-01	4.90E-01	3.24E-01	1.04E-01	1.48E-02	1.87E-03
770	9.61E-01	7.92E-01	4.89E-01	3.25E-01	1.04E-01	1.50E-02	1.87E-03
780	9.61E-01	7.92E-01	4.89E-01	3.25E-01	1.04E-01	1.50E-02	1.87E-03
790	9.64E-01	7.98E-01	4.92E-01	3.27E-01	1.05E-01	1.54E-02	1.98E-03
800	9.64E-01	7.98E-01	4.92E-01	3.27E-01	1.05E-01	1.54E-02	1.98E-03
810	9.64E-01	8.00E-01	4.92E-01	3.27E-01	1.05E-01	1.56E-02	1.99E-03
820	9.64E-01	8.00E-01	4.92E-01	3.27E-01	1.05E-01	1.56E-02	1.99E-03
830	9.67E-01	8.01E-01	4.92E-01	3.28E-01	1.06E-01	1.60E-02	2.16E-03
840	9.67E-01	8.01E-01	4.92E-01	3.28E-01	1.06E-01	1.60E-02	2.16E-03
850	9.60E-01	8.00E-01	4.90E-01	3.28E-01	1.06E-01	1.63E-02	2.39E-03
860	9.60E-01	8.00E-01	4.90E-01	3.28E-01	1.06E-01	1.63E-02	2.39E-03
870	9.59E-01	7.98E-01	4.88E-01	3.27E-01	1.06E-01	1.65E-02	2.63E-03
880	9.59E-01	7.98E-01	4.88E-01	3.27E-01	1.06E-01	1.65E-02	2.63E-03
890	9.56E-01	8.00E-01	4.87E-01	3.27E-01	1.07E-01	1.69E-02	2.76E-03
900	9.56E-01	8.00E-01	4.87E-01	3.27E-01	1.07E-01	1.69E-02	2.76E-03
910	9.49E-01	7.98E-01	4.75E-01	3.19E-01	1.06E-01	1.67E-02	2.84E-03
920	9.49E-01	7.98E-01	4.75E-01	3.19E-01	1.06E-01	1.67E-02	2.84E-03
930	9.48E-01	8.02E-01	4.76E-01	3.21E-01	1.06E-01	1.69E-02	2.94E-03
940	9.48E-01	8.02E-01	4.76E-01	3.21E-01	1.06E-01	1.69E-02	2.94E-03

950	9.68E-01	8.02E-01	4.77E-01	3.23E-01	1.05E-01	1.69E-02	3.13E-03
960	9.68E-01	8.02E-01	4.77E-01	3.23E-01	1.05E-01	1.69E-02	3.13E-03
970	9.50E-01	8.20E-01	4.87E-01	3.30E-01	1.08E-01	1.72E-02	3.27E-03
980	9.50E-01	8.20E-01	4.87E-01	3.30E-01	1.08E-01	1.72E-02	3.27E-03
990	9.51E-01	8.21E-01	4.87E-01	3.31E-01	1.08E-01	1.74E-02	3.38E-03
1000	9.51E-01	8.21E-01	4.87E-01	3.31E-01	1.08E-01	1.74E-02	3.38E-03
1010	9.55E-01	8.24E-01	4.87E-01	3.32E-01	1.09E-01	1.76E-02	3.50E-03
1020	9.55E-01	8.24E-01	4.87E-01	3.32E-01	1.09E-01	1.76E-02	3.50E-03
1030	9.56E-01	8.28E-01	4.88E-01	3.34E-01	1.09E-01	1.77E-02	3.61E-03
1040	9.56E-01	8.28E-01	4.88E-01	3.34E-01	1.09E-01	1.77E-02	3.61E-03
1050	9.63E-01	8.38E-01	4.92E-01	3.36E-01	1.09E-01	1.77E-02	3.71E-03
1060	9.63E-01	8.38E-01	4.92E-01	3.36E-01	1.09E-01	1.77E-02	3.71E-03
1070	9.62E-01	8.13E-01	4.77E-01	3.26E-01	1.09E-01	1.83E-02	3.80E-03
1080	9.62E-01	8.13E-01	4.77E-01	3.26E-01	1.09E-01	1.83E-02	3.80E-03
1090	9.62E-01	8.18E-01	4.76E-01	3.25E-01	1.09E-01	1.83E-02	3.85E-03
1100	9.62E-01	8.18E-01	4.76E-01	3.25E-01	1.09E-01	1.83E-02	3.85E-03

Preliminary Calibration of the Photometrics PXL1300L CCD Camera*

Steve Shiang-Feng Chen*
Jerry Wei-Chieh Li*
Kenneth E. Torrance†
S. N. Pattanaik‡

PCG-96-1 March 4, 1996

This report describes the preliminary spectroradiometric calibration of a CCD camera system, which consists of a high dynamic range (12 bit), liquid cooled scientific grade CCD camera used in conjunction with a series of narrow band and neutral density filters. The purpose of the calibration is to extend the camera system into a *spectral camera*, capable of measuring scene images that would provide, not only color information, but *quantitative spectrum data* for every pixel of a viewed scene. The measured images from such a *spectral camera* can eventually be compared with the synthetic images generated using physically based algorithms for illumination exchange.

The present report provides spectral transmittance curves for the narrow band and neutral density filters used with the CCD camera, and the results of various linearity checks on the camera. The report provides the *spectral response function* for the camera and *preliminary spectral reconstructions* for wide and narrow band light sources.

*An early version of this report was submitted by the first two authors towards the partial fulfillment of their M.Eng. degree in Mechanical & Aerospace Engineering, under course M&AE 690 (8 credits).

†Professor, Sibley School of Mechanical and Aerospace Engineering, Cornell University.

‡Post Doctoral Research Associate, Program of Computer Graphics, Cornell University.